5-23-1961

The Control and Measurement of Minute Curvatures In a Steel Shaft

Donald F. Wilkes

THE CONTROL AND MEASUREMENT OF MINUTE CURVATURES IN A STEEL SHAFT • WILKES

THE CONTROL AND MEASUREMENT OF MINUTE CURVATURES IN A STEEL SHAFT

By

Donald F. Wilkes

A Thesis

Submitted in Partial Fulfillment of the

Requirements for the Degree of

Master of Science in Mechanical Engineering

The University of New Mexico

1961

This thesis, directed and approved by the candidate's committee, has been accepted by the Graduate Committee of the University of New Mexico in partial fulfillment of the requirements for the degree of

MASTER OF SCIENCE

E L Castetter
Dean

May 23, 1961
Date

Thesis committee

R C Dart
Chairman

Frederick R Sahs

C T Snow

TABLE OF CONTENTS

TABLE OF CONTENTS (cont)

* Appendix I has been omitted because of security classification.

LIST OF ILLUSTRATIONS

LIST OF ILLUSTRATIONS (cont)

LIST OF ILLUSTRATIONS (cont)

THE CONTROL AND MEASUREMENT OF MINUTE CURVATURES IN A STEEL SHAFT

Introduction

The primary purpose of this thesis was the solution of several special problems relating to the establishment, adjustment, and measurement of small elastic curvatures and the associated strains in a metal shaft. The solution of these problems was an important link in the development of a new type of seismometer for measuring extremely long period earth vibrations (up to 60 seconds).[1]* To achieve the sensitivity and long natural period of vibration required for accurate measurements of long-period waves,[2] the seismometer employs a seismic mass which is suspended on an air film and constrained to follow an essentially horizontal guide rod. The guide rod, which was originally straight, is bowed elastically through use of a straining frame to form a plane curve which is concave upward. This combination of guidance and support forms a lightly damped gravity pendulum in which the seismic mass always seeks the lowest point on the curve. The natural period of this pendulum must be adjustable between the limits of 20 and 200 seconds to allow both ease of setup and high-fidelity performance. This is equivalent to saying that the guide-shaft radius of curvature must be adjustable from about 327 feet up to about 32,700 feet.

---

*Superscript numbers in [ ] brackets refer to references listed in the bibliography, page 81.

The Thesis Problems

Purpose

The problem of introducing these curvatures into the guide rod and measuring them was the principal concern of this thesis. Secondary objectives were: (1) to evaluate semiconductor strain gages for measuring minute strains, (2) to explore new ways to obtain precise functions through controlled elastic deformation, and (3) to develop a feasible technique for obtaining semicontinuous plots of minute elastic curves. A more complete explanation of the seismometer and the origin of the thesis problems is presented in Appendix I.

Scope

The following five closely related subprojects were undertaken in order to satisfy the primary purpose and still confine the thesis work to reasonable bounds.

1. The design of a straining frame to accurately induce and regulate the guide-shaft curvature. This frame was to be made compatible with the seismometer and designed for high stability with respect to time and temperature variations.

2. The calibration of the straining frame for theoretical periods and radii of curvature between 20 seconds or 350 feet and 200 seconds or 35,000 feet.

3. The verification of this calibration by completely different means.

4. The study of the fine details of several typical elastic curves introduced by loading, shaft weight, etc., so that the linearity of the seismometer may be evaluated.

5. The development of a measuring technique with sufficient accuracy and resolution to allow nearly continuous plots of minute curvatures to be drawn. The plotting of several

typical curves and the comparison of these with theoretical curves. This type of information was needed in order to evaluate and scientifically eliminate unwanted forces that were introduced into the seismometer by the suspension and readout systems.

In addition to the range of shaft curvatures already mentioned (350 feet to 35,000 feet), the following restrictions were imposed on the shaft and formulation of the problems because of the seismometer application: (1) The shaft was made of steel; (2) the shaft had a uniform 7/16-inch outside diameter and is 5-1/2 inches long; (3) the straining-frame load points were symmetrically oriented 3.375 inches and 4.375 inches apart to give approximately constant moment bending in the section between the two center load points; (4) only central loadings representative of interesting seismic mass loadings were considered; and (5) only approximately the center 2 inches of shaft curvature were of particular interest.

Method

The theory of shaft flexure is relatively simple and extremely accurate for small deflections. Thus the problems of this thesis were created by the degree of precision required in the measurements rather than by any complication of theory. Direct physical measurement of these elastic curves was not feasible because of the high degree of resolution needed. Some of the curves of interest had maximum deflections of about 4×10^{-6} inches in a 3-3/8-inch span. Another serious limitation on direct physical measurement was imposed by the best attainable surface finishes (1/2 to 1/4 μ in rms). The range of shaft curvatures needed in the 7/16-inch-diameter shaft corresponded to maximum strains of from 1.5 to 15 μ in/in. Conventional foil or wire resistance strain gages will not reliably give this type of resolution.

To overcome these limitations, two special techniques were employed: (1) semiconductor resistance strain gages and (2) measurement of light-wave interference patterns. The semiconductor resistance strain gages were chosen because they are from 30 to 100 times more sensitive than

conventional strain gages. Strain readings taken with semiconductor gages mounted to a dummy shaft were used in conjunction with flexure theory to calibrate the straining apparatus. The step of verification was made by timing the period of vibration of the seismic mass under different straining-frame settings. Fine detail study and continuous plotting were accomplished by taking measurements from photographs of optical fringe patterns set up on a dummy shaft. This dummy shaft was equipped with a very narrow, optically flat surface. The fringe pattern was set up between this flat and the reference-glass flat in the interferometer used. This procedure was chosen because no contact is made with the shaft,and a very precise quantity, the wavelength of helium green light, is used as the standard.

Straining-Frame Design

The design of a straining frame stable enough for use as a base for a 200-second seismometer required special attention. Practical considerations showed that tilts induced in the guide rod by the occurrence of stress relief or differential thermal expansion in any part of the seismometer structure would have to be held to less than 1×10^{-8} radians per week to make the instrument's extremely sensitive readout system useable. The important design considerations will now be discussed.

Shaft Dimensions and Load-Point Spacing

A 7/16-inch nominal diameter was selected for the guide rod because precision metal bushings were available in this diameter for use in developing the hydrodynamically suspended seismic mass needed in the seismometer. A minimum spacing between the inner walls or inner load-point surfaces of the straining frame of 3 inches for a 2-inch-long bushing was experimentally established. Lesser spacing resulted in excessive axial forces due to the aerodynamics of the spinning bushing. The requirements of extreme straightness, roundness, and constancy of diameter imposed on the guide rod by its role in the air-bearing suspension made it desirable to maximize the lateral stiffness of the rod for grinding. This was done by

making the rod as short as possible. The configuration and material shown in Figure 1 were chosen as the best compromise.

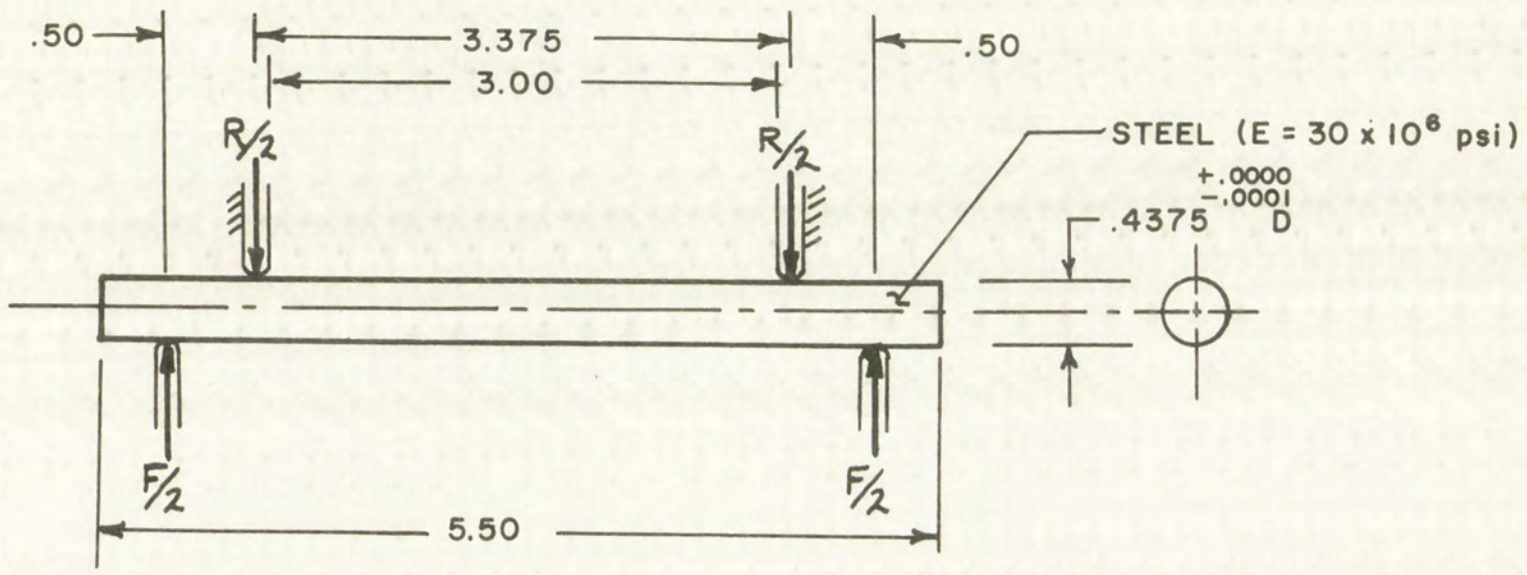

Figure 1. Straining-Frame Geometry

The method chosen for making the minute settings required of the straining frame was to use a large deflection of a spring element to produce a relatively small change in spring force. Practically, this can be done by using a fine pitch screw to extend a weak spring. The choice of the best screw and spring requires a knowledge of the resolution in force and range of forces needed. The maximum radius of curvature of interest for the constant-moment section of the guide rod (for 200-second period, R_c = 32,700 feet) corresponds to a central deflection, δ, of 7.3×10^{-6} inches in 3.375-inch central span. A maximum error of ± 1 percent was desired for all period settings. Thus, since the period of a gravity pendulum is:

$$T = 2\pi \sqrt{\frac{R_c}{g}}$$

where

T = period of vibration (sec)

R_c = radius of curvature (in), and

g = gravitational constant = 386 in/sec^2,

and the radius of curvature in the constant moment is

$$R_c \propto \frac{1}{\delta}$$

where

δ = the central deflection (in)

thus the equation for the natural period of vibration may be written as

$$T \propto \sqrt{\frac{1}{\delta}} \quad \text{or} \quad T = C\sqrt{\frac{1}{\delta}}$$

where

C = constant = 0.538 in this situation.

Let $\Delta\delta$ equal the maximum permissible error in δ, and ΔT equal the maximum permissible error in T (1 percent of the nominal period T in this case). Thus, if the period T were set into the frame, the measured or true period should be within 1 percent of T. This may be written

$$T - \Delta T = C\sqrt{\frac{1}{\delta + \Delta\delta}} = 0.99T,$$

from which

$$\Delta\delta = \frac{C^2}{(T - \Delta T)^2} - \delta$$

for $T = 200$ seconds, $\Delta T = 2$ seconds, and $\delta = 7.3\ \mu$ in; therefore, the resolution required in the central deflection is

$$\Delta\delta = \frac{(0.538)^2}{(198)^2} - 7.30 \times 10^{-6} = 7.39 - 7.30 \approx 0.1\ \mu \text{ in.}$$

In order to determine the degree of force resolution needed, the $\Delta\delta$ calculated above will be converted into a maximum permissible change in force, ΔF.

Since only an approximation is needed, the rod will be assumed weightless and without any bushing load. For a constant moment section, the central deflection is given by the formula:

$$\delta = \frac{Fd\ell^2}{16EI}$$

where

d = spacing between the inner and outer load points = 0.5 in

$E = 30 \times 10^6$ psi

$$I = \frac{1}{4}\pi r^4 = \frac{\pi}{4}(0.2188)^4 = 1.8 \times 10^{-3} \text{ in}^4$$

$\ell = 3.375$ in

or in terms of permissible errors,

$$\Delta\delta = \frac{\Delta F d \ell^2}{16EI} .$$

Solving for ΔF, the desired resolution in force is

$$\Delta F = \frac{16EI\Delta\delta}{\ell^2 d} = \frac{16 \times 30 \times 10^6 \times 1.8 \times 10^{-3} \times 1 \times 10^{-7}}{(3.375)^2 \times 0.5}$$

$$= 0.0152 \text{ lbs}$$

$$= 1.52 \times 10^5 \Delta\delta \text{ lbs.}$$

Using the same formulas, one finds that the maximum force needed (for 20-second period, $\delta = 7.3 \times 10^{-4}$ inches) is

$$F_{max} = 1.52 \times 10^5 \times 7.3 \times 10^{-4} = 111 \text{ lbs.}$$

If 1 inch of spring deflection is arbitrarily selected to give this maximum force, the spring constant becomes $k_S = 111$ lbs/in.

If the 0.0152-pound resolution determined necessary above is to be maintained, this means that the 1 inch of spring deflection must be broken down into 111/0.0152 = 7300 parts, or 1 inch/7300 = 0.000137-inch increments. An 80-pitch thread is about the finest practical thread. This

pitch has a lead of 0.0125 inch per revolution so that each revolution would have to be broken into approximately 100 increments. Additional setting accuracy can be gained by adding a vernier scale to the 100-increment dial to further break each of these increments into 10 parts. This design was used: (1) 1-inch maximum travel, (2) $k_S \approx 111$ lb/in, (3) 80-pitch thread, and (4) scales and vernier to break each revolution into 1000 parts.

Material Selection

Hot-rolled 1018 steel was chosen for the basic structural material because it is soft, easy to machine, stable with time, easy to weld, and gives minimum distortion during machining. After welding, several times during rough machining, and again before final machining, the 1018 parts were uniformly heated to provide stress relief and were then slowly cooled to room temperature. This process reduced the warping, during and after machining, to the lowest possible figure. All parts of the frame except the spring and load points were made of 1018 steel. The spring was made of plain, heat-treated, high-carbon spring wire to match as closely as possible the thermal expansion of the rest of the frame.

Load-Point Design

The internal surfaces of the load rings were given a 1/2-inch radiused profile so that there would be a repeatable point (more realistically, an elliptical area) of contact, see Figure 2.

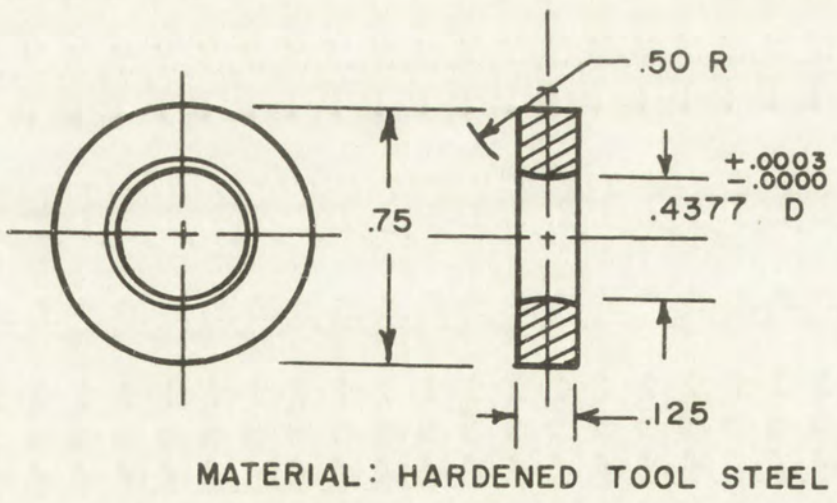

Figure 2. Load Ring

These rings were made of hardened tool steel to withstand the high contact stresses without yielding.

Elimination of Stress Risers

In the interest of even greater stability, all welds were ground smooth and all machined parts amply filleted to eliminate stress concentrations which might possibly throw certain areas of the frame into the yield stress region during use.

Final Design

The final straining-frame design layout, a photo of the frame, and a photograph of the parts is shown in Figures 3, 4, and 5. Notice that the minimum thickness of any structural part is 0.25 inch. This design includes all of the features and considerations mentioned above. In addition, all waste motions were reduced to the absolute minimum possible with hand fitting. This frame has been used successfully for more than 1 year, and all indications show that both the material and method of construction are adequate for the final instrument design. Detailed drawings of the parts are included in Appendix II.

Selection and Mounting of Semiconductor Resistance Strain Gages for Straining-Frame Calibration

The extreme resolution required in the straining-frame adjustment had to be matched with an equally sensitive method of calibration if the straining-frame settings were to be useful in establishing long periods of vibration for the seismometer. A simple calculation converts the required straining-frame resolution ($\Delta F = 0.0152$ pounds) into an equivalent resolution in maximum strain, $\Delta\epsilon$.

$$\Delta\epsilon = \frac{\Delta F dy}{2EI} = \frac{0.0152 \times 0.5 \times 0.21875}{2 \times 30 \times 10^{6} \times 1.8 \times 10^{-3}} = 1.54 \times 10^{-8} \text{ in/in}$$

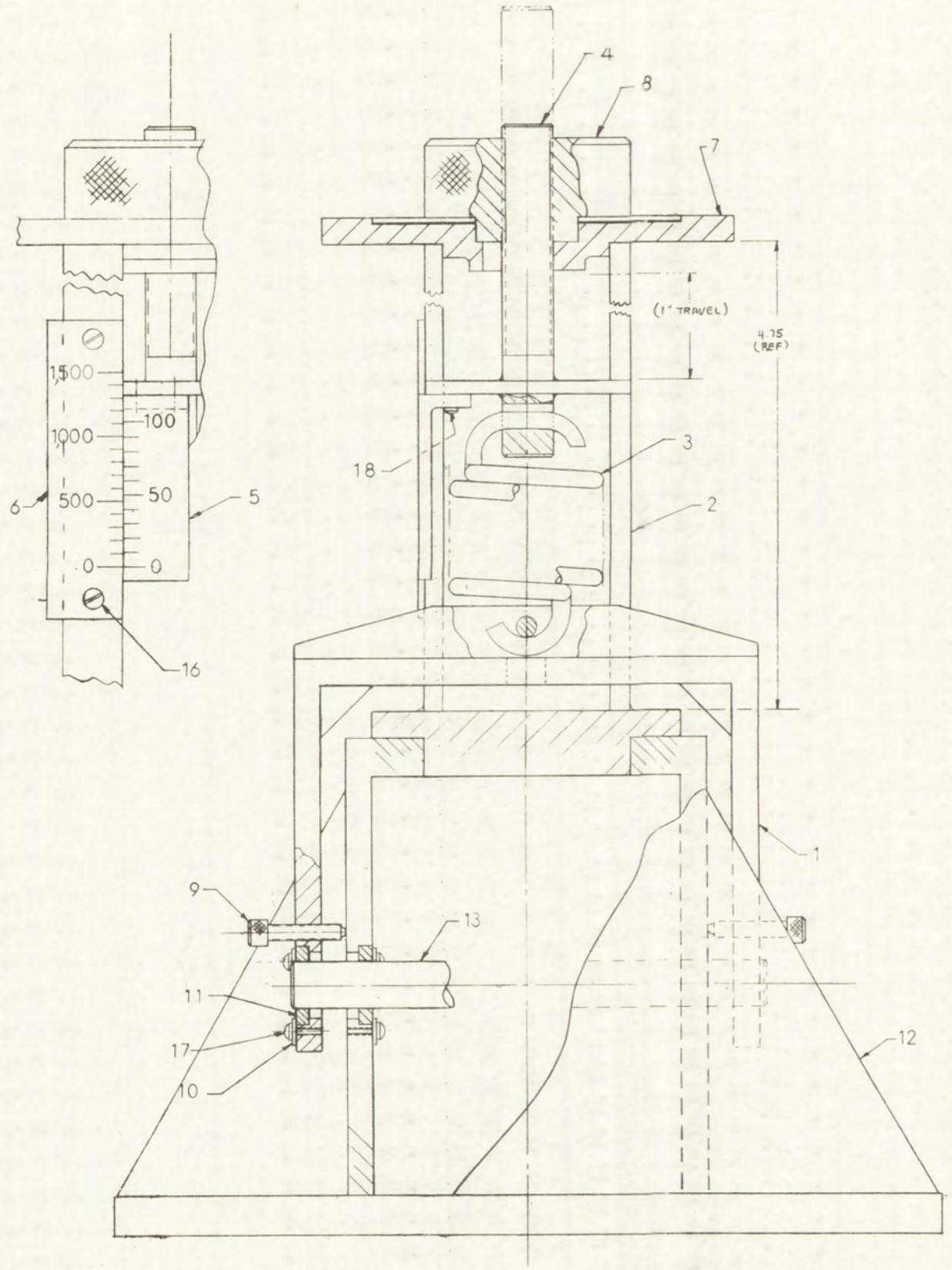

Figure 3. Seismometer Test Fixture

1	Frame, Shaft
2	Frame, Spring
3	Spring, Tension
4	Shaft Threaded
5	Calibration, Bracket
6	Calibration, Plate
7	Cover Plate
8	Knob
9	Screw, Balancing
10	Washer, Retaining
11	Bearing
12	Base
13	Shaft

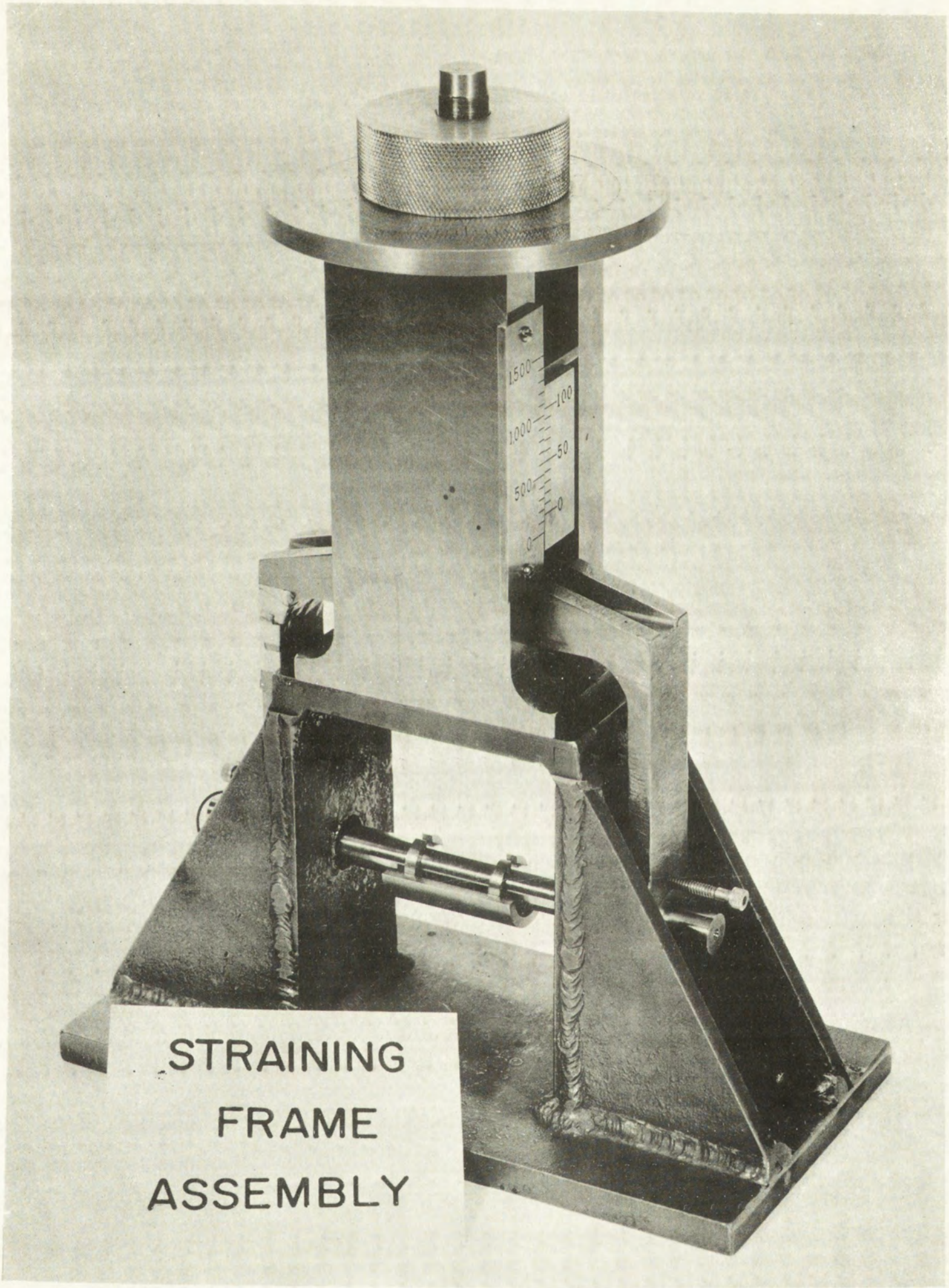

Figure 4. Straining-Frame Assembly

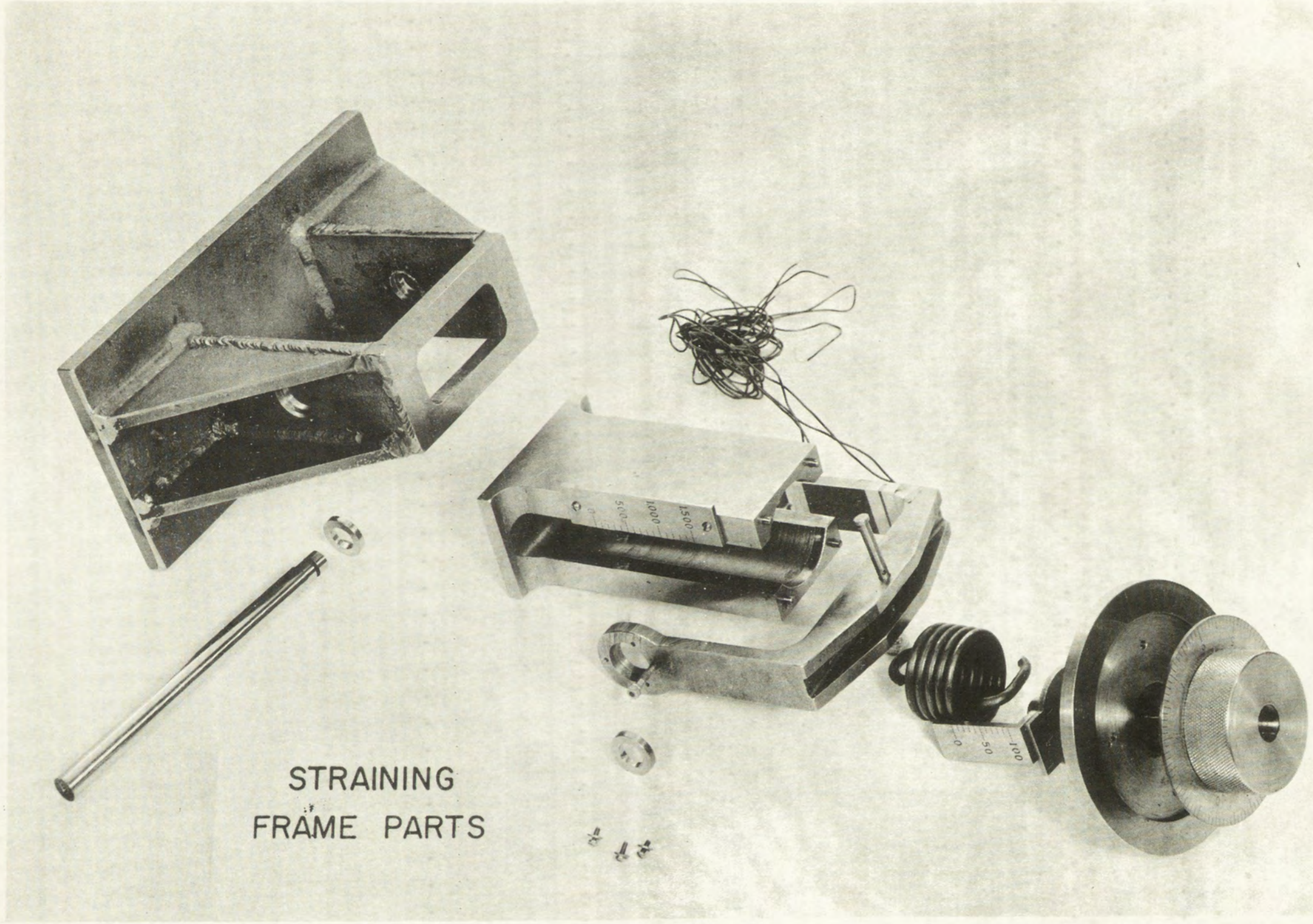

Figure 5. Straining-Frame Parts

where

d = spacing between inner and outer load points = 0.5 in,

y = distance from neutral axis to most distant fiber = r = 0.2187 in.

The maximum strain resolution feasible with conventional wire-type strain gages and conventional strain-indicating equipment is about 1 μ in/in. Thus, about $(1.54 \times 10^{-8})/(1 \times 10^{-6}) \approx 70$ times more gage sensitivity would be needed to use a conventional strain indicator for the straining-frame calibration. Fortunately, a new type of highly sensitive resistance strain gage making use of semiconductor materials and the piezoresistive effect has appeared on the market. These new gages do have from 30 to 100 times the sensitivity of wire gages, but they are so new that very little is known of their behavior and stability. It was realized that further study and experiment were required to insure their suitability for the straining-frame calibration.

Principle of Semiconductor Gage Performance

The piezoresistive effect exhibited by properly oriented germanium and silicon under stress may be used to form very sensitive strain gages.[3][4][5] Both of these materials have cubic crystalline structure and, in the unstressed condition, are isotropic with respect to electrical resistivity. Under stress the electrical resistivity becomes anisotropic. It is this resistance change that makes them useful as resistance strain gages. Elongated shapes of minimal cross-sectional area are generally used for strain-gage elements so that the stiffness in the longitudinal direction is minimized and the surface area per unit length is maximized (to insure good bonding). For greatest sensitivity, the crystal lattice of the semiconductor material must be properly oriented with respect to the longitudinal axis of the element. The chart below (Figure 6) shows the direction and theoretical maximum gage factors attainable for properly "doped" or treated n- and p-type compositions.[6]

Material	Unstressed volumetric resistivity, ρ (ohm-cm)	Orientation of longitudinal axis for maximum sensitivity	Maximum gage factor $\frac{\Delta R/R}{\epsilon}$
Ge (p-type)	1.1	Equal angles with three crystal axes	+101.5
Ge (n-type)	16.6	Equal angles with three crystal axes	-157
Si (p-type)	7.8	Equal angles with three crystal axes	+175
Si (n-type)	11.7	Parallel to a crystal axis	-133

Figure 6. Table of Piezoresistive Properties

The maximum gage factors are generally not sought in semiconductor gage design because increased temperature sensitivity accompanies the heavy doping required. See References [3] through [9] for a more complete mathematical and physical description of semiconductor resistance gage performance.

Semiconductor Gage Selection

Types Available -- Only three companies were making semiconductor gages during work on this thesis. Design data on these three types are presented in Figure 7.

Thermal Behavior and Stability

All semiconductor resistance strain gages are very temperature-sensitive.[6][8] A graph of the temperature characteristics of the Model 711 Strainistor is shown in Figure 8; it is typical of the three types presently available. It is apparent that large thermal errors may be obtained, even with normal temperature variations. All of the manufacturer's data show that near-perfect temperature compensation can be achieved through use of two gages mounted to the same type of material in adjacent legs of the

	Manufacturer	No. of Gage	Shape and Gage Length	Material	Nominal Resistance, R (ohms)	Gage Factor $\frac{\Delta R/R}{\varepsilon}$	Linearity for Full Scale, for Single Gage (%)	Maximum Useful Strain (μ in/in)	Maximum Recommended Current (ma)
1	Bell Telephone Laboratories (experimental gages)	-	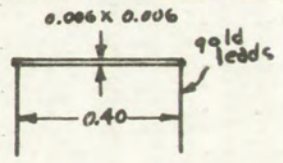	Ge (n-type)	70	65-75	?	?	?
2	Century Electronics	Strainistor Model 711	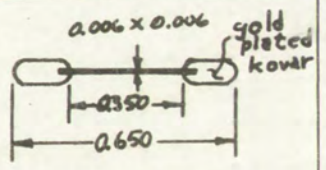	Si (p-type)	120 ohms ±5% (in matched pairs 120 ohms ±0.5%)	120-140	2.5	±2000	30
3	Kulite Bytrex Corporation	Kulite Model DA-101	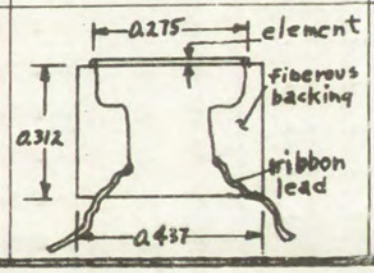	Si (p-type)	62±2	118±5%	?	±1500	20

	Recommended Bonding Agent	Bonding Technique	Lead Attachment	Difficulty of Gage Attachment	Comments
1	C-4 EPY-150	Must first apply insulating layer and let harden, then bond gage itself.	Solder to existing gold-plated lead (hard to keep from melting).	Very difficult to handle and position. Very brittle.	Not commercially available.
2	Eastman 910 EPY-150 Mithra No. 200	Must first apply insulating layer and let harden, then bond gage itself.	Solder to thin plates to end of gage. (Very hard to keep from breaking bond with soldering heat.	Comes with handling frame. Easy to handle and bond, but frame obscures element and makes positioning difficult.	Cost $35.00 each. More information available on this gage than on Bytrex type.
3	A-2 EPY-150	Bonds directly.	Solder to metal ribbons (easy).	Easy to handle and position.	

Figure 7. Semiconductor Gage Comparison Table

MODEL 711 STRAINISTOR

LOT NO. 101 SENSITIVITY FACTOR 123 ±5% DATE 3-25-60

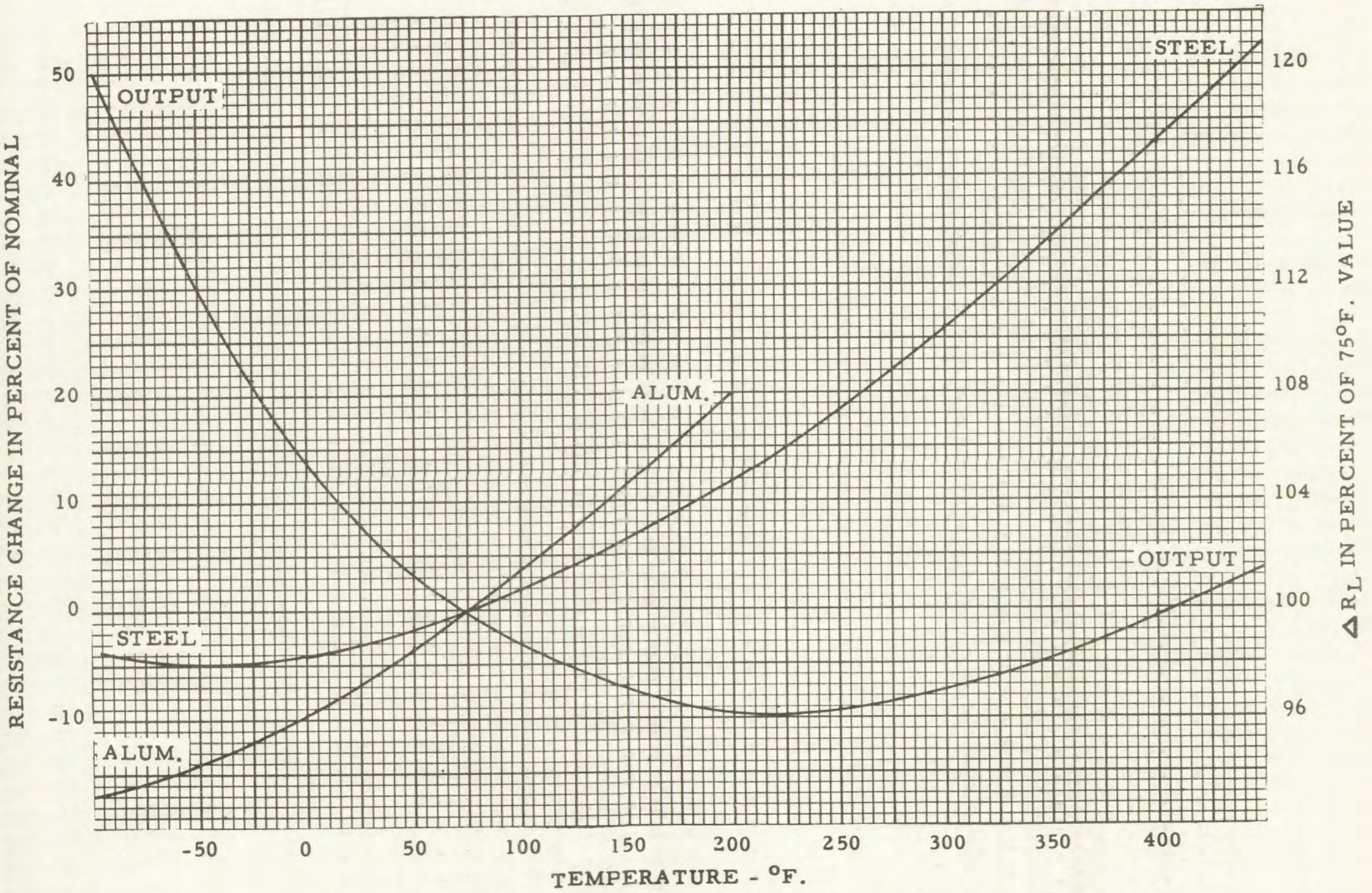

Figure 8. Typical Temperature Characteristics

indicator bridge circuit. This may be done either with one active and one dummy gage or with two active gages in the same manner that wire gages are temperature-compensated. With two active temperature-compensating gages, Strainistor claims a departure from linearity over the entire usable range of 2000 μ in/in of 2 percent. In contrast, the departure with one active gage over the same range is 10 percent.

The thermal behavior and linearity were not particularly important considerations in selection of a gage for the straining-frame calibration because temperature compensation with two active gages was to be employed. The final calibration was to be carried out in a $\pm 1^{\circ}$F temperature-controlled room, and the maximum measured strain was to be only 100 μ in/in or about 5 percent of the rated maximum for the gages. Stability, however, was a major consideration. A 1-month stability test was run on BTL germanium gages, using two A-18 SR-4 wire gages for comparison (see Figure 9). Both types were bonded with Armstrong's C-4 epoxy cement. A Baldwin-Lima-Hamilton SR-4 Type N strain indicator was used. The test was made under the following controlled conditions: (1) temperature was controlled within $\pm 1^{\circ}$F; (2) test was run under a cover to protect gages from thermal radiation and heat currents; (3) a set testing cycle was used; (4) gages were mounted in temperature-compensating pairs; (5) gages were lightly strained to 42 μ in/in for the entire time; (6) gage readings were taken, then the gage positions in the bridge were reversed, new readings made, and the average of these two readings was used to reduce indicator drifts to a minimum; and (7) readings were taken twice daily 5 days per week.

The strain-indicator gage factor selector was set at 1.8 for both gages. This meant that the germanium gages should have been $\frac{67.3}{1.8} \approx 37$ times more responsive to cold flow of the epoxy bonding material than the SR-4's. As the curves show, the two types of gages showed approximately the same apparent drift tendencies and even about the same statistical variation. Thus, it must be concluded that the indicator drift was by far the major source of instability and that, on the basis of this test, one would have to say that the germanium gages were at least as stable as the SR-4's. Apparently, indicator drift would be more of a problem in calibration than gage draft.

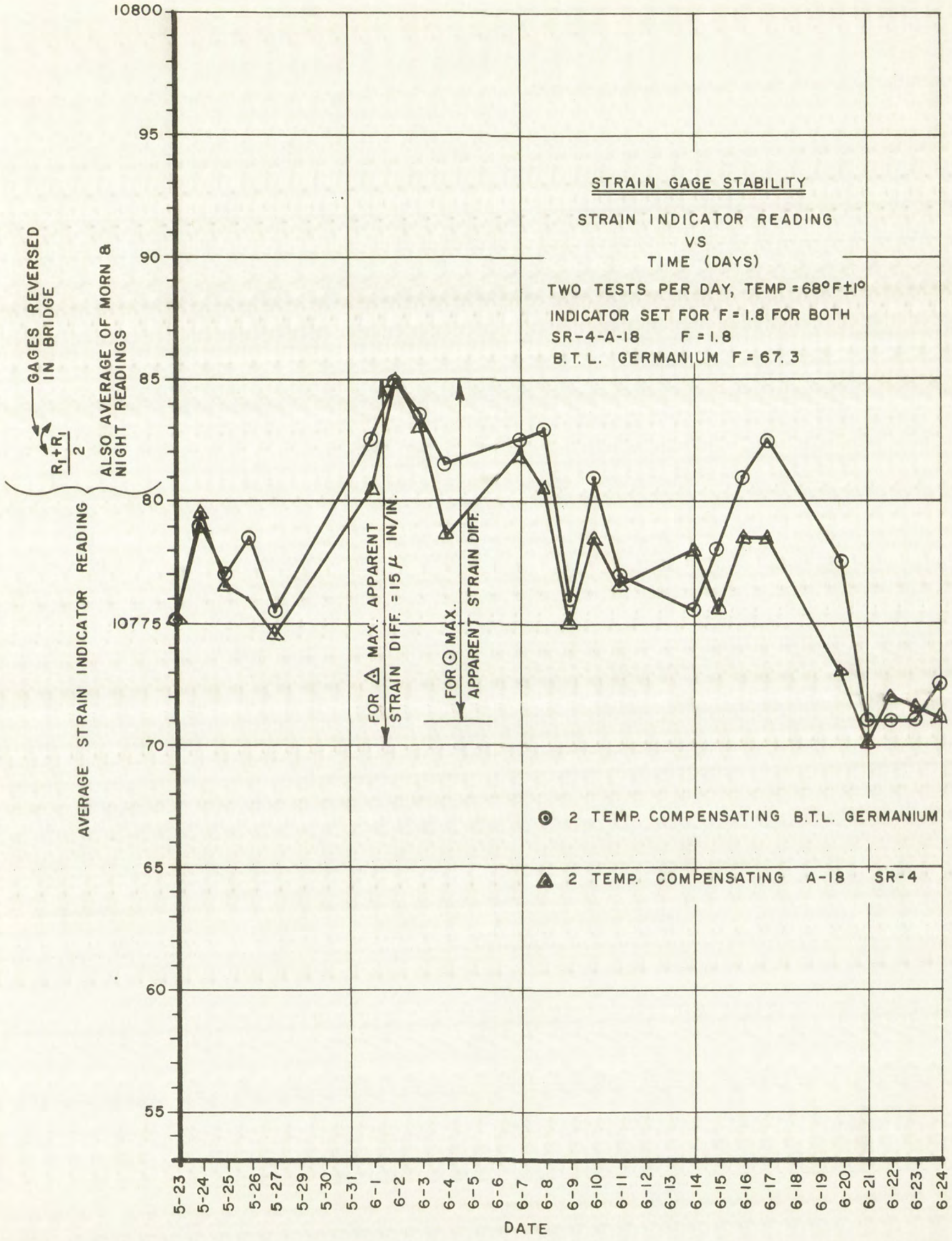

Figure 9. Strain Gage Stability with Time

Mounting Considerations

The natural location for gages to calibrate the straining frame would be at the center of a dummy shaft (identical to the seismometer guide rod). The best combination of temperature compensation and sensitivity would be realized with gages mounted at the top and bottom of the shaft in positions to measure the maximum tensile and compressive strains, and connected in adjacent legs of the indicator bridge.[10] Thus, the gage selection should be made on the basis of the best gage for mounting parallel to the longitudinal axis of a 7/16-inch-diameter dummy shaft.

A comparison of shape, sensitivity, and availability of information showed the Strainistor Model 711 to be the best choice for the calibration even though it was harder to handle and position than the Kulite DA-101. In addition, the Kulite gage was too wide for convenient mounting to the shaft. See Figure 10a for a picture of the Strainistor in the holding bracket with which it comes.

Special Problems

Mounting and testing the strainistor gages presented special problems. Baldwin-Lima-Hamilton EPY-150 epoxy cement was chosen for the bonding agent because it is convenient to use (it comes in a two-chambered plastic tube; mixing of the two ingredients is done inside the tube) and has been especially developed for strain-gage work. First, two sets of gage locating lines were carefully scribed into the shaft at diametrically opposite locations. When the surface was slightly roughened with 320-grit emery paper and thoroughly cleaned with acetone, a coat of EPY-150, about 0.003 inch thick, was brushed on the mounting areas and allowed to cure. A positioning jig was made using a V-block for holding and centering the shaft and a rectangular guide hole (which just fit the Strainistor holder) to act as a guide for the gage. Next, a liberal coat of EPY-150 was brushed on the gage area and the gage positioned with the aid of the jig. The gage holder was left to supply the needed bonding pressure. Once the epoxy had cured, the holder was removed and a thin additional layer of epoxy applied over the top of the gage element. Next, the leads were soldered to the end tabs. Extreme care was needed to avoid loosening the epoxy bond during soldering

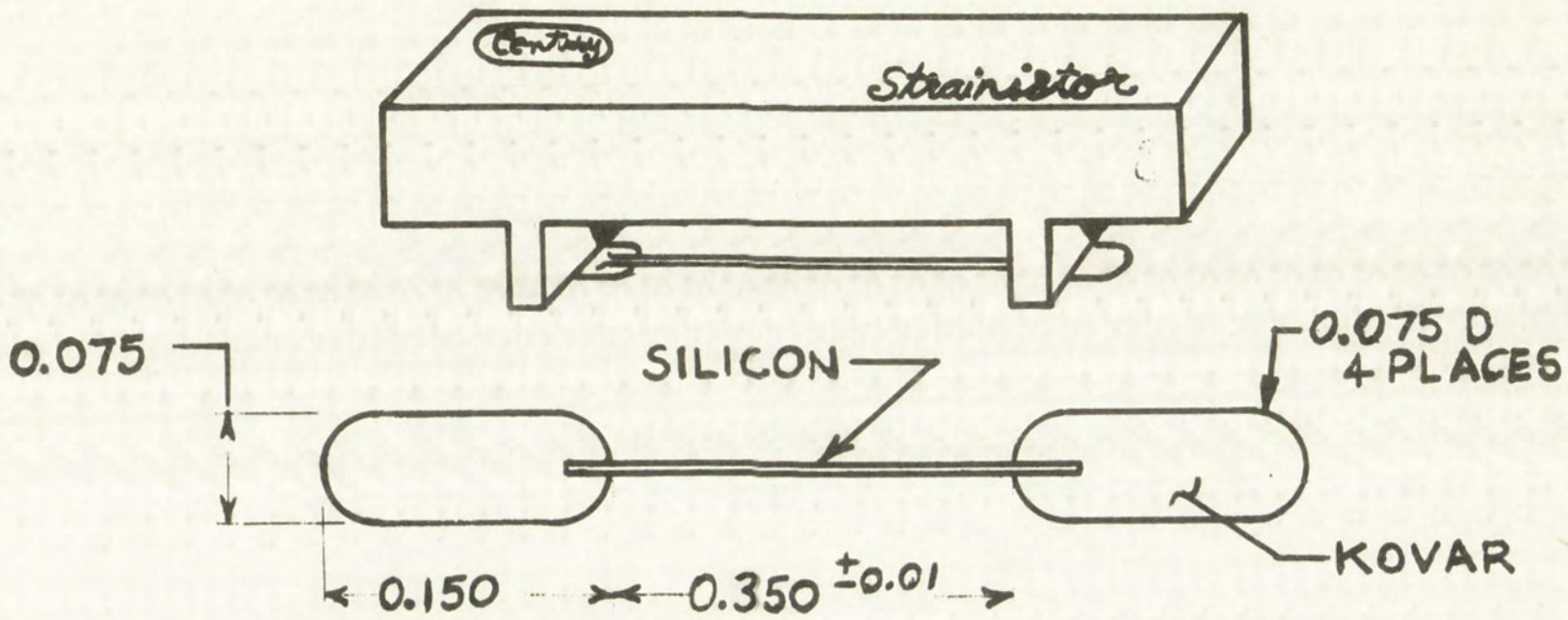

Figure 10(a). Model 711 Strainistor Gage in Handling Frame

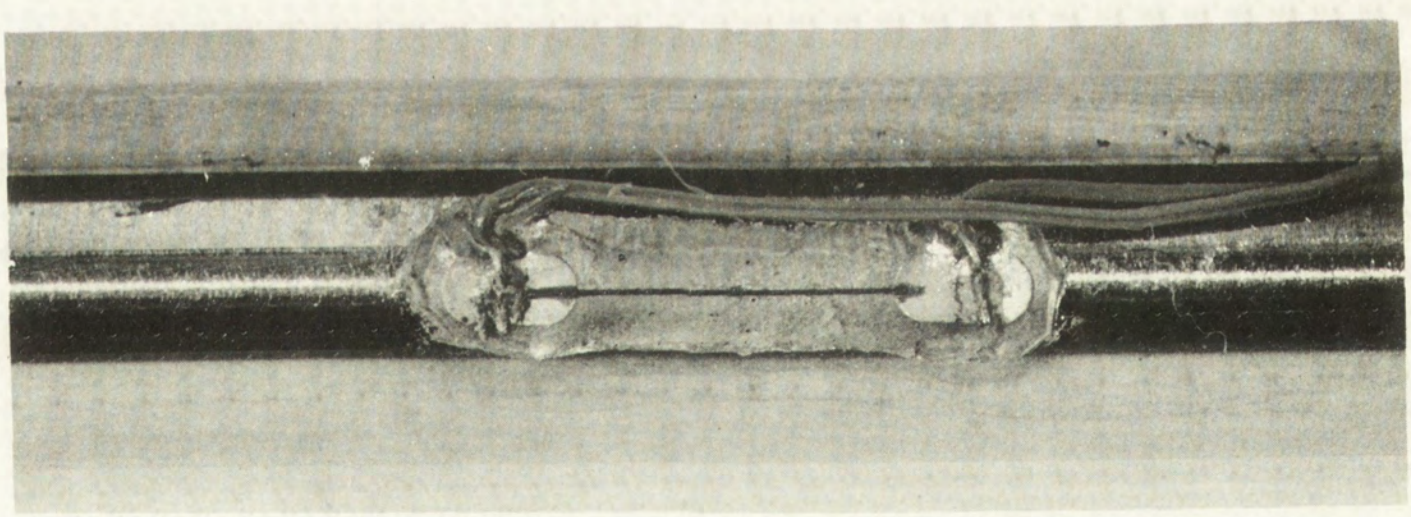

Figure 10(b). Mounted Semiconductor Resistance Strain Gage

(one gage was ruined in learning how to do this). A 7-watt iron, 230°F solder, and rapid soldering were needed. See Figure 10b for a photo of the final mounted gages.

Once the gages were mounted, new problems were encountered. Due to their extreme sensitivity, strain indicator drift became important and allowance for drift had to be made by setting up an exactly timed testing rhythm and then correcting on the basis of the rate of drift determined by the error in closure after the test. The mounted gages were very well temperature-compensated and indicated very little change in strain (only 1 or 2 μ in/in) when one end of the dummy shaft was touched with a soldering iron. The slightest unbalance in the radiant energy reaching the two gages gave very large indicated strain variations, and it was found necessary to carry on the final calibration with a black box completely surrounding the shaft and gages (see Figure 11).[9] Even with the radiation shield in place, large indicator-needle fluctuations were obtained by moving the lead wires or by the presence of any part of the operator's body in the vicinity of the gages, leads, or indicator. This effect was attributed to electrical capacitance changes. The leads were firmly taped and the indicator placed several feet away from the straining frame to minimize these variations. Even then the final readings had to be taken with the operator's hands at least 1 foot away from the indicator.

Another problem, which would not have appeared with regular gages, was encountered with these gages. The small movements of the extremely rigid straining fixture about the test-bench surface, which occurred during setting changes, gave variations in indicated strain. The fixture was firmly clamped to the bench to eliminate this problem. Once these sources of error were recognized and the proper precautions were employed, no great trouble in stability of readings was encountered. With indicator drift correction and only small changes in setting, the frame dial would repeat strain settings as shown on the indicator to about 3×10^{-8} in/in rms (as determined from 30 readings). On the basis of 30 carefully controlled readings, a straining-frame hysteresis between the settings of 610, 600, and 590 showed that an average of 6.9×10^{-8} in/in hysteresis occurred in the

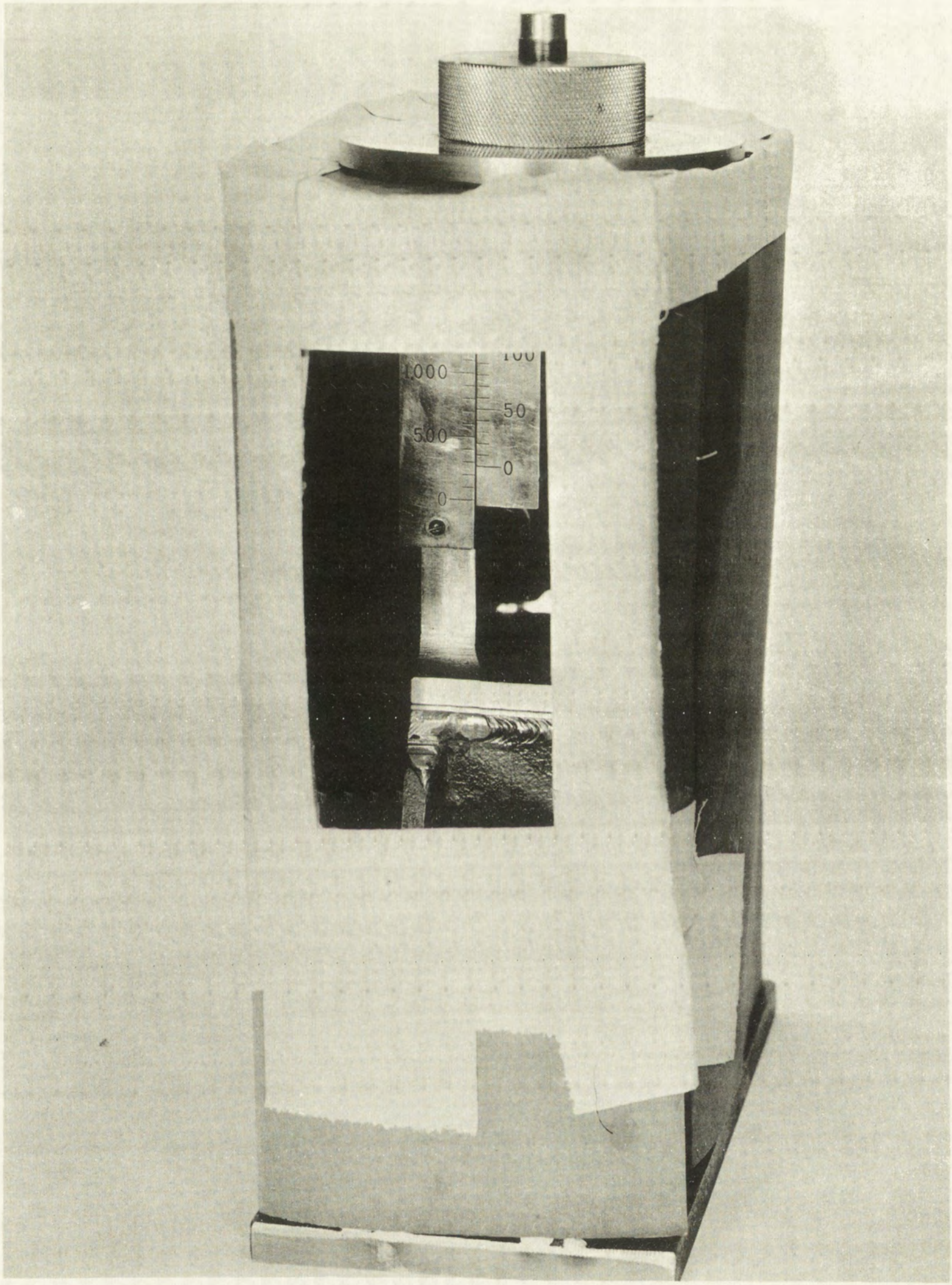

Figure 11. Straining Frame and Radiation Shielding

straining frame between an increase in setting of 10 and a decrease in setting of 10. Also, during this test, the rms variation about the mean for increasing settings was 2.18×10^{-8} in/in and 4.12×10^{-8} in/in for decreasing settings. This suggests that final settings should always be made in the direction of increasing settings.

Straining-Frame Calibration

The work of straining-frame calibration consisted of four phases: (1) spring constant determination, (2) obtaining indicated strain versus setting, (3) gage-factor determination, and (4) the final calibration for period of vibration versus setting, based upon both experimental data and flexure theory.

Spring-Constant Determination

The spring constant for the straining-frame spring was determined by measuring the spring length inside the end hooks for different static loads. See Figure 12 for a plot of these data. Although the spring was not intended to have a preload force (bottomed coils), the actual spring turned out to have a 7-pound preload force. This would not be desirable for the final 200-second seismometer, but would be all right for developmental work up to 100 seconds. Thus, a spring with a 7-pound preload and a spring constant (as determined from Figure 12) of 121.3 lb/in was used.

Indicated Strain Versus Setting

The dummy shaft equipped with two centrally mounted semiconductor strain gages was centered in the straining frame. All of the previously mentioned precautions (such as using radiation shielding, taping leads, etc.) were taken to insure the best possible data. The gage factor selector on the strain indicator was set for a gage factor of 2 because the correct gage factor was not yet known and would be much larger than the maximum selector setting. A complete set of readings, from a maximum straining-frame setting of 800 down to 250 in increments of 50 and then down to the minimum load setting of 141.3 in increments of 10, was made. Then the same

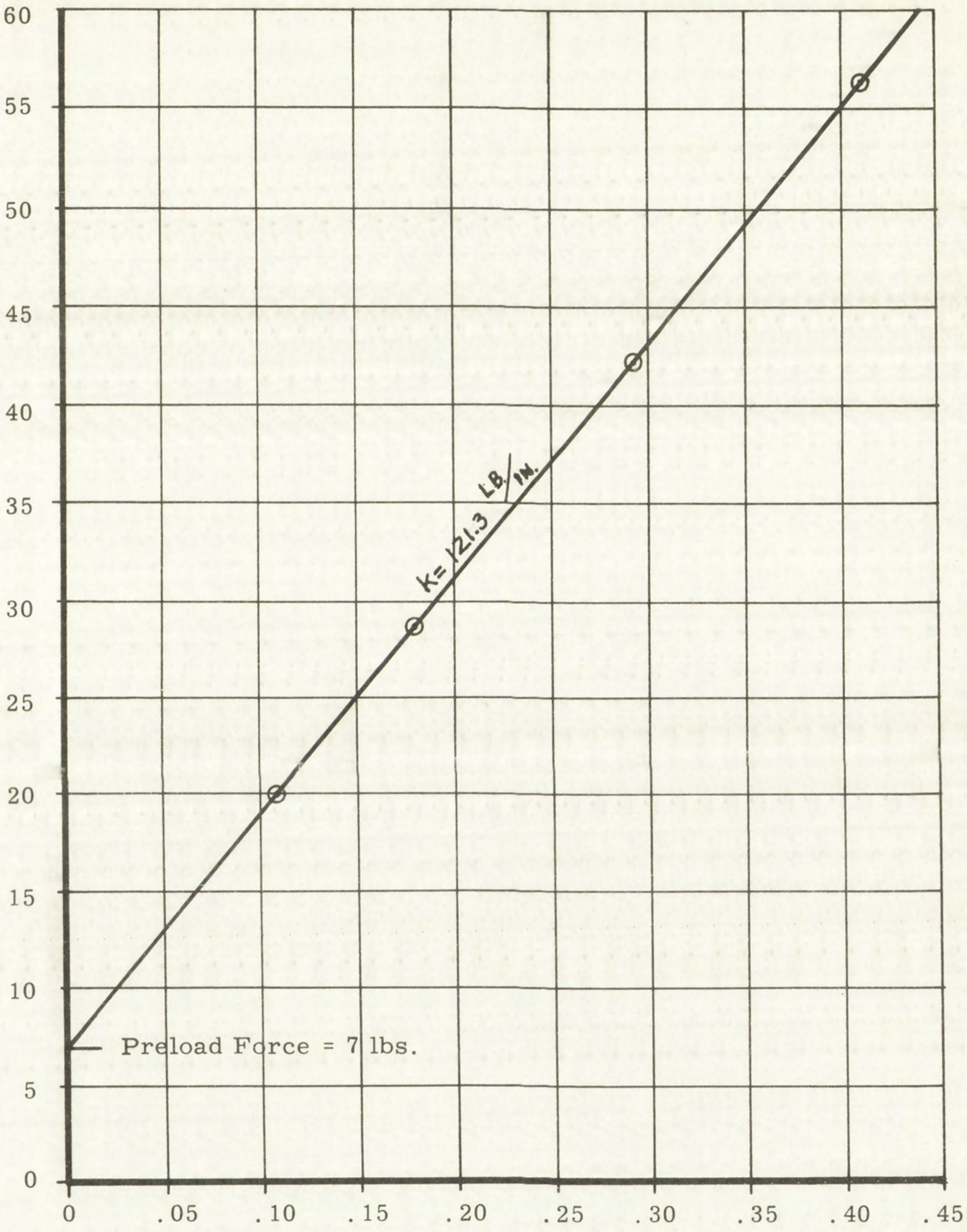

Figure 12. Straining-Frame Spring Force Versus Deflection

procedure was reversed until the 800 setting was again reached. After each new setting, the indicator knob was moved as quickly as possible to null the indicator and maintained as closely as possible to null for exactly 30 seconds before taking the reading. Figure 13 shows this run and the resulting indicator drift. The average of the two readings for each setting is plotted as the heavy solid line. Note that the strain curve departs abruptly from the linear spring portion for settings below about 170. This is because of the effect of the straining-frame weight and the preload spring force. Insufficient detail is available from this curve because of the wide point spacing in the critical region of settings below 170. Another run was made to better define the region of greatest interest, 250 to 140. Here, a more accurate method of drift correction was used. At each straining-frame setting, a reading was taken after 30 seconds at null as before, then the tension on the straining frame was reduced to the minimum value and the indicated strain at this setting was recorded after 30 seconds at null. Then the tension was readjusted to the initial reading and the strain reading taken after 30 seconds at null. For each run, the average difference in indicated strain between the two identical settings and the zero or minimum indicated strain was used as the corrected measured strain. This procedure was duplicated for all points from 250 to 170 in increments of 10, from 170 to 150 in increments of 5, and from 150 to 140 in increments of 1. See Figure 14 for a plot of these data. For both Figure 13 and Figure 14, the theoretical frame setting for the intercept of the asymptote for values greater than 170 with the zero indicated strain axis, was 98, showing that the two methods gave the same results. The theoretical zero strain setting for a perfectly linear spring with no preload and a weightless shaft and straining frame was 107. The actual minimum strain setting occurred at 140 because of the spring preload, straining-frame weight, and shaft weight. Note that, below a setting of 142.5, the shaft became bowed in the opposite direction due to the weight of the straining frame.

Gage-Factor Determination

The average gage factor for the two calibrating gages was determined by a combination of theory and experimental data. The spring constant was

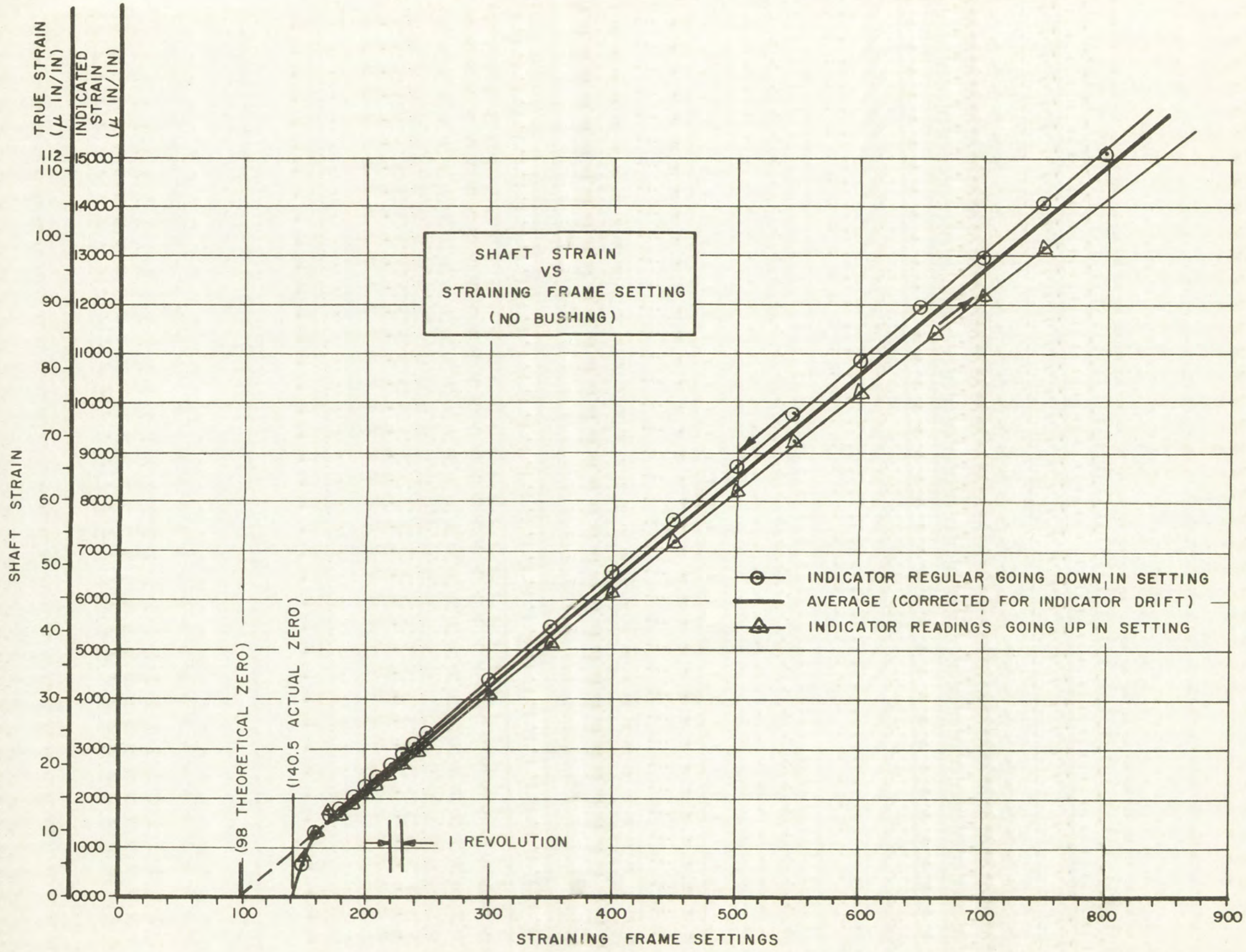

Figure 13. Shaft Strain Versus Straining-Frame Setting (140-800)

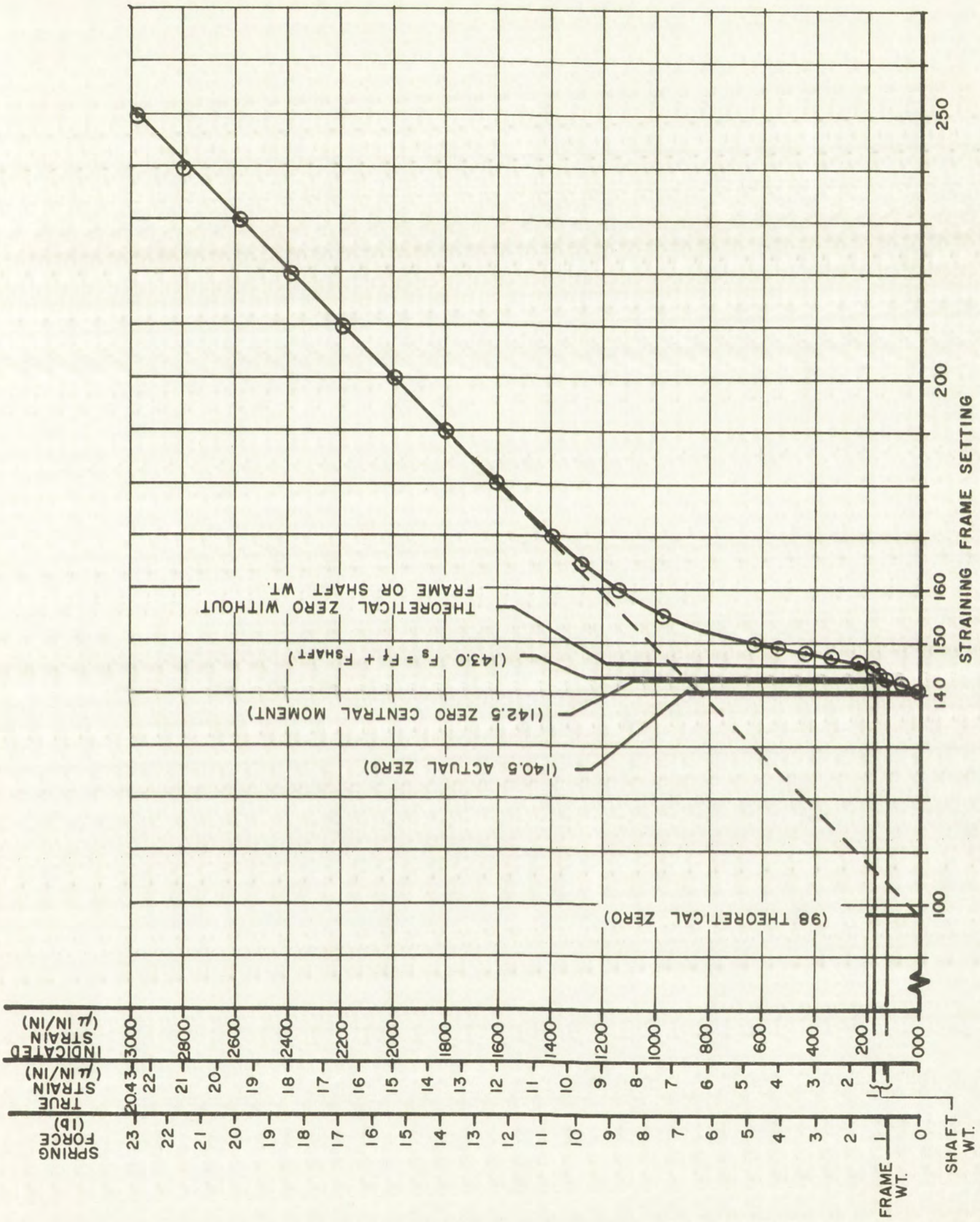

Figure 14. Shaft Strain Versus Straining-Frame Setting (140-250)

already found to be 121.3 lb/in. The straining-frame setting knob was equipped with an 80-pitch thread which has a lead of 0.0125 inch per revolution; therefore, the change in spring force per revolution is

$$\Delta F/\text{rev} = 0.0125\ k = 0.0125 \times 121.3 = 1.51625 \text{ lb/rev.}$$

The maximum stress in a flexural member is

$$S = \frac{My}{I} = \frac{M}{Z},$$

where

y = the distance from the neutral axis to the fiber = r in the case of a round rod,

Z = the section modulus

$$= \frac{\pi r^3}{4} = \frac{\pi(0.21875)^3}{4} = 8.17 \times 10^{-3} \text{ in}^3.$$

The moment, M, in the constant-moment section is

$$M = \frac{F}{2} \times 0.5 = 0.25\ F.$$

Equating this M to the M derived from the stress formula yields

$$0.25\ F = ZS = 8.17 \times 10^{-3} S$$

or

$$S = 30.60\ F.$$

But stress is proportional to strain; hence,

$$S = 30.60\ F = E\epsilon,$$

from which

$$\epsilon = \frac{30.60\ F}{E}.$$

Thus, the actual change in strain per revolution of the straining knob is

$$\epsilon/\text{rev} = \frac{30.60}{E} \times \frac{F}{\text{rev}} = \frac{30.60 \times 1.51625}{30 \times 10^6} = 1.548\ \mu \text{ in/in/rev},$$

but the indicated strain per revolution as determined from the upper part of the curve in Figure 14 was found to be 207 μ in/in/rev. Therefore, the conversion factor for changing from measured strain to true strain (with the indicator gage selector set at 2.00) would be the ratio

$$\frac{1.548}{207} = 7.48 \times 10^{-3}.$$

The average gage factor, $\frac{\Delta R/R}{\epsilon}$, for the two strainistor calibrating gages is

$$\frac{\Delta R/R}{\epsilon} = \frac{1}{7.48 \times 10^{-3}} = \frac{\text{Number of active gages}}{\text{indicator gage factor setting}} = \frac{1}{7.48 \times 10^{-3}} \times \frac{2}{2} = 133.7$$

This value is within the range 120 to 140, specified by the manufacturer. The conversion factor was used to add a true strain scale to Figures 13 and 14.

Final Calibration

The final calibration of the straining frame, in terms of period of vibration versus setting, had to account for the shaft deflections due to straining-frame loading, shaft weight, and bushing load. Also, the effective length of the suspended air-bearing bushing had to be included. The various deflections could be calculated separately and then added to obtain the resultant by making use of the principle of superposition. Calculations of the first two deflections are straightforward, but the way the bushing load is applied from a spinning bushing 1.56 inches long to a curved shaft through an air film is not readily subject to analysis. The three accompanying Figures 15a, 15b, and 15c, show in a qualitative way what is known about the distribution of pressure in straight-sleeve hydrodynamic gas bearings.[11][12]

The effect of a slightly downward bow in the shaft should be to change the axial pressure distribution as shown by the dotted lines in Figure 15c. Either the straight-shaft axial pressure distribution or the estimated distribution for the curved shaft would be fairly well approximated by two equal vertical forces (each equal to one-half the bushing weight) located halfway

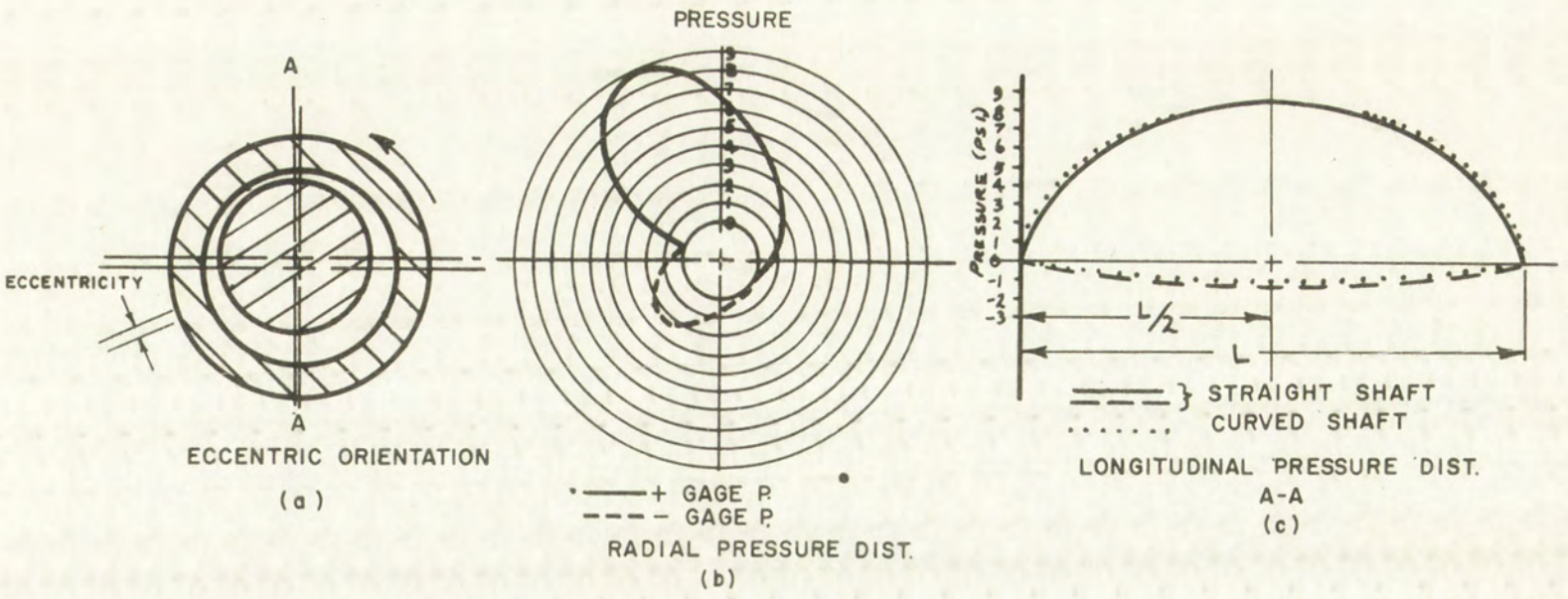

Figure 15. Qualitative Hydrodynamic Gas-Bearing Information

between the bushing center (shaft center) and the ends of the bushing. The effect of this simplified loading would be easy to calculate, since the seismic bushing normally makes very short axial excursions (a maximum of about 0.010 inch) about the shaft centerline; therefore, it will be assumed to be located at the center and stationary.

The three loading conditions to be superimposed are shown schematically below.

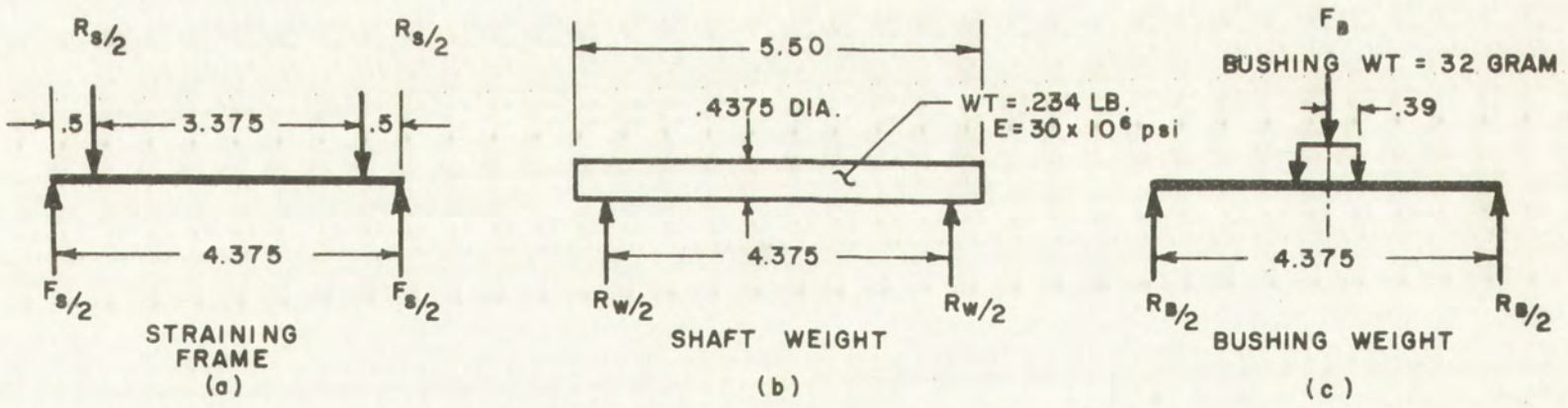

Figure 16. Loading Conditions

Strains due to the first two loadings (shown in Figures 16a and 16b) are automatically included in the setting versus strain plots (shown in Figures 16a and 16b) for the position of the gages. The effect of bushing weight must be added to predict the true strain or central moment for the final seismometer shaft. The bending moment or curvature of the central 2 inches of the shaft is constant due to the condition shown in Figure 16a, is not constant due to the condition shown in Figure 16b, and is constant inside the central 0.78 inch but not constant outside this region for Figure 16c. If the shaft curvatures at the two resultant bushing load points shown in Figure 16c (0.39 inch from centerline) are assumed to be controlling the period of vibration, it is reasonable to use the resultant moment at these locations as the criterion for period. The period will be calculated on this assumption and the additional assumption that this resultant moment is constant for small displacements. In truth, the resultant moment will be higher inside the 0.39-inch point and lower outside, but this average value is assumed for simplicity. The problem, then, is to convert the measured central strains into corrected resultant moments at the 0.39-inch load points. Referring to Figure 17, the moment due to the straining frame at position 3 is

$$M_{3F_S} = \frac{d}{2}\left(F_S - F_f\right) = \frac{0.5}{2}\left(F_S - 0.978\right) = 0.25\ F_S - 0.2445\ \text{in/lb.}$$

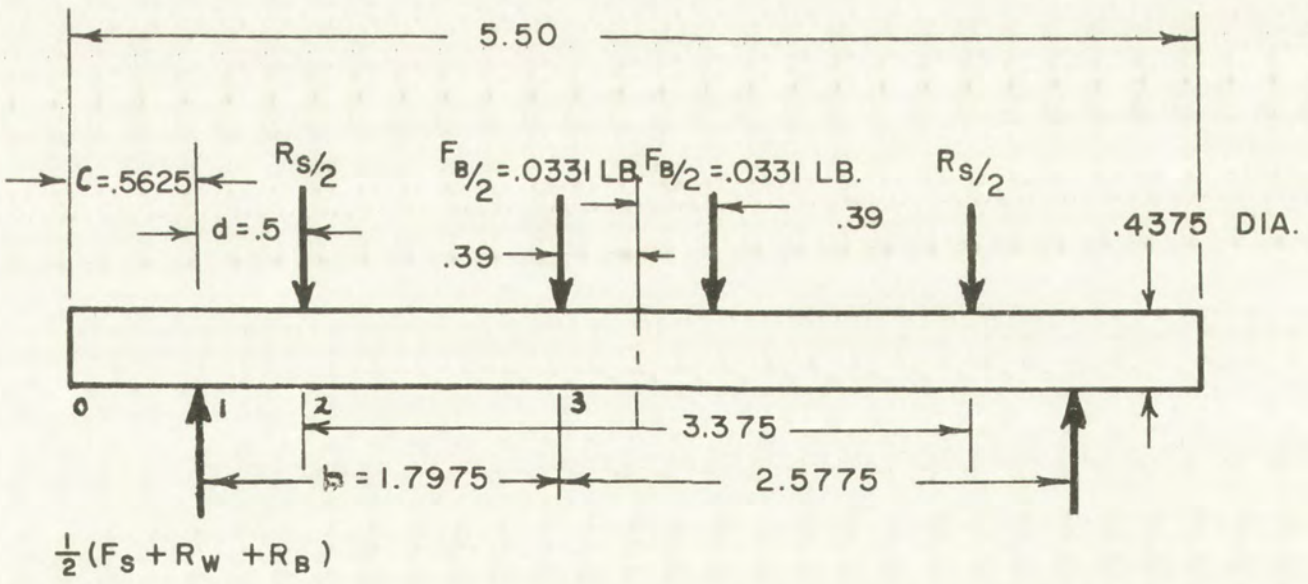

Figure 17. Combined Loading

The moment at 3 due to shaft weight is

$$M_{3W_S} = \frac{W_S b}{2}\left(1 - \frac{c}{b} - \frac{b}{\ell}\right) = \frac{0.234 \times 1.798}{2}\left(1 - \frac{0.5625}{1.798} - \frac{1.798}{5.5}\right) = 0.0758 \text{ in-lb.}$$

The moment at 3 due to bushing weight is

$$M_{3W_B} = \frac{W_B}{2} \times b = 0.0331 \times 1.798 = 0.0596 \text{ in-lb.}$$

Therefore, the resultant effective moment at 3 is

$$M_{3\text{Resultant}} = M_{3F_S} + M_{3W_S} + M_{3W_B} = 0.25\, F_S - 0.2445 + 0.0758$$

$$+ 0.0596 = 0.25\, F_S - 0.1091.$$

The period versus central deflection or moment for a constant-moment section will now be calculated. For a gravity pendulum, the period of vibration is given by the formula

$$T = 2\pi\sqrt{\frac{R_c}{g}}$$

where

R_c = the length of the pendulum arm or radius of curvature in the present case.

The central deflection in a constant-moment section is given by the formula

$$\delta_{max} = \frac{Fd\ell^2}{2 \times 8EI} = \frac{F \times 0.5 \times (3.375)^2}{2 \times 8 \times 1.8 \times 10^{-3} \times 30 \times 10^6}$$

$$= 6.59771 \times 10^{-6} F$$

Referring to Figure 18, it can be seen that

$$\tan\theta = \frac{\delta}{1.6875} \approx \sin\theta = \frac{1.6875}{R_c}$$

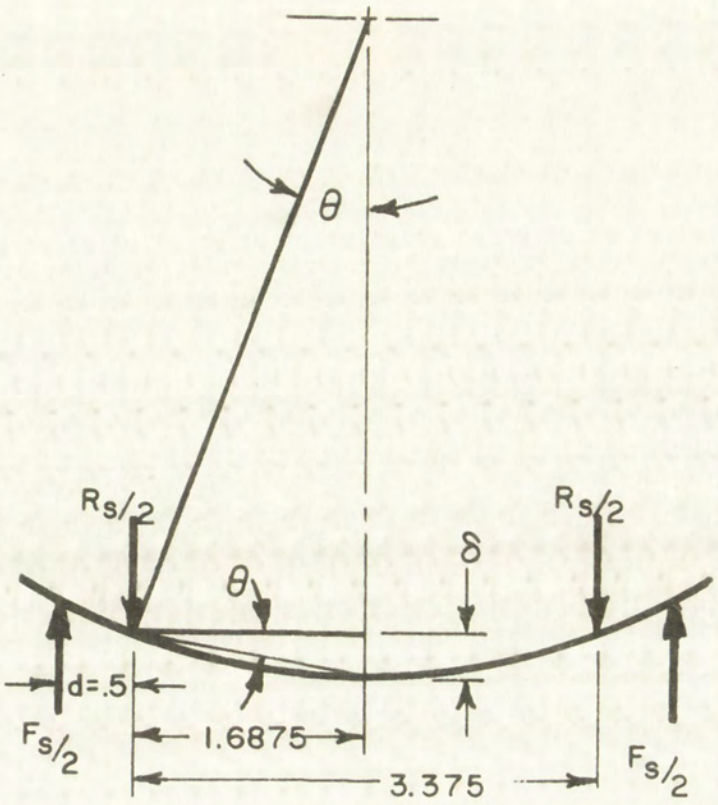

Figure 18. Central Deflection for Given Radius of Curvature

and that, therefore,

$$R_c \approx \frac{(1.6875)^2}{\delta} = \frac{2.84766}{\delta} \text{ in.}$$

Thus, the theoretical period for the constant-moment section is

$$T_{\text{theoretical}} = \frac{2\pi}{\sqrt{g}} \sqrt{R_c} = 0.319\sqrt{R_c}$$

or

$$= 0.319\sqrt{\frac{2.84766}{\delta}} = 0.538\sqrt{\frac{1}{\delta}} \text{ sec.}$$

See Figure 19 for the data reduction and conversion of indicated strain measurements to final period data. Figure 20 shows the final calibration of period of vibration versus setting.

(1)	(2)	(3)	(4)	(5)	(6)	(7)	(8)	(9)
Straining Frame Setting	Change in Setting Measured from Theoretical Zero (98)	Spring Deflection (in.)	Spring Force, F_S (lb)	True Moment for Period, M_T (in-lb)	Central Deflection, S_T (x 10^{-6} in.)	Radius of Curvature, R_C (x 10^{-6} in.)	$\sqrt{R_C}$ (x $10^{3/2}$ in.)	True Period, T (sec)
	Correction made from Figure 14 for all Straining-Frame Settings in (1) less than 190	Column (2) x 0.00125	F_S = (3) x k (k = spring const. 121.3 (lb/in)	$M_T = 0.25F_S - 0.1091$ $= 0.25 \times (4) \times 0.1091$	$\delta_T = \frac{M_T l^2}{16EI}$ $= 26.35 M_T \times 10^{-6}$ Central def. for a constant moment of M_T	$R_C = (\frac{l}{2})^2 \times \frac{1}{\delta_T}$ $= \frac{2.84766}{\delta}$		$T = 2\pi\sqrt{\frac{R_C}{G}} = 0.319\sqrt{R_C}$
810.00	712.0	0.8900	108.0	26.89	708	4.02	63.5	20.25
800.00	702.0	0.8775	106.5	26.51	698	4.08	64.0	20.4
750.00	652.0	0.8150	98.9	24.52	645	4.42	66.5	21.2
700.00	602.0	0.7530	91.4	23.49	619	4.60	67.9	21.6
650.00	552.0	0.6905	83.8	20.84	550	5.18	72.0	23.0
600.00	502.0	0.6280	76.2	18.93	499	5.71	75.6	24.1
550.00	452.0	0.5655	68.7	17.07	450	6.33	79.7	25.4
500.00	402.0	0.5030	61.1	15.17	399	7.15	84.6	27.0
450.00	352.0	0.4400	53.4	13.22	348	8.19	90.6	28.9
400.00	302.0	0.3775	45.8	11.33	299	9.53	97.8	31.2
350.00	252.0	0.3150	38.25	9.45	249	11.4	106.8	34.1
300.00	202.0	0.2525	30.65	7.55	199	14.3	119.6	38.2
250.00	152.0	0.1900	23.05	5.65	149	19.1	138.3	44.2
240.00	142.0	0.1775	21.55	5.28	139	20.4	143.0	45.7
230.00	132.0	0.1650	20.02	4.89	129	22.1	148.8	47.5
220.00	122.0	0.1525	18.50	4.52	119	23.9	154.7	49.4
210.00	112.0	0.1400	17.00	3.14	109	26.1	161.7	51.6
200.00	102.0	0.1276	15.48	3.76	99.2	28.7	169.7	54.1
190.00	92.0	0.1150	13.97	3.38	89.2	31.9	178.8	57.1
180.00	81.5	0.1019	12.38	2.99	78.8	36.1	190.2	60.7
170.00	71.0	0.0888	10.78	2.59	68.2	41.8	204.5	65.3
160.00	57.5	0.0719	8.72	2.07	54.6	52.1	228.5	73.0
150.00	32.0	0.0400	4.86	1.11	29.2	97.5	313.0	100.0
149.00	27.5	0.0344	4.17	0.937	24.7	115.2	340.0	108.5
148.00	23.0	0.0288	3.49	0.767	20.2	141.0	376.0	120.0
147.00	14.0	0.0175	2.123	0.425	11.2	254	505	161.0
146.00	11.5	0.0144	1.748	0.331	8.72	327	573	182.8
145.00	9.0	0.0112	1.360	0.234	6.16	462	681	217
144.00	8.0	0.0100	1.213	0.1975	5.20	548	741	236
143.00	7.5	0.00937	1.150	0.182	4.79	595	773	247
142.00	3.7	0.00462	0.561	0.0343	0.904	3150	1780	568
141.00	0.5	0.000675	0.759	-0.0870		-	-	-
140.50	0.0	0.00000	0.0000	-0.106				

Figure 19. Final Straining-Frame Calibration Table

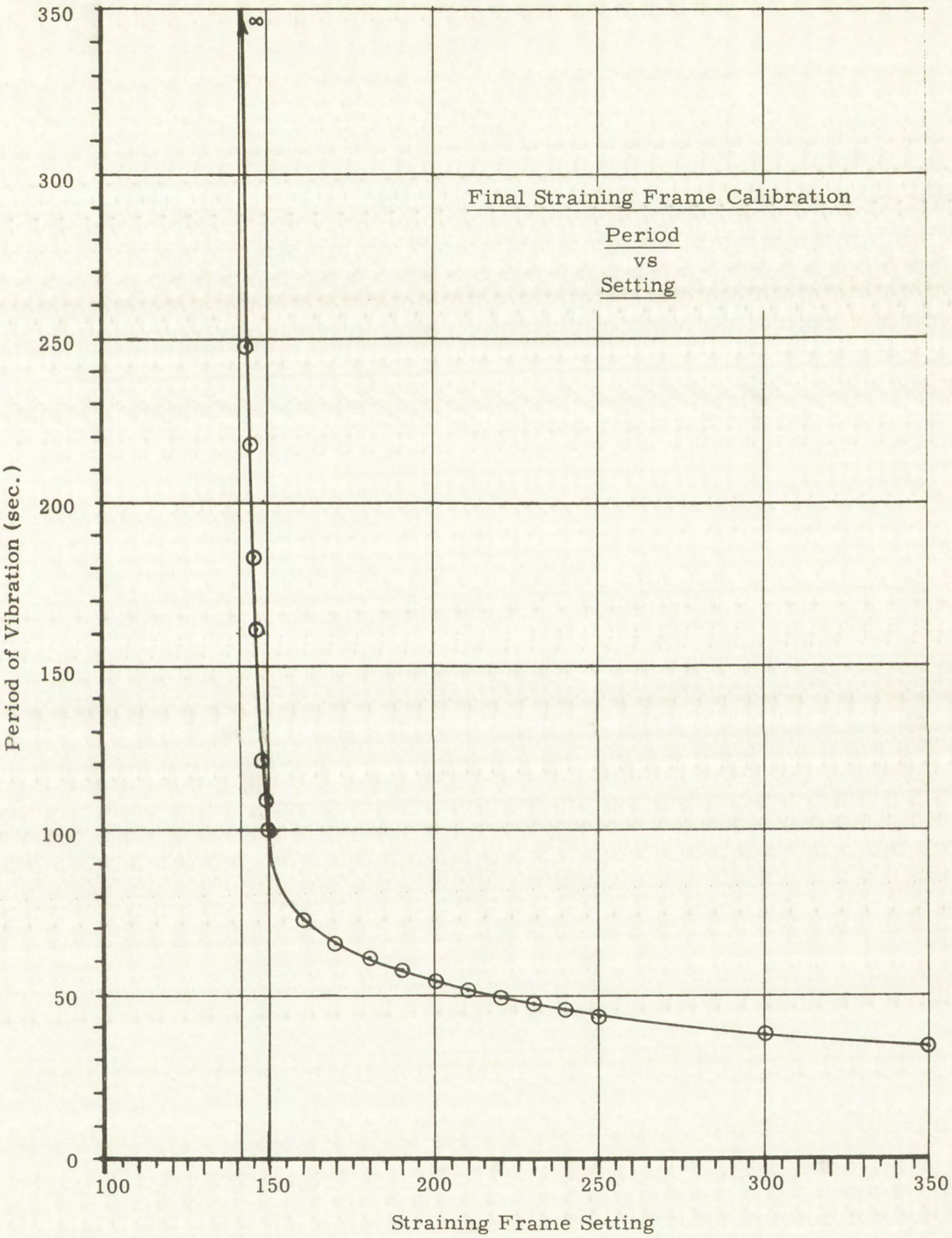

Figure 20. Theoretical Period Versus Straining-Frame Setting

Optical Interference Measurements

Semiconductor strain gages were ideal for the straining-frame calibration but would not be good for obtaining continuous plots because:

1. Finite gage length results in an average strain reading over the gage length (0.350 inch).
2. The large number of gages needed would drastically alter the elastic properties of the shaft if they were simultaneously mounted to the same shaft.
3. A large number of these gages would be too costly ($35 each).
4. There is insufficient room to mount enough gages (at least 20 would be needed in the center 2 inches of the shaft).

Optical interference methods, in addition to being inherently accurate, do not require contact with the shaft. Because most engineers have had little experience with interferometry, a brief description of the principle will be presented.

The Principle of Interferometry

There are many types of interferometers and usually each type is best suited for a particular job. The range of uses runs from measuring the surface flatness of gage blocks to the measuring of the optical diameters of distant stars. In all cases, however, an interference condition between two or more coherent light beams is utilized. Normally, monochromatic light from a single source is divided into two or more beams which are then superimposed after doing something to one or more of the beams. After the beams have been recombined, the intensity in the region of superposition is found to vary from point to point between maxima which exceed the sum of the intensities of the individual beams and minima which may be zero. There are two main methods of obtaining multiple beams from a single source:

1. Division of wave front, in which one beam passes through apertures placed side by side. This method requires the use of a point source to maintain coherency.

2. Division of amplitude, in which the beam is divided at one or more partially reflecting surfaces. Here, an extended source may be used and greater fringe contrast and intensity obtained.

The type of interferometer commonly used for comparing gage block lengths and measuring surface flatness is referred to as a Fizeau-type or gage-measuring interferometer. This was the only type available to the writer which had sufficient field of view for the shaft-measuring job. See Figure 21 for an optical schematic of a gage-measuring interferometer. In this type of interferometer, the interference pattern is the result of standing waves created in the region between the reference optical flat and the surface being investigated by multiple reflections of the light beam. This situation is shown, greatly exaggerated, in Figure 22.

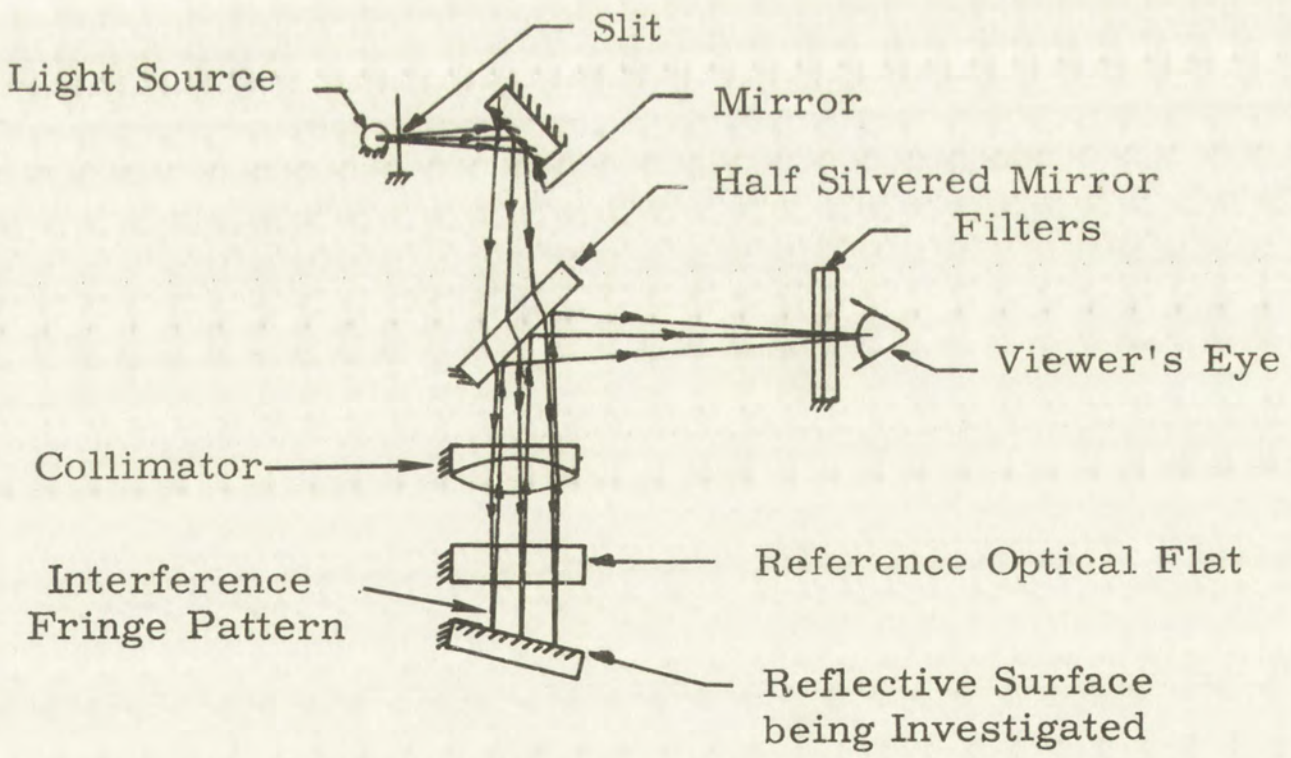

Figure 21. Gage-Measuring Interferometer

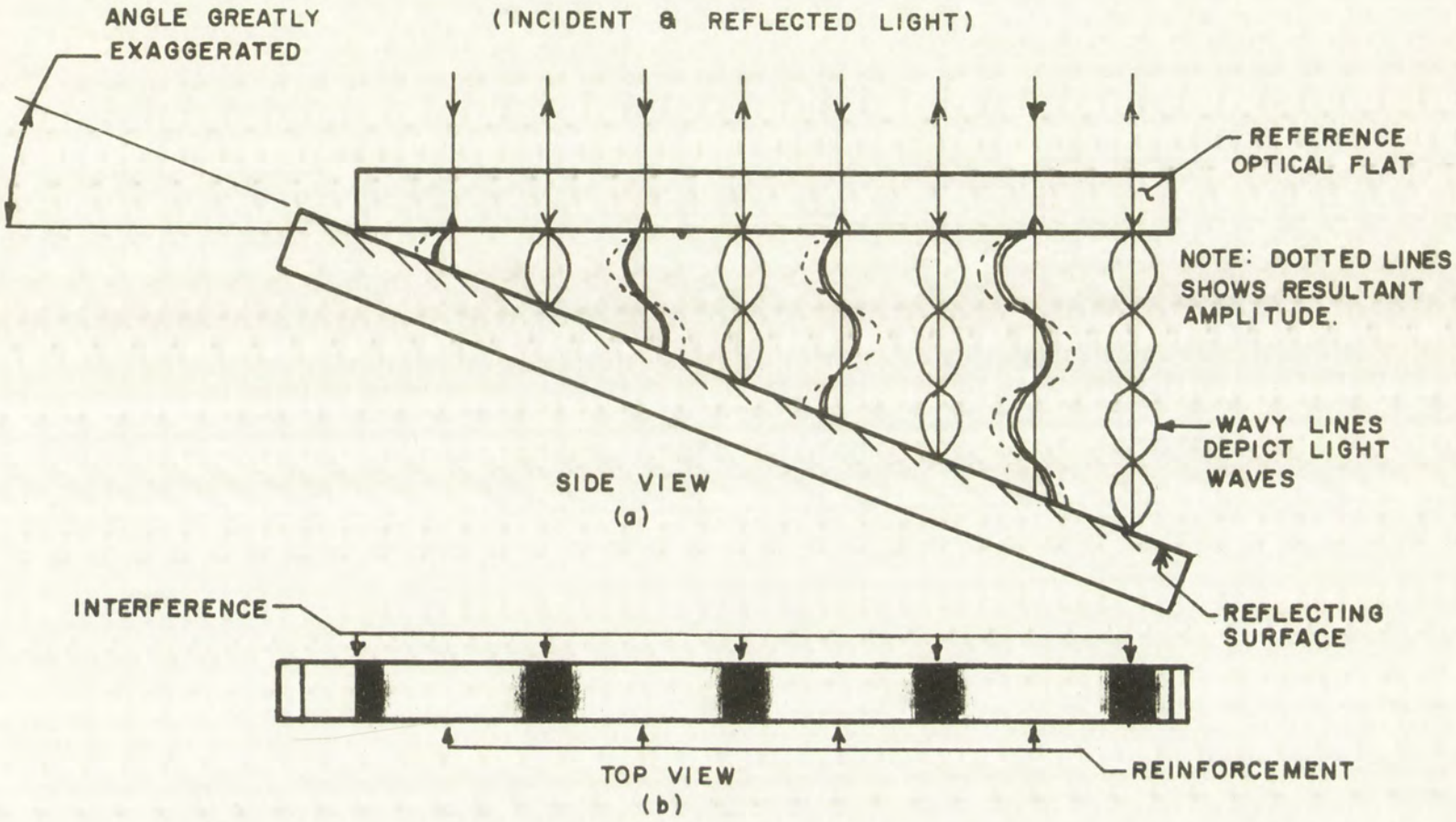

Figure 22. Standing-Wave Fringe Pattern

In this diagram, points 1, 3, 5, and 7 represent dark fringes or nodes. At all of these points, the resultant light-wave amplitude is zero; thus, there is complete dark. Points 2, 4, and 6 are antinodes or bands of maximum light intensity. Here, the resultant amplitude is seen to be greater than the amplitudes of the two reflected waves.[13]

Measuring Technique

The technique of measuring minute shaft curvatures with light interference patterns will also be explained with exaggerated diagrams. Assume that a reference optical flat is resting upon the curved surface to be measured, as shown in Figure 23, and that a monochromatic collimated light beam is impinging normal to the reference flat. A vertical scale and parallel horizontal lines depicting integral multiples of $\lambda/2$ have been superimposed on the figure. It can be seen that an interference fringe will occur at

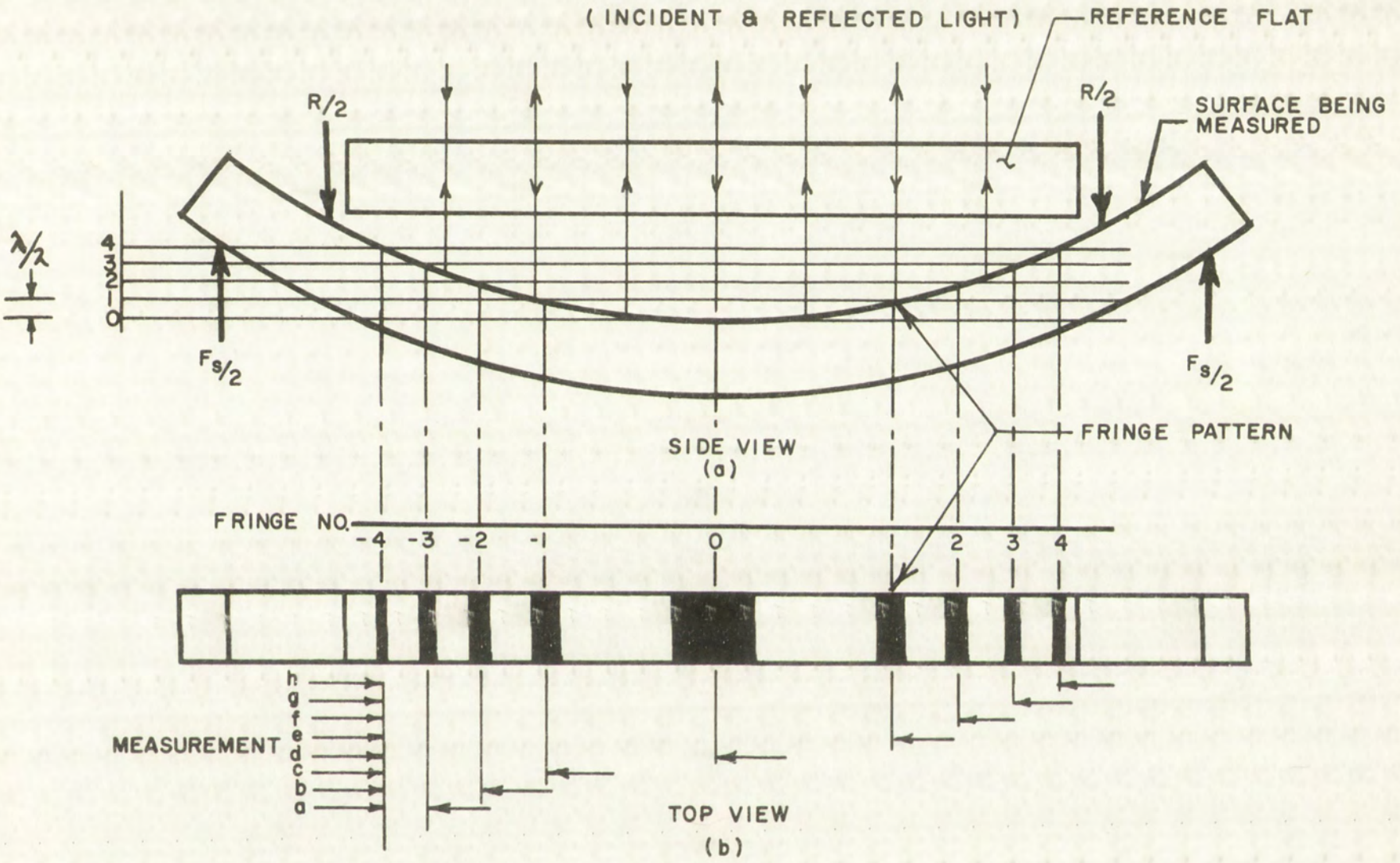

Figure 23. Measuring Curves with Interference Fringes

the intersections of the $\lambda/2$ lines with the curved surface. Figure 23b shows the top view of this hypothetical fringe pattern (in both views, 23a and 23b, only the centerline of the fringe has been drawn). It would be possible to measure the horizontal positions of the fringes in view 23b and then replot the shaft curvature to any vertical scale desired (to emphasize a minute curve, for instance), knowing that each successive fringe represents a change in vertical spacing of $\lambda/2$ of the measuring light. This measurement could be conveniently done from a photograph of the original fringe pattern. For small curvatures, only a very few fringes would appear in the arrangement shown in Figure 23a, and then it would be difficult to determine the exact centers of the fringes for measurement. Figure 24a-d shows an improved way of measuring small curvatures with the same apparatus.

Here, the curved surface is tilted so that the average fringe is narrow enough so that the center of the fringe can be easily and accurately determined. (The optimum width would usually be such that the fringes on the photograph were just slightly wider than the hairline of the measuring instrument.) In this case, the picture contains many more fringes than before, and each fringe may be more accurately located. The method of plotting will now be explained. Referring to Figure 24c, which shows the data-reduction process for the curve in Figure 24a, colum 2 is the measured horizontal position of the various fringes. Column 3 is the theoretical fringe order (not an integer) at the position shown in column 2, assuming a perfectly flat surface of the same average slope as the curved surface. (This theoretically flat surface is also shown in Figure 24a.) Column 4 is the vertical difference between the theoretical flat and the curve in fringes ($\lambda/2$) at each position shown in column 2. Figure 24d shows a plot of columns 2 and 4 with the column 4 scale greatly exaggerated.

Selection of Interferometer

In order to use the method of measurement outlined in the preceding section, several requirements had to be met:

1. The interferometer had to have at least a 2-inch field of view.
2. The interferometer had to have provisions for delicate

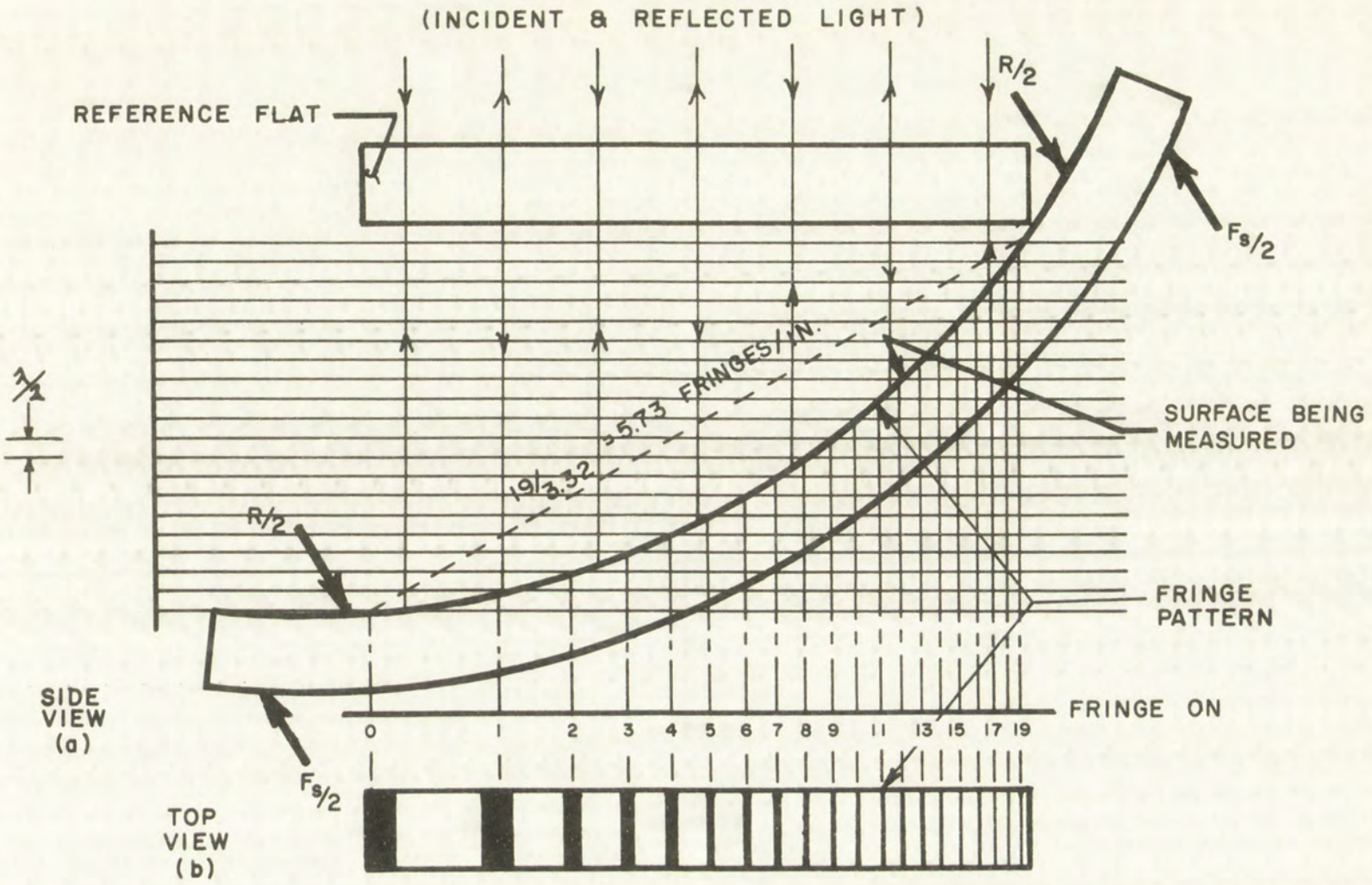

TABLE			
1 NO.	2 MEAS (IN)	3 THEOR	4 DIFF. (FRINGES)
0	0	0	0
1	.66	3.78	2.78
2	1.03	5.90	3.90
3	1.31	7.51	4.51
4	1.53	8.77	4.77
5	1.73	9.91	4.91
6	1.91	10.93	4.93
7	2.08	11.90	4.90
8	2.21	12.67	4.67
9	2.37	13.58	4.58
10	2.49	14.26	4.26
11	2.60	14.90	3.90
12	2.71	15.53	3.53
13	2.81	16.10	3.10
14	2.91	16.68	2.68
15	3.00	17.19	2.19
16	3.09	17.70	1.70
17	3.18	18.22	1.22
18	3.26	18.67	.67
19	3.32	19.02	0

(c)

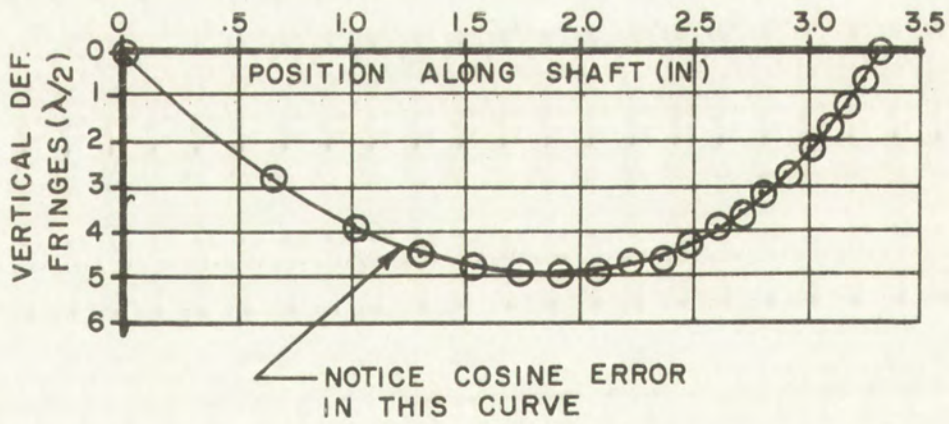

VERTICAL DEFLECTION VS POSITION
(d)

Figure 24. Improved Method for Measuring Curves with Interference Fringes

manipulation of the slope between the reference flat and the shaft to optimize the fringe spacing.

3. The interferometer had to be compatible with photography so that pictures of the fringe patterns could be made.

4. The interferometer had to allow close spacing between the reference flat and the bowed shaft, so that the fuzziness and lack of intensity which accompany high fringe orders with light which is not truly monochromatic would be eliminated.

5. The interferometer reference flat had to have the proper reflectivity for viewing polished metals.

6. The dummy straining shaft had to be equipped with an optically flat surface.

Of the available interferometers, the instrument which came closest to meeting these requirements was located in the Sandia Corporation Primary Mechanical Standards Laboratory (see Figure 25). This interferometer had originally been designed for Naval Ordnance use and was quite old. It had been revamped and equipped with better filters. It is used primarily in measuring the surface flatness of gage blocks. The material and coating of the reference flat had been selected so that its index of refraction provided a reflected light intensity approximately equal to that of flat polished steel; hence, it was ideal for measuring polished metal surfaces. The field of view of this instrument was approximately 2.5 inches, and the interferometer table was equipped with fine tilting screws. The interferometer head was mounted on a slide rod and could be driven up and down with a rack-and-pinion drive. The extending viewing tube formed a natural place for clamping a camera mount. The instrument was located in a room in which the temperature was kept at standard room temperature, within $\pm 1^{\circ}$F; the humidity was controlled; and there was only light foot traffic and no heavy machinery close by. Also, the room was easily darkened for taking photographs. With this interferometer (which uses a helium light source and is filtered to pass only the green helium line), a spacing between

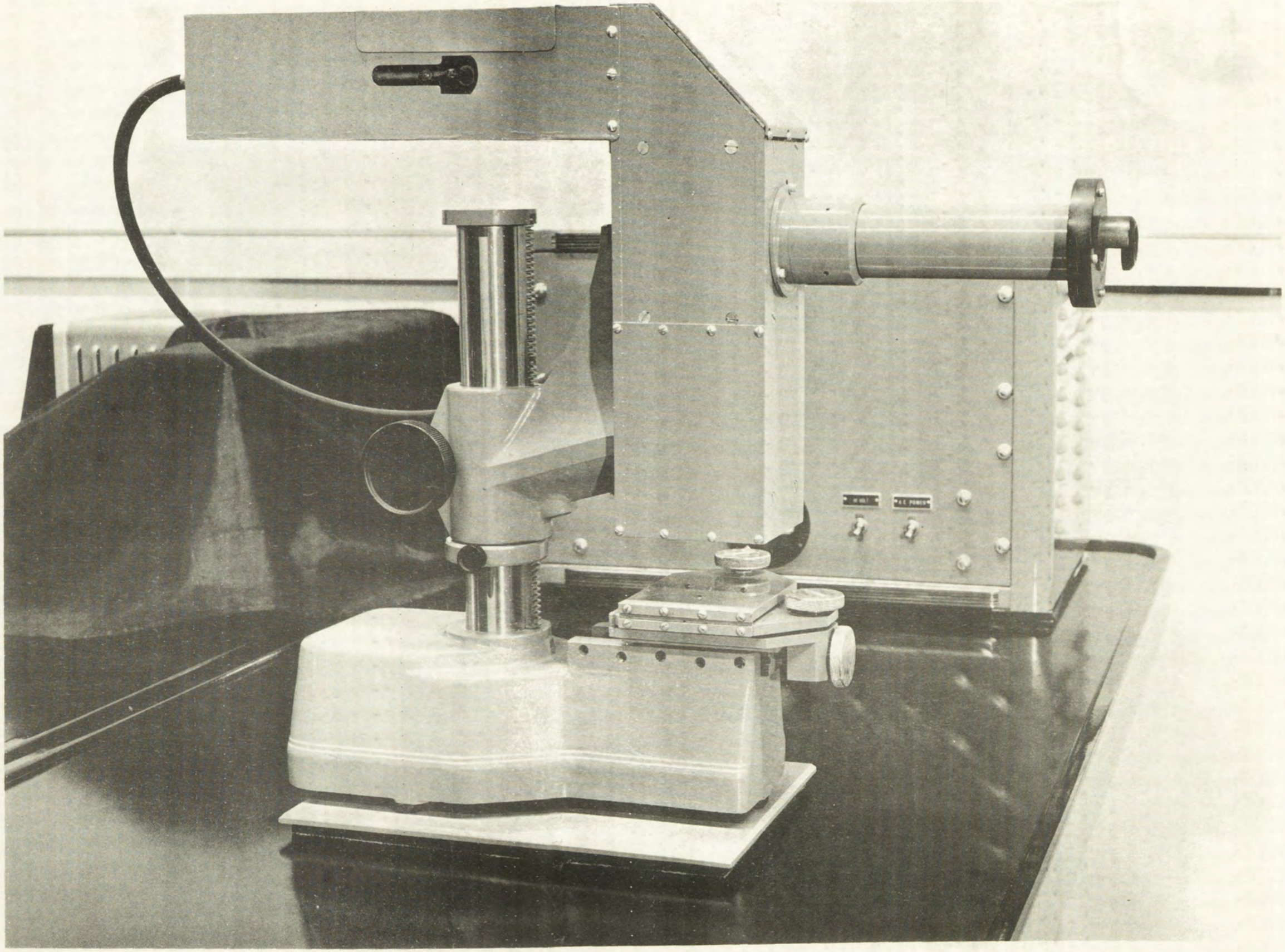

Figure 25. Gage-Measuring Interferometer

the reference flat and shaft of greater than 2 inches resulted in too much fading and fuzzing of the fringe lines to be usable. Thus, a transfer straining frame had to be built to allow the reference flat to be positioned within 2 inches of the shaft surface. The original dummy shaft was equipped with two diametrically opposite optically flat surfaces, 0.023-inch wide, located at 90 degrees from the two strain gages. These flats were formed by first surface-grinding and then hand-lapping with longitudinal strokes on a cast-iron lapping plate charged with 50-μin. diamond grit. Since the flat area was only 0.023 inch wide, a small toolmaker's clamp was attached to one end of the shaft in outrigger fashion to establish the third point of the final lapping plane and prevent rounding of the flat surface. The final flat obtained was flat within 2 μ in. in 5-1/2 inches of length, and the surface finish was about 1 μ in. rms with longitudinal lay.

Transfer Straining Frame

The method used for setting up a predictable shaft curvature with a transfer frame was, first, to put the desired setting into the dummy shaft with the original straining frame; then the indicated strain at this setting was obtained with the semiconductor gages. The dummy shaft was then removed and put into the transfer straining frame. The transfer straining frame was adjusted to give the same indicated strain and the shaft was then rotated 90 degrees to place the optically flat surface in the correct position to set up the interference fringe pattern. A simple transfer frame was made of five basic pieces (see Figures 26 and 27): (1) a heavy structural part of 1018 hot-rolled steel, (2) four hardened load rings similar to those used in the regular straining frame, (3) a 0.125-inch-thick flat spring made of tool steel and equipped with centrally located half-round pivot points, (4) two threaded outer load-point housings, and (5) two fine-pitch adjusting screws.

Photographic Considerations

A 35-mm Practina FX camera with an f/2 lens was available which would accommodate the 18-inch focal length needed to take pictures through

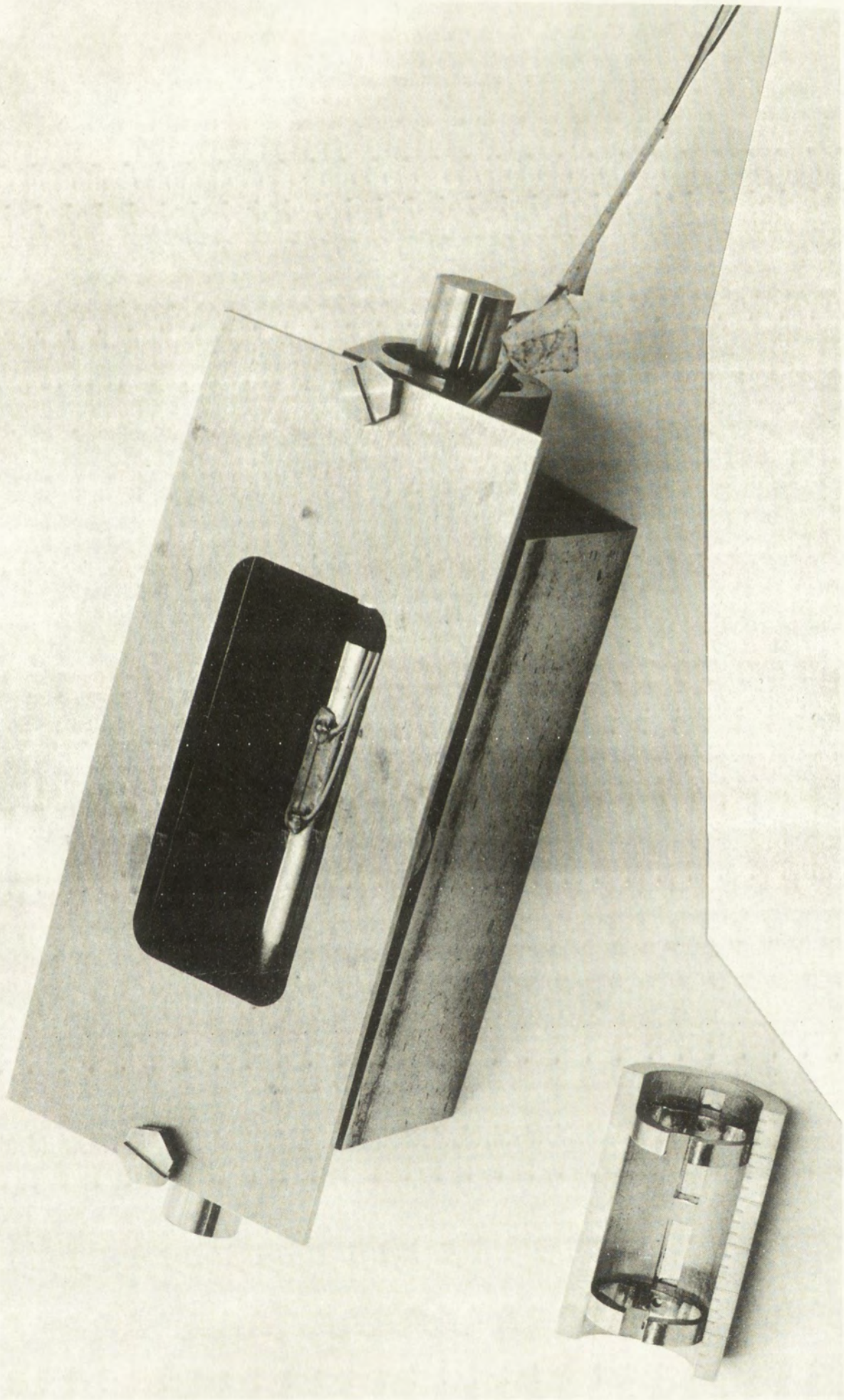

Figure 26. Transfer Straining Frame

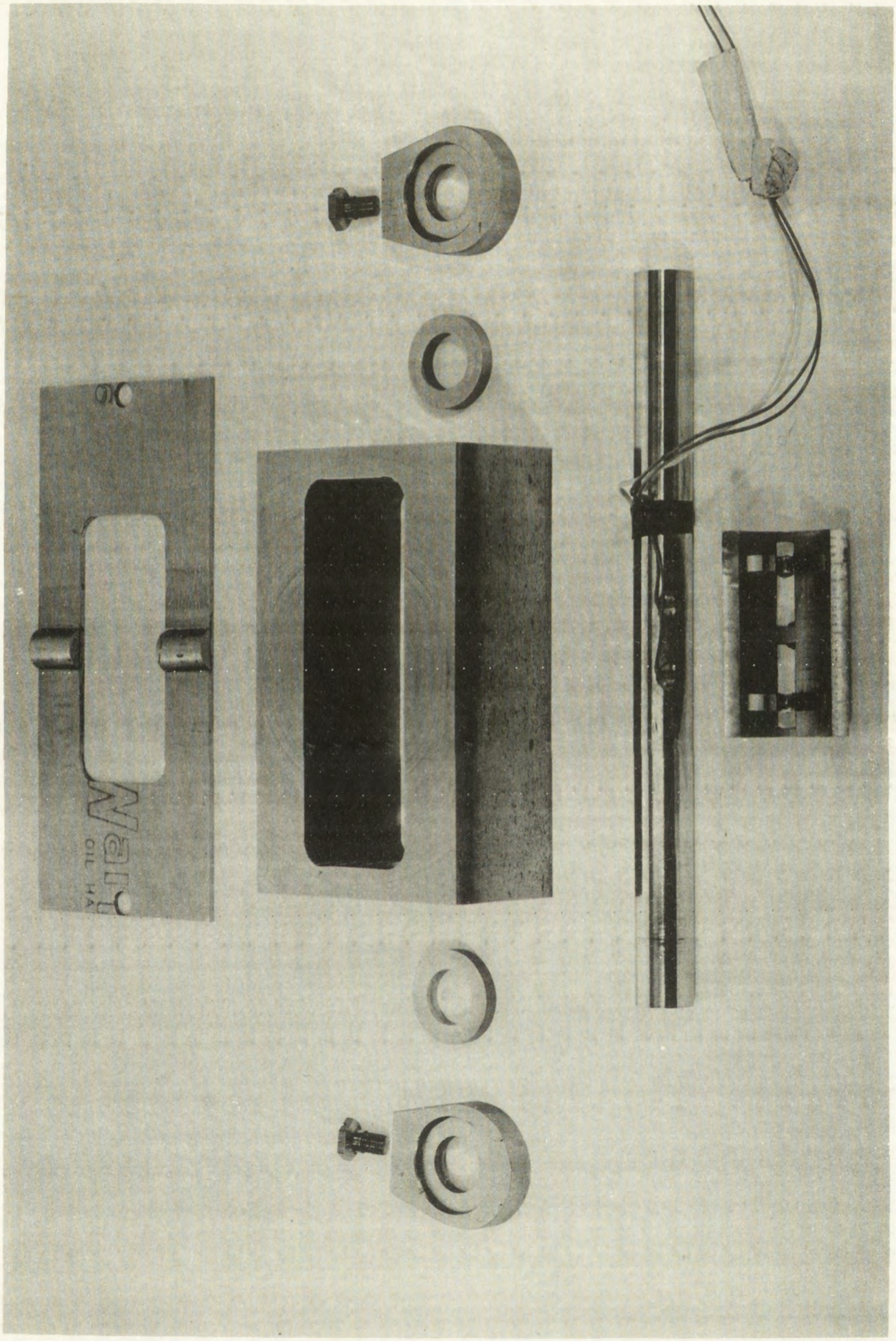

Figure 27. Transfer Straining Frame

the interferometer. The small amount of light given off by the 0.023-inch-wide fringe pattern 18 inches away would definitely mean a time exposure. It had already been noted that a slight vibration of the interferometer table caused the fringes to become fuzzy to the eye, so it was easy to see that extreme stability of the camera and interferometer were required for sharp time exposures. The electrical inlet cord from the helium exciter unit to the interferometer was vibration isolated to reduce a 60-cycle vibration. A sample series of photographs was made to determine in advance the suitability of the camera and to establish the best camera settings and times of exposure. The results showed that about 3 minutes in an entirely dark room was best. In the interest of uniformity, a remote shutter release and stop watch were used and the operator left the immediate area during the exposure. A fine-grained German film was used to allow ultimate resolution from the finished negatives. See Figure 28 for an enlarged print of a typical shaft fringe pattern (no difference in fringe spacing is discernible to the naked eye). See Figure 29 for a tabulation of the final photographs taken. All 33 negatives are available, but only 11 of them have been analyzed.

Data Reduction

The process of data reduction used follows the same general pattern as discussed in the section on measurement technique; however, several additional steps were necessary to get the data into a usable final form. A preliminary step was added to ease the fringe measurements and reduce the chances for errors in counting fringes. This consisted of (1) taping the negative to be measured to a glass microscope stage with masking tape, (2) taping a straightedge formed of 0.002-inch-thick brass shimstock along the edge of the fringe pattern, and (3) scribing a line in the brass opposite each fifth fringe. (The lines corresponding to each tenth fringe were made longer and were numbered for positive identification.) A fine needle ground to an even sharper point was used as a scriber. The scribing operation was done under 40x magnification. This numbering system eliminated further counting of the fringes, but the final measurements were taken directly from the negative.

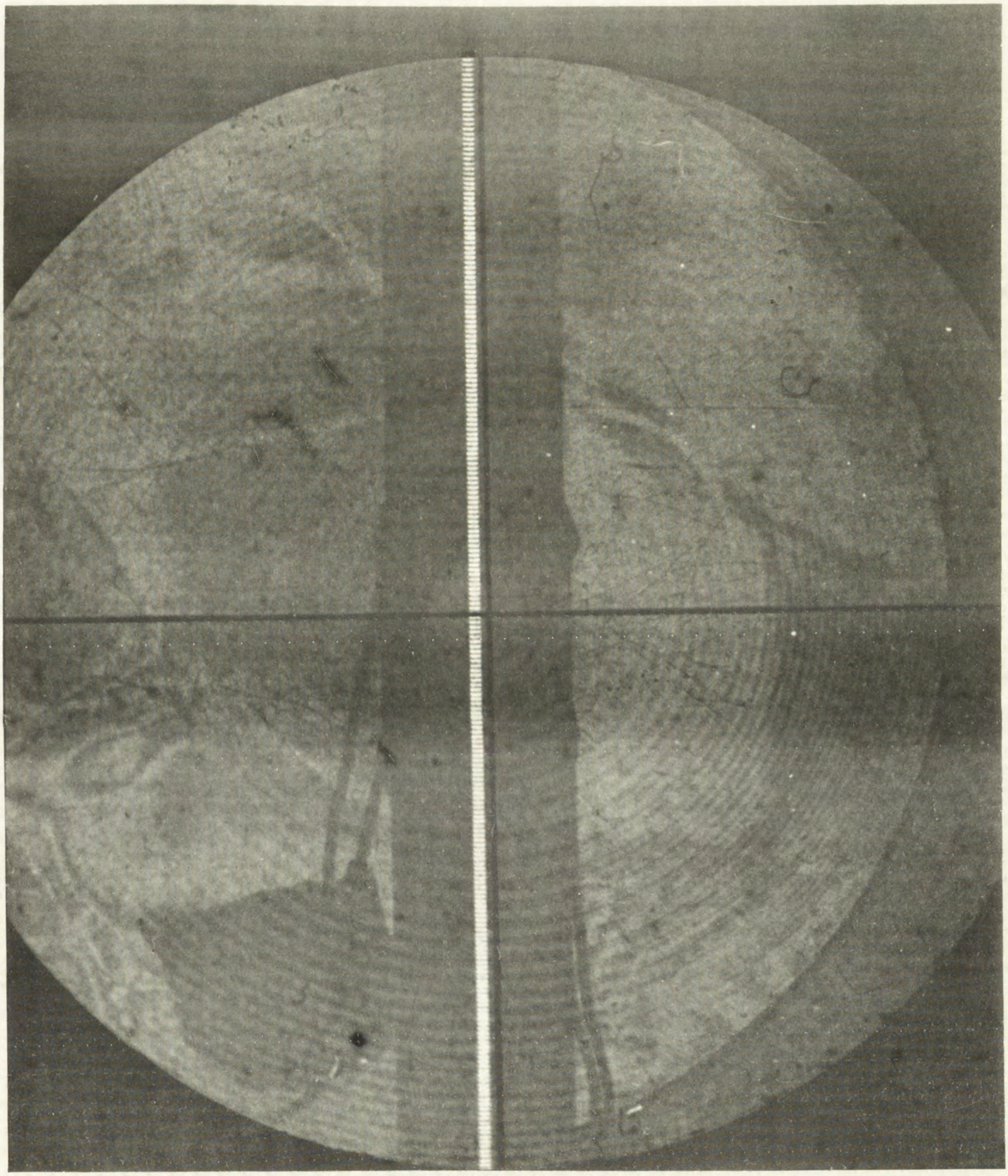

Figure 28. Typical Fringe Pattern

Negative No.	Strain Setting Before Rotation (Does not Correct for Indicator Drift)	Straining-Frame Setting (Neglecting Indicator Drift)	Central Loading (grams)	Central Loadpoint Spacing (in.)	Approximate Fringe Spacing	f Setting at 17.5-in. Distance	Exposure Time	Data Reduced?	Comments
1	16700	250	None		Close	1.65	3	Yes	
2	16700	250	None		Close	1.65	6	No	
3	16700	250	None		Close	1.65	3	No	19.2 distance
4	16700	250	None		Close	1.75	3	No	focused with
5	16700	250	None		Wide	1.75	3	No	light
6	14810	160	None		Close	1.75	3	Yes	
7	14810	160	None		Close	1.75	6	No	
8	14810	160	None		Wide	1.75	3	No	
9	14810	160	None		Wide	1.75	6	No	
10	13860	No Frame	None		Close	1.75	3	Yes	
11	13860	No Frame	None		Close	1.75	6	No	
12	13860	No Frame	None		Wide	1.75	3	No	Misfire
13	13860	No Frame	None		Wide	1.75	3	No	
14	13860	No Frame	None		Wide	1.75	6	No	
15	13860	No Frame	None		Very Close	1.75	3	Yes	
16	13987	No Frame	32	0.75	Close	1.75	6	Yes	
17	13987	No Frame	32	0.75	Close	1.75	3	No	
18	13987	No Frame	32	0.75	Wide	1.75	6	No	
19	13987	No Frame	32	0.75	Wide	1.75	3	No	
20	14810	160	32	0.75	Close	1.75	6	Yes	
21	14810	160	32	0.75	Close	1.75	3	No	
22	14810	160	32	0.75	Wide	1.75	6	No	
23	14810	160	32	0.75	Wide	1.75	3	No	
24	14810	160	32	0.75	Close	1.75	3	No	Central Load Off Center
25	14810	160	32	0.75	Very Close	1.75	3	No	Central Load Off Center
26	14810	160	32	0.75	Very Close	1.75	3	No	Central Load Slightly Off Center
27	13987	No Frame	32	0.75	Very Close	1.75	3	No	Slightly Off Center
28	13987	No Frame	32	1.00	Very Close	1.75	3	No	Slightly Off Center
29	Shaft lying directly on 3-inch diameter reference optical flat.				Close	1.75	3	No	
30	0.001-inch graduated steel scale on reference flat.				Close	1.75	3	No	
31	0.001-inch graduated steel scale on reference flat.						2		Random flash-light
32	0.001-inch graduated steel scale on reference flat.						2	Yes	Random bare bulb
33	0.001-inch graduated steel scale on reference flat.						10	Yes	Room light, 10 minutes

Figure 29. Photographic Data, 35-mm Practina Fx f/2 Lens

Explanation of the process of data reduction will be done by discussing the steps shown in Figure 30 for the data reduction of exposure No. 1. Columns 1 and 2 make up the initial measured data. Column 1 lists the position being measured. Usually this corresponds with one of the "tenth" lines scribed on the brass reference piece because only every tenth fringe was measured. Column 2 is the horizontal position measurement obtained from the negative with the aid of a toolmaker's microscope (see Figure 31 for a picture of this instrument). The micrometer wheels on this microscope read directly to 1×10^{-4} inches and, with practice, one may extrapolate to an accuracy of $\pm 1 \times 10^{-5}$ inches. The fifth decimal place in the horizontal-position measurements was retained until the final step of data reduction, to maintain the best statistical accuracy possible.

The initial measured data were reduced as follows. A new fringe number scale was formed in column 3 to limit the data reduction to the region of interest (some of the additional information in this column was needed to establish the centerline and to check the validity of the end points used in column 3). Column 4 converted the readings in column 2 into positions along the negative from the zero point in column 3. Column 5 lists the theoretical fringe order for the position shown in column 4, assuming a perfectly straight shaft. The number in column 5 was obtained by multiplying column 4 by the average number of fringes per inch of negative, n_t/ℓ_t, which in this case was 130/0.32413 = 401.073 fringes per inch (notice this number is not an integer). Column 6 represents the vertical deviation of the curved shaft from the theoretical straight surface joining the 0 and 130 fringes at each horizontal position shown in column 4 (deviation measured in fringes or multiples of $\lambda/2$). The number in column 6 was obtained by subtracting column 5 from column 1. Column 7 converted column 4 into the true measurement along the shaft. The conversion factor for this operation was obtained by dividing the true diameter of the reference flat by the diameter of the reference flat measured from the negative. Column 8 converted the vertical deviation (in fringes) into actual deflection measured in μin. This was done by multiplying the deflection in fringes by 10.7457, the exact length of $\lambda/2$.

		Initial Measured Data		Measured Data Reduction						Final Measured Data	
	Step	(1)	(2)	(3)	(4)	(5)	(6)	(7)	(8)	(9)	(10)
	Symbol	N	$\bar{L}$(in.)	n	$\bar{\ell}$(in.)	$\gamma = 4 \times \frac{n_t}{\ell_t}(\text{in.})^{-1}$	Δ_γ	ℓ(in.)	δ ($\times 10^{-6}$ in.)	ℓ(in.)	δ ($\times 10^{-6}$ in.)
	Explanation	Fringe No. or Position on Negative	Position Reading from Negative (Toolmaker's Microscope)	Fringes Renumbered for Convenience	Position from New Zero in (3)	Theoretical Fringe for Positions in (4) if shaft were straight $\frac{n_t}{\ell_t} = \frac{130}{0.32413} = 401.073$	Measured Deflection in Fringes Δ_γ = (3) - (5)	True Position Along Shaft (4) x 6.36321 6.36321 = Dist. Scaling Factor	Measured Deflection in Inches (6) x $\frac{\lambda}{2}$ $\frac{\lambda}{2} = 10.7457 \times 10^{-6}$ in.	True Position (7) Rounded Off	Measured Deflection (8) Rounded Off
Data	Left Edge, Circle	1.22808									
	Left Edge, Frame Aperture	1.33139									
	1	1.33303									
	10	1.35510	0	0.00000	0.0000	0.0000	0.00000	00.0000	0.000	00.00	
	20	1.37749	10	0.02239	8.9800	1.0200	0.14247	10.9599	0.142	10.96	
	30	1.40030	20	0.04520	18.1285	1.8715	0.28762	20.1092	0.288	20.11	
	40	1.42329	30	0.06819	27.3492	2.6508	0.43391	28.4828	0.434	28.48	
	50	1.44672	40	0.09162	36.7463	3.2537	0.58300	34.9610	0.583	34.96	
	60	1.47067	50	0.11557	46.3520	3.6480	0.73540	39.1978	0.735	39.20	
	70	1.49501	60	0.13991	56.1141	3.8859	0.89028	41.7539	0.890	41.75	
				℄ -0.15676				-0.99753	-0.998		
	80	1.51942	70	0.16432	65.9043	4.0957	1.04560	44.0083	1.046	44.01	
	90	1.54490	80	0.18980	76.1237	3.8763	1.20774	41.6508	1.208	41.65	
	100	1.57073	90	0.21563	86.4834	3.5166	1.37210	37.7859	1.372	37.79	
	110	1.59682	100	0.24172	96.9474	3.0526	1.53812	32.8002	1.538	32.80	
	120	1.62357	110	0.26847	107.6761	2.3239	1.70833	24.9703	1.708	24.97	
	130	1.65097	120	0.29587	118.6655	1.3345	1.88268	14.3392	1.883	14.34	
	140	1.67923	130	0.32413	129.9998	0.0000	2.06251	00.0000	2.063	00.00	
	144	1.69080									
	Right Edge, Frame Aperture	1.69234								Final Measured Data Plotted in Fig. 32	

Figure 30. No. 1 Sample Measured Data

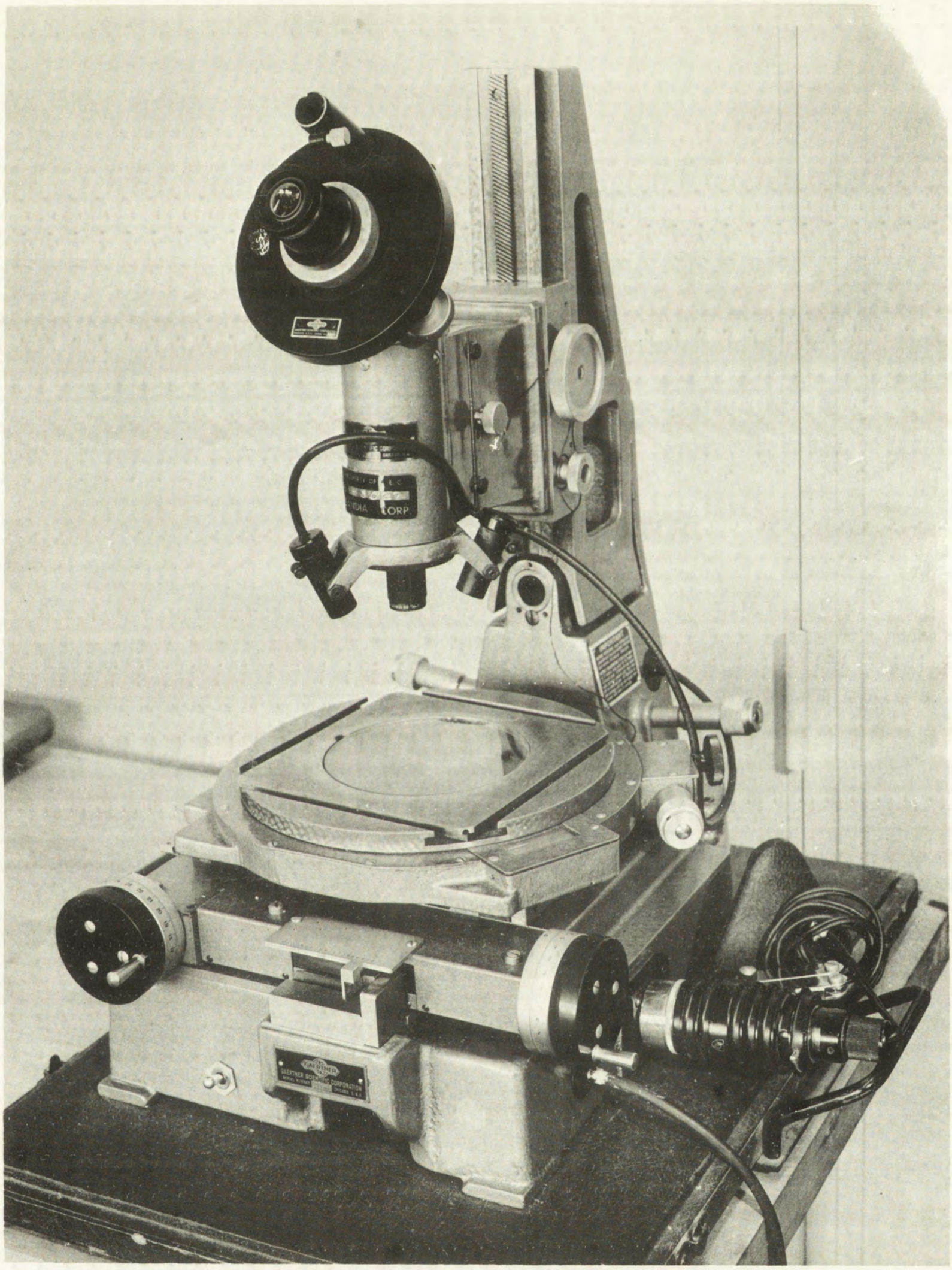

Figure 31. Toolmaker's Microscope

The final data appear in columns 9 and 10 and were obtained by merely "rounding off" columns 7 and 8. The final data for negative No. 1 are shown plotted in Figure 32.

Data Correction

A study of all of the final measured data from the 11 negatives which were analyzed showed that the reference flat on the interferometer had an over-all sag and a central discontinuity, both of which were distorting the final measured data. In addition, an unknown amount of photographic distortion undoubtedly was present. Figure 33 shows the way the correction to the final data was established. Columns 1, 2, 3, 9, and 10 for both No. 15 and No. 10 correspond to those already explained for No. 1 (naturally, all of the intervening steps were carried through). Negative Nos. 15 and 10 are of the shaft sagging under its own weight. The final measured data (9 and 10) are plotted in Figure 34. Notice that the measured data are negative in value, signifying an upward curvature, when the shaft was known to be slightly bowed downward. This could only occur if the reference flat were sagging more than the unstrained shaft. Because there was a slight central discontinuity and because the axial fringe measurements were not equally spaced on each side of the axial centerline, the two final measured data curves were essentially folded over at the centerline and the points all transferred to a single side of the folded graph. An averaged smooth curve was drawn through these points. See Figure 35 for a plot of the smoothed data which is the average of No. 10 and No. 15. The same folding and graphical averaging technique was applied to the final measured data for No. 1 (see Figure 36). The smoothed and averaged measured deflection at every 0.1 inch along the shaft was read off Figures 35 and 36, and appears as columns A and B of Figure 37 and columns 11 and 12 of Figure 38. The final correction curve is derived graphically in Figure 35 and in tabular form in Figure 37. The derivation is by addition of the theoretical deflection of the shaft under its own weight to the smoothed and averaged measured deflection obtained from negative Nos. 10 and 15. The final correction for each 0.1 inch along the center 2 inches of the shaft is shown in column D of Figure 37. The final correction shown in column D appears in column 13

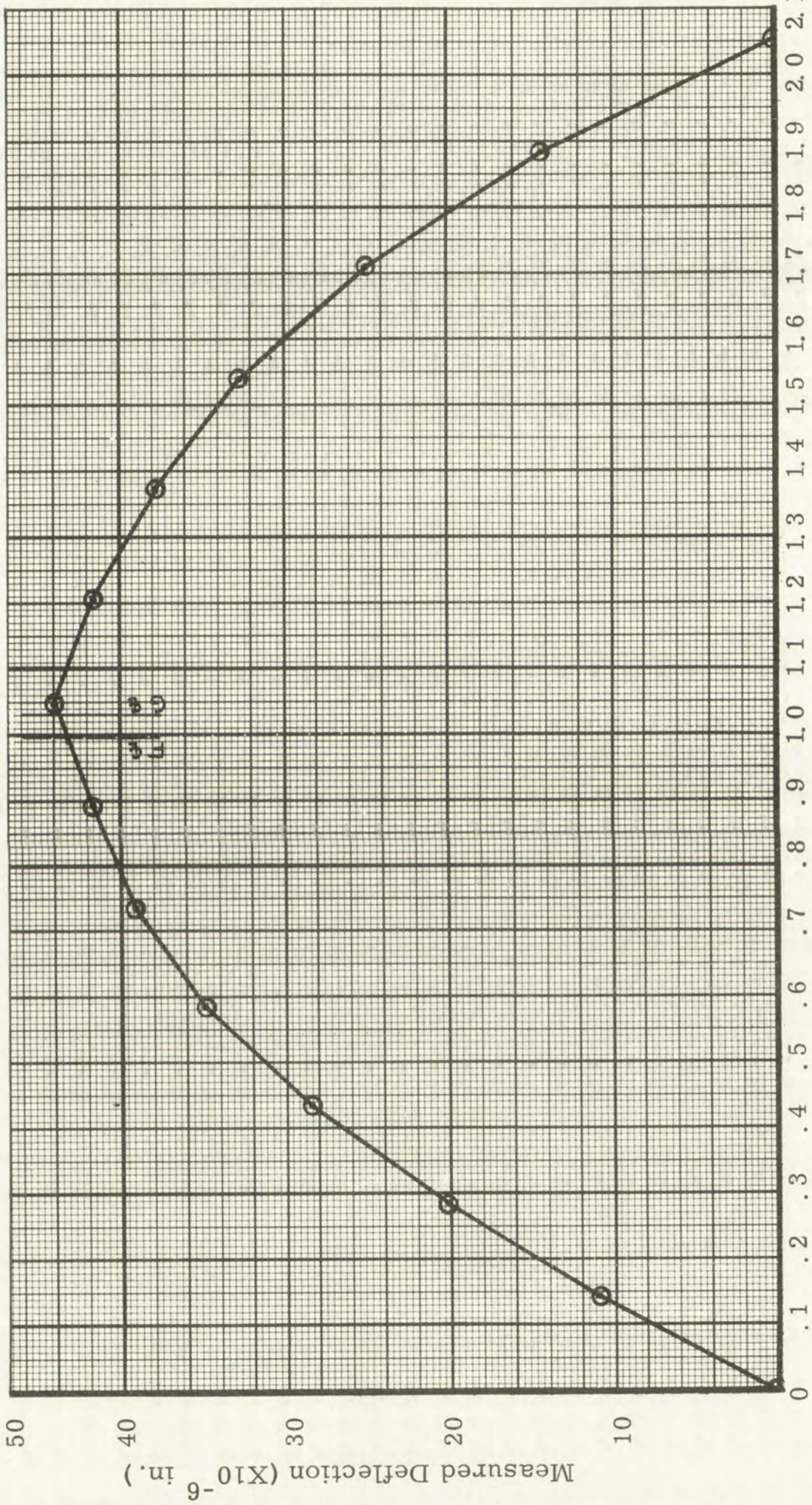

Figure 32. No. 1 Measured Deflection Versus Shaft Position

Step	No. 15 - Shaft Weight Only (Close Fringe Spacing)					No. 10 - Shaft Weight Only (Wide Fringe Spacing)				
	Initial Measured Data			Final Measured Data		Initial Measured Data			Final Measured Data	
	(1)	(2)	(3)	(9)	(10)	(1)	(2)	(3)	(9)	(10)
Symbol	N	L(in.)	n	ℓ(in.)	δ(x10^{-6}in.)	N	$\bar{L}$(in.)	n	ℓ(in.)	δ(x10^{-6}in.)
	Left Edge, Circle	1.26897				Left Edge, Circle	1.33888			
	0	1.26999				0	1.34025			
	10	1.28546				10	1.36790			
	20	1.30090				20	1.39572	0	0.00	0.00
	30	1.31651				30	1.42295	10	0.174	2.13
	40	1.33182	0	0.000	0.00	40	1.45043	20	0.350	5.26
	50	1.34719	10	0.098	1.98	50	1.47775	30	0.525	7.75
	60	1.36232	20	0.195	2.26	60	1.50493	40	0.670	9.67
	70	1.37774	30	0.294	4.60	70	1.53179	50	0.871	10.31
	80	1.39306	40	0.392	6.22	80	1.55867	60	1.043	11.03
	90	1.40831	50	0.490	7.35	$\bar{L}$	----1.56463----		----1.081	
	100	1.42356	60	0.587	8.48	90	1.58537	70	1.214	11.02
	110	1.43875	70	0.684	9.18	100	1.61188	80	1.383	10.25
	120	1.45383	80	0.781	9.10	110	1.63807	90	1.551	8.19
	130	1.46909	90	0.879	10.30	120	1.66440	100	1.720	6.70
Data	140	1.48410	100	0.975	9.72	130	1.69053	110	1.887	4.40
	$\bar{L}$	----1.49387----		----1.047		140	1.71669	120	2.054	2.22
	150	1.49918	110	1.071	9.64	150	1.74284	130	2.222	0.00
	160	1.51417	120	1.167	8.92	160	1.76910			
	170	1.52917	130	1.263	8.27	167	1.78752			
	180	1.54416	140	1.359	7.54					
	190	1.55922	150	1.455	7.32					
	200	1.51415	160	1.551	6.17					
	211	1.59053	171	1.656	4.60					
	221	1.60545	181	1.751	3.38					
	231	1.62037	191	1.847	2.16					
	241	1.63533	201	1.942	1.22					
	251	1.65025	211	2.038	0.00					
	261	1.66532								
	271	1.68014								
	281	1.69517		See Figure 34 for plot					See Figure 34 for plot	
	291	1.71023								
	296	1.71776								

Figure 33. Sample Data for Determination of Correction for Flat Sag
(Continued in Figure 37)

Final Measured Data

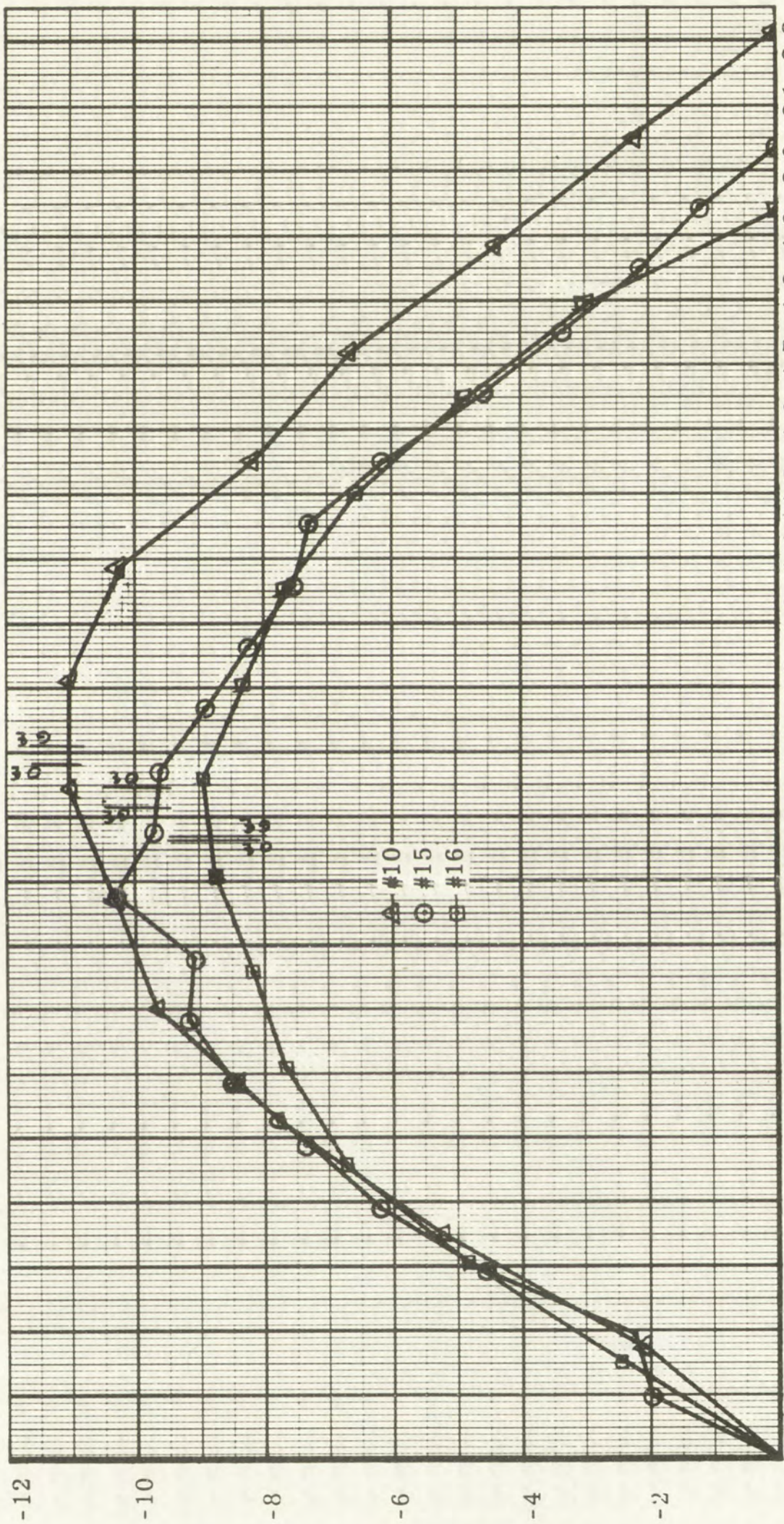

Figure 34. Nos. 10, 15, and 16 Measured Deflection Versus Shaft Position

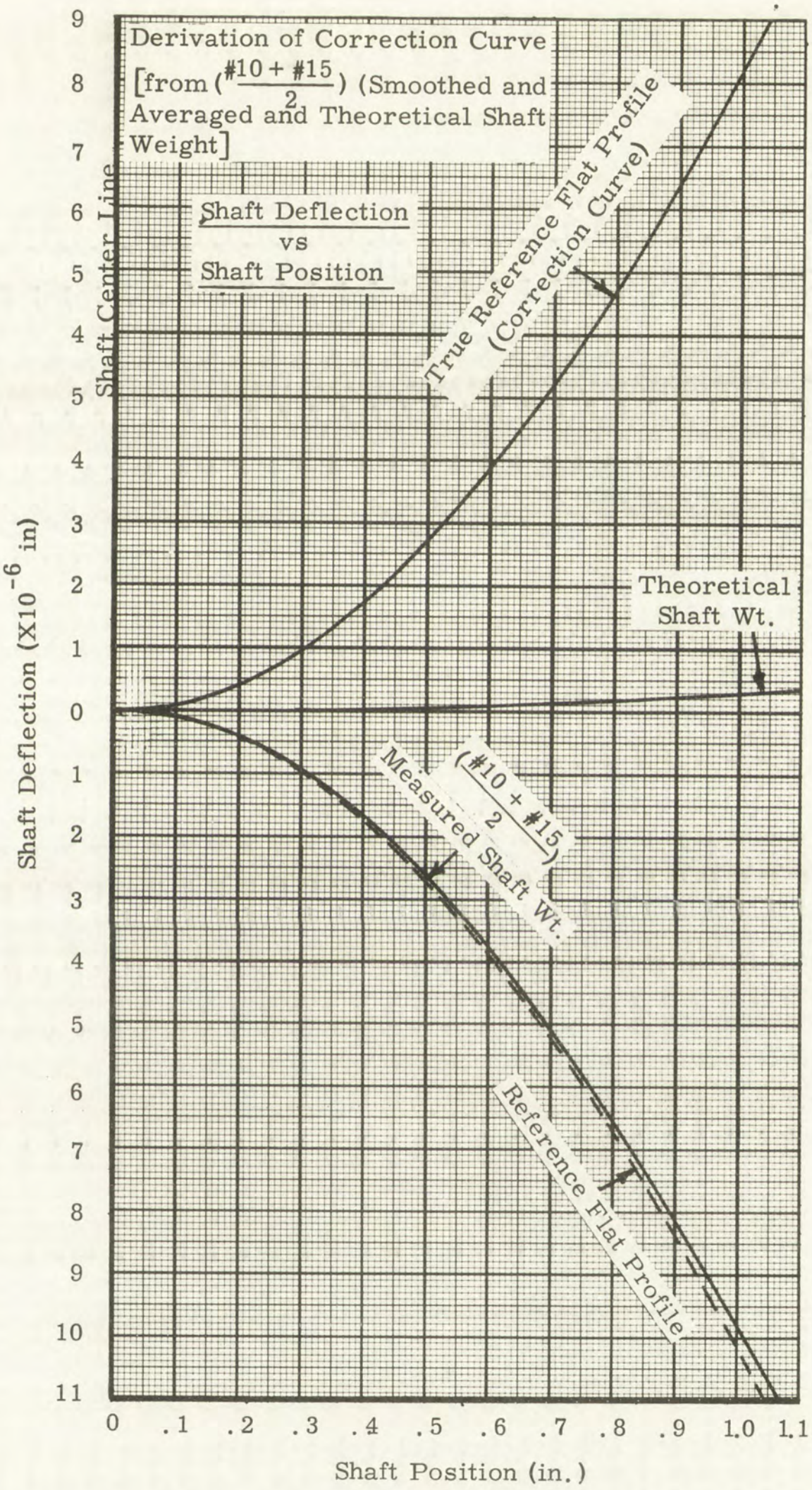

Figure 35. Nos. 10 and 15 Smoothed and Averaged Measured Shaft Deflection Versus Shaft Position (Theoretical Shaft Weight and Reference Flat Profile)

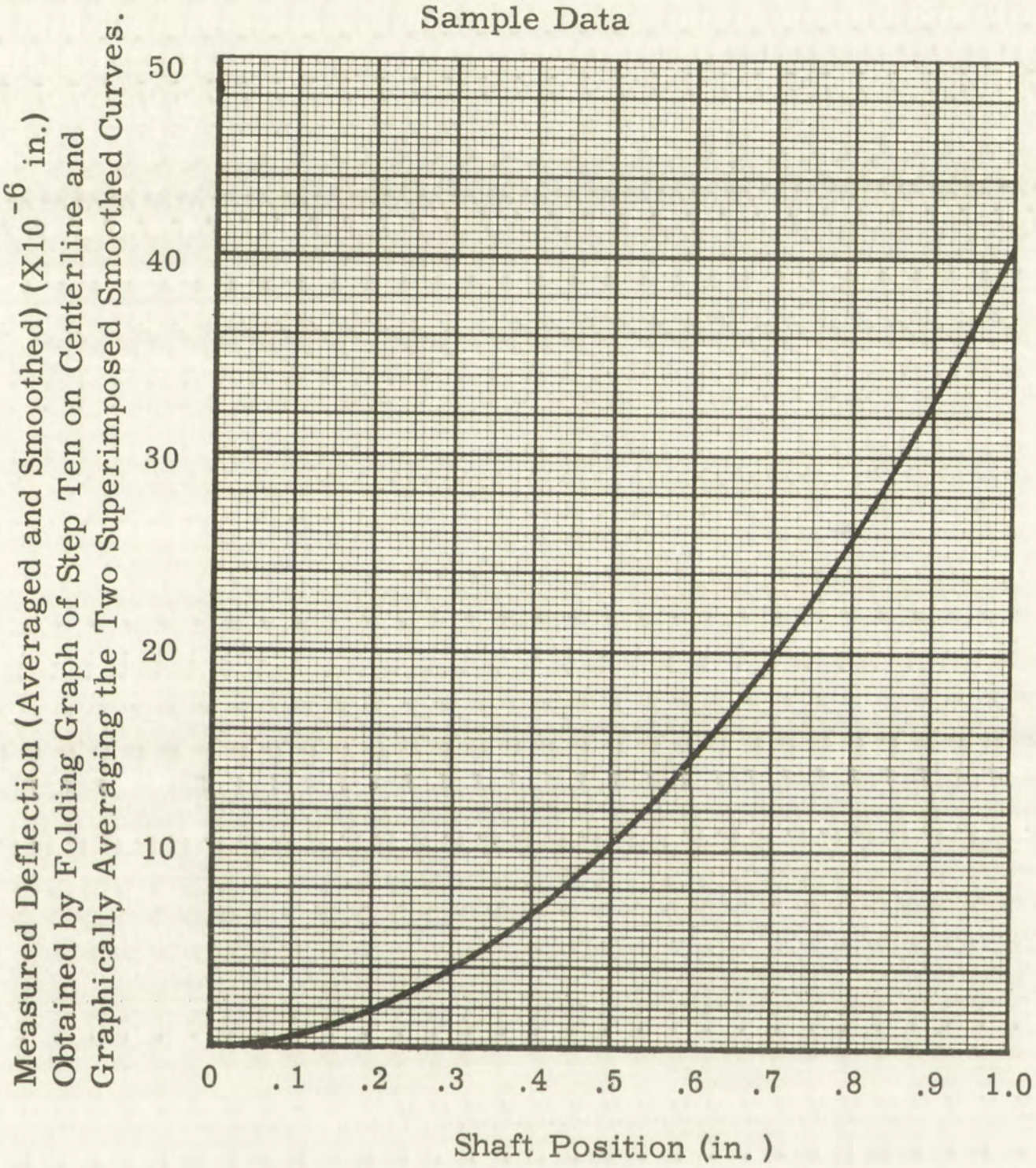

Figure 36. No. 1 Smoothed and Averaged Measured Shaft Deflection Versus Shaft Position

Explanation	Step	Ⓐ	Ⓑ	Ⓒ	Ⓓ
	Symbol and Units	ℓ (in.)	$t(\times 10^{-6}$ in.)	$\hat{\delta}$ $(\times 10^{-6}$ in.)	$c(\times 10^{-6}$ in.)
		Shaft Position Measured from Longitudinal $\mathcal{C}_L$	Theoretical Deflection for Shaft Weight Only (See Page ___ for Derivation)	Measured Deflection for Shaft Weight Only $\hat{\delta} = (\frac{\delta_{10} + \delta_{15}}{2})$ Averaged and Smoothed from Figure 34	Correction for Flat Sag Ⓓ = Ⓑ - Ⓒ (To be added to all measured deflections)
Data		Shaft $\mathcal{C}_L$	0.000	-0.00	0.00
		0.1	0.004	-0.12	0.124
		0.2	0.014	-0.43	0.44
		0.3	0.030	-0.93	0.96
		0.4	0.053	-1.64	1.69
		0.5	0.083	-2.58	2.66
		0.6	0.118	-3.73	3.84
		0.7	0.158	-5.04	5.20
		0.8	0.203	-6.52	6.72
		0.9	0.253	-8.09	8.34
		1.0	0.306	-9.78	10.09
			See Figure 35 for plots		

Figure 37. Final Data for Correction of Errors Introduced by Master Flat Sag (Both No. 10 and No. 15, Averaged for Distortion Reference)

No. 1 - Correction of Measured Data for Flat Sag					No. 1 - Determination of rms Measuring Error					
Step	11	12	13	14		15	16	17	18	19
Explanation	Shaft Position Measured from Longitudinal ℄	Deflection Averaged and Smoothed (Taken from Figure 37	Correction for Reference Flat Sag (Taken from data for Figure 37)	Final Deflection (Corrected Deflection) 12 and 13		Fringe No.	Measured Shaft Position (9)	|Difference| Between 10 and Corresponding Value from Figure 37	(17)^2	rms Error per Measured Point
Data	Shaft ℄ 0.000	0.00	0.00	0.00	1	0	0.000	0	0	
	0.100	0.50	0.12	0.62	2	10	0.142	0.3	0.09	0.509 µin.
	0.200	1.65	0.44	2.09	3	20	0.288	0.7	0.49	
	0.300	3.45	0.96	4.41	4	30	0.434	0.5	0.25	
	0.400	6.13	1.69	7.82	5	40	0.583	0.05	0.0025	
	0.500	9.57	2.66	12.23	6	50	0.735	0.4	0.16	
	0.600	13.88	3.84	17.72	8	60	0.890	0.7	0.49	
	0.700	19.34	5.20	24.54	9	70	1.046	0.8	0.64	
	0.800	25.85	6.72	32.57	10	80	1.208	0.02	0.0004	
	0.900	33.05	8.34	41.39	11	90	1.372	0.1	0.01	
	1.000	40.90	10.09	50.99	12	100	1.538	0.2	0.04	
					13	110	1.708	0.5	0.25	
					14	120	1.883	1.1	1.21	
					15	130	2.063	0	0	
				See Figure 36 for plot					$\sum_{0}^{14}$ = 3.6329	
									$\frac{\Sigma}{14}$ = 0.2595	
									rms - error = $\sqrt{0.2595}$ = 0.509 µin.	

(NOTE: All Data on This Page are to be x10^{-6} in.)

Figure 38. No. 1 Final Corrected Data

of Figure 37. The final corrected data for No. 1 is shown in column 14 of Figure 38 and is the sum of columns 12 and 13.

Columns 15 through 19 of Figure 38 show the method used in determining the rms measuring error. The final smoothed and averaged measured curve of Figure 36 was superimposed on the initial measured data curve (Figure 32) and the deviation at each measured shaft position recorded in column 17. These deviations were squared in column 18, these squares were averaged, and the square root was then extracted. The final rms measuring error occurs in column 19.

Remaining Optical Measurement Data

The final measured data for negatives 6 and 20 are shown in Figure 39 and for negative 16 in Figure 40. The smoothed and averaged measured data for curves 1, 6, 16, and 20 are shown in Figure 41. The final corrected data for these curves are tabulated in Figure 42 and plotted along with curve 15 in Figure 43. Figures 44, 45, and 46 show the final corrected plots in comparison with theoretical curves. Figure 47 shows the statistical variation obtained in closely spaced measurements and the central reference flat discontinuity in a plot of approximately the center 0.2 inch as the shaft.

Accuracy and Errors

The wavelength of helium green light is known to 10^{-13} inches ($\lambda/2 = 10.74570045$ inches). Additional accuracy is gained due to the sharpness of the dark fringes in helium green (see Figure 28). The dark interference fringes are nearly one-fourth the width of the light bands. The sources of error other than in the reference flat, which has already been discussed, are: (1) the accuracy of the transfer operation, (2) the accuracy of the optical flats, and (3) the accuracy of measurements. The sources of error in the transfer operations are threefold: (1) the difference in moment of inertia between

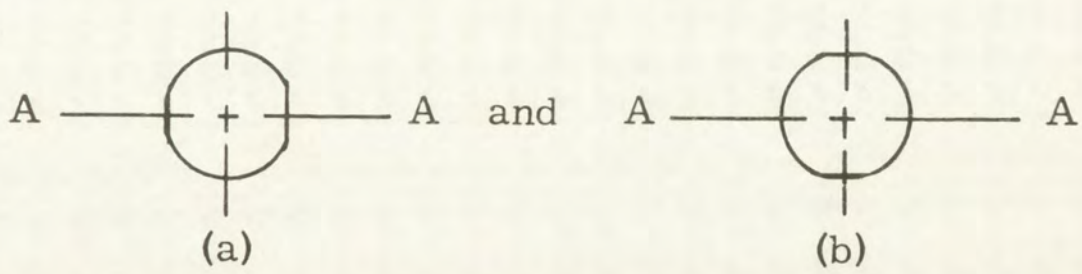

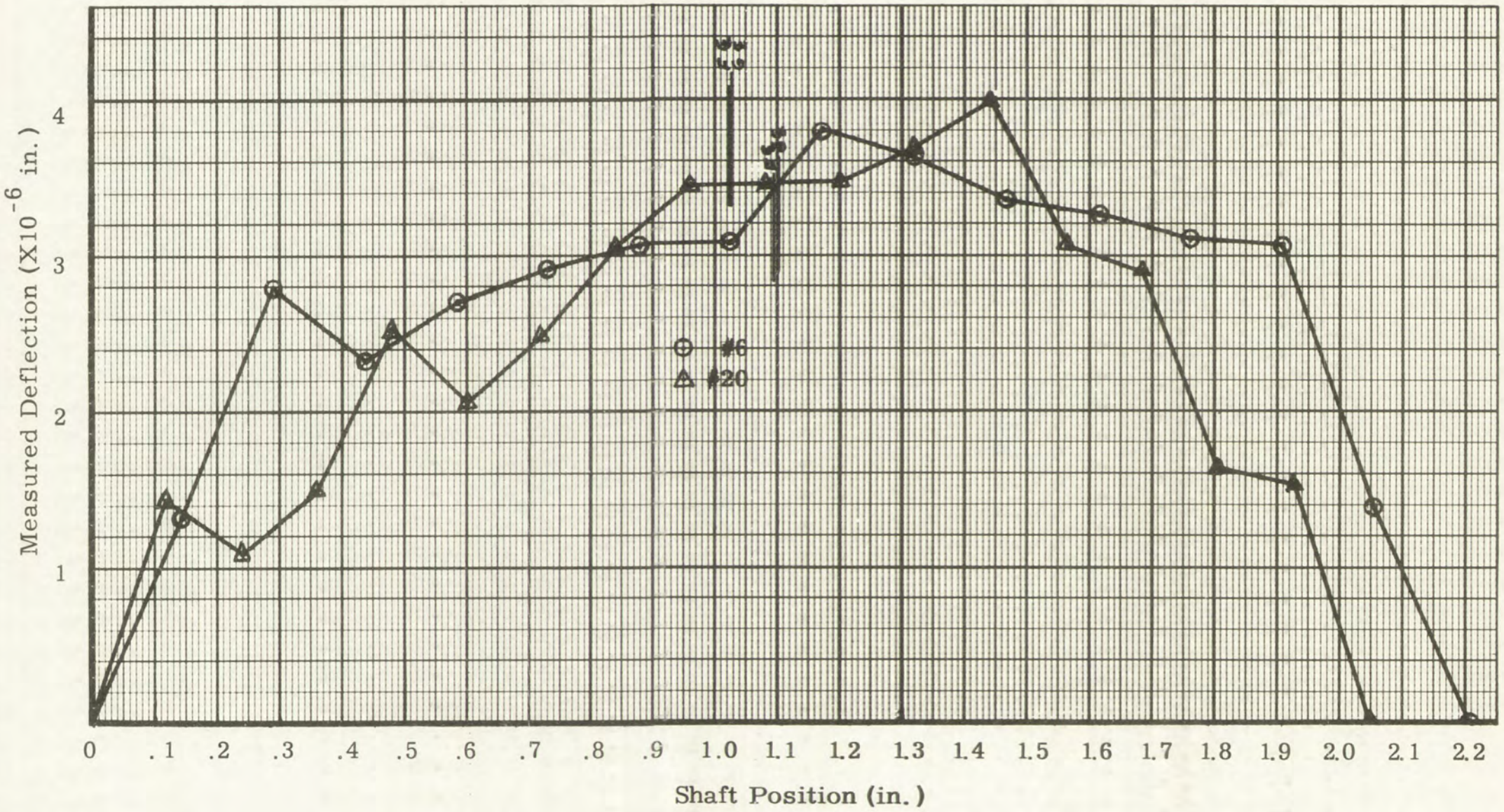

Figure 39. Nos. 6 and 20 Measured Deflection Versus Shaft Position

Final Measured Data

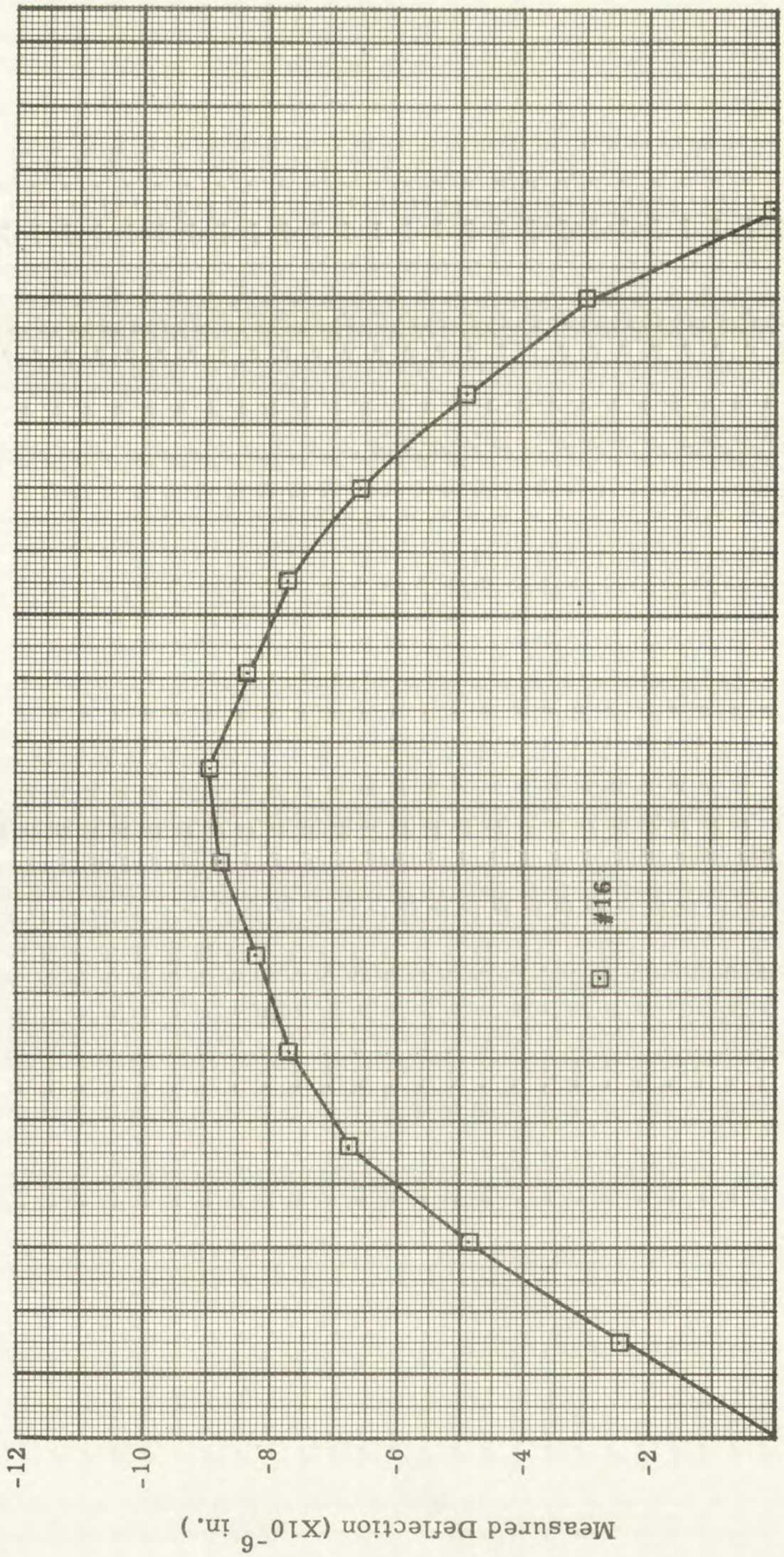

Figure 40. No. 16 Measured Deflection Versus Shaft Position

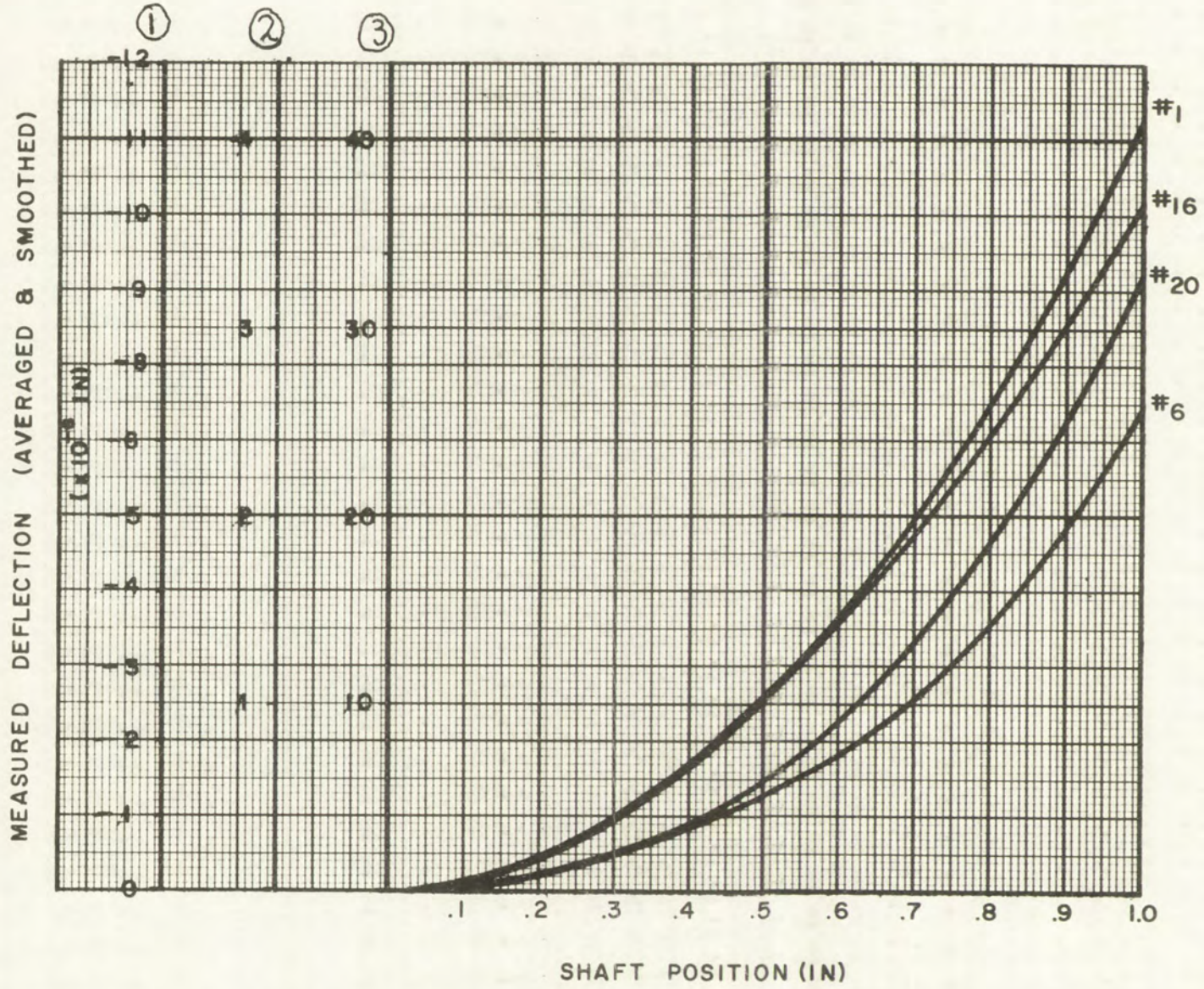

PHOTO	SET	BUSHING ?	SCALE
#1	250	NO	③
#6	160	NO	②
#16	0	YES	①
#20	160	YES	②

Figure 41. Nos. 1, 6, 16, and 20 Measured Deflection (Averaged and Smoothed) Versus Shaft Position

Shaft Position from ℄ (in.)	No. 1 (μin.)	No. 6 (μin.)	No. 16 (μin.)	No. 20 (μin.)
0	0	0	0	0
0.1	0.62	0.14	0.014	0.126
0.2	2.09	0.53	0.03	0.55
0.3	4.41	1.15	0.05	1.19
0.4	7.82	2.03	0.09	2.06
0.5	12.23	3.18	0.18	3.25
0.6	17.72	4.58	0.30	4.74
0.7	24.54	6.22	0.46	6.53
0.8	32.57	8.14	0.64	8.57
0.9	41.39	10.25	0.79	10.79
1.0	50.99	12.65	0.97	13.37

Figure 42. Final Corrected Data

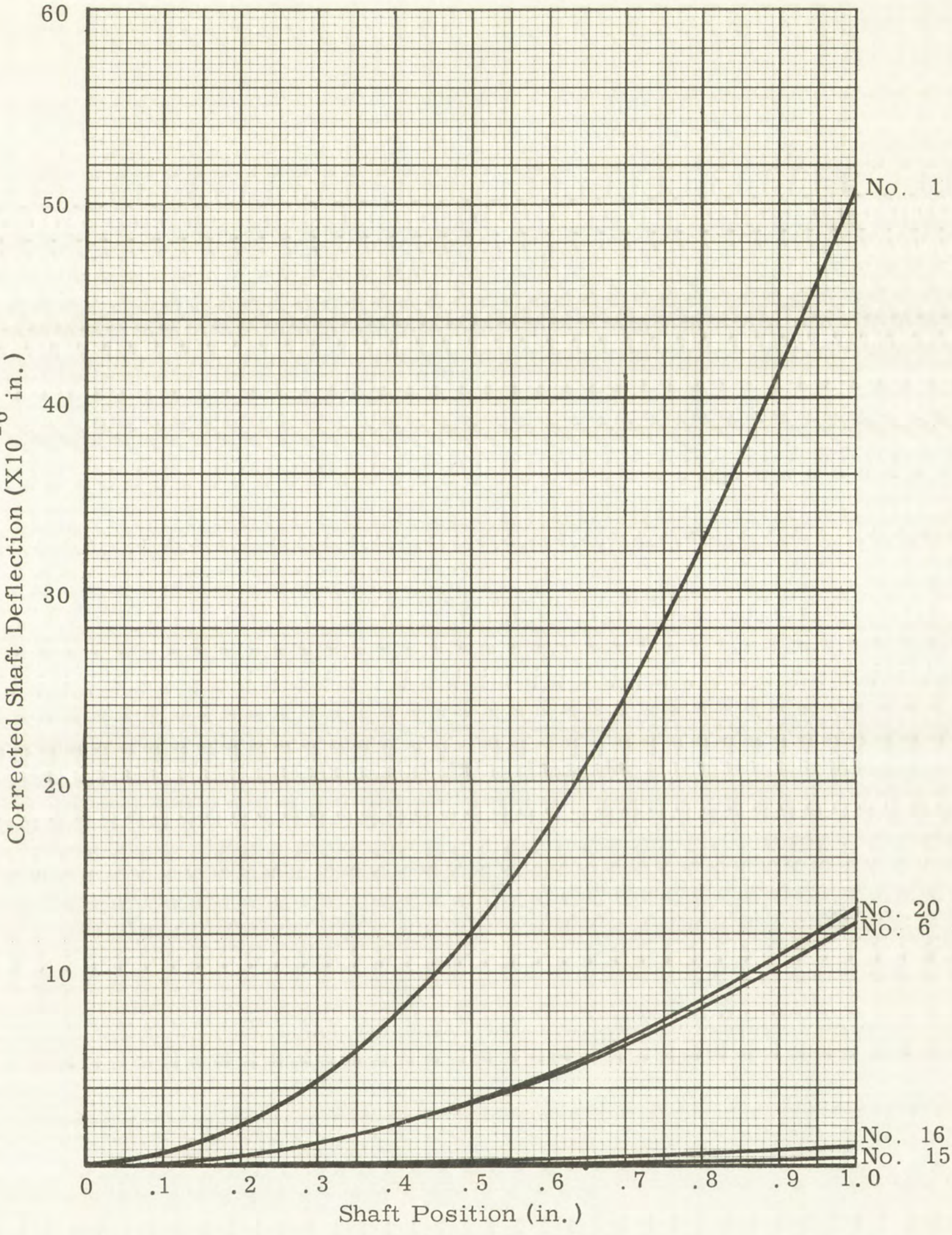

Figure 43. Final Corrected Shaft Deflection Versus Shaft Position (All Curves)

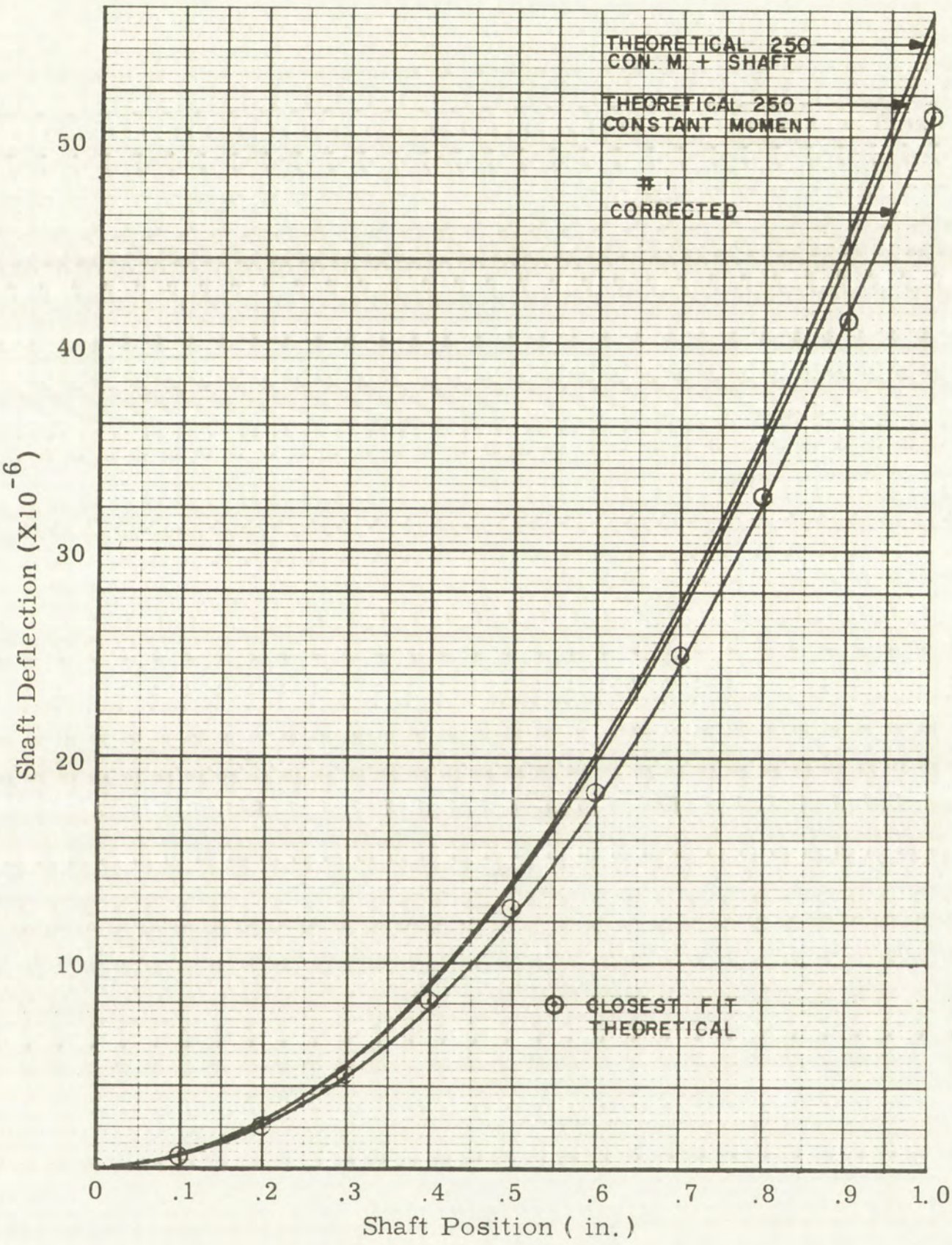

Figure 44. No. 1 Final Corrected Data Compared with Theoretical Curves
Shaft Deflection Versus Shaft Position

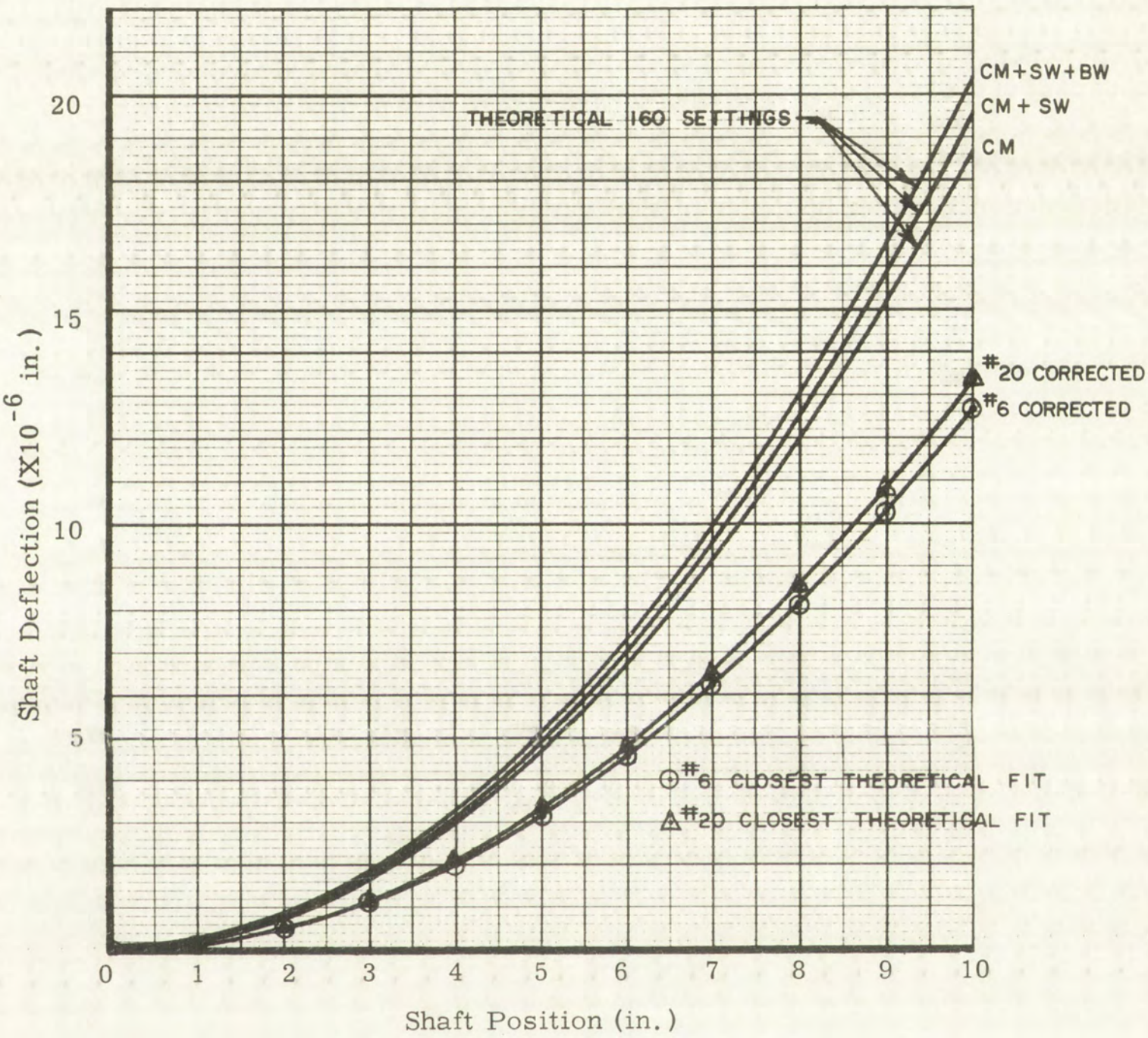

Figure 45. No. 6 and No. 20 Final Corrected Data Compared with Theoretical Curves
Shaft Deflection Versus Shaft Position

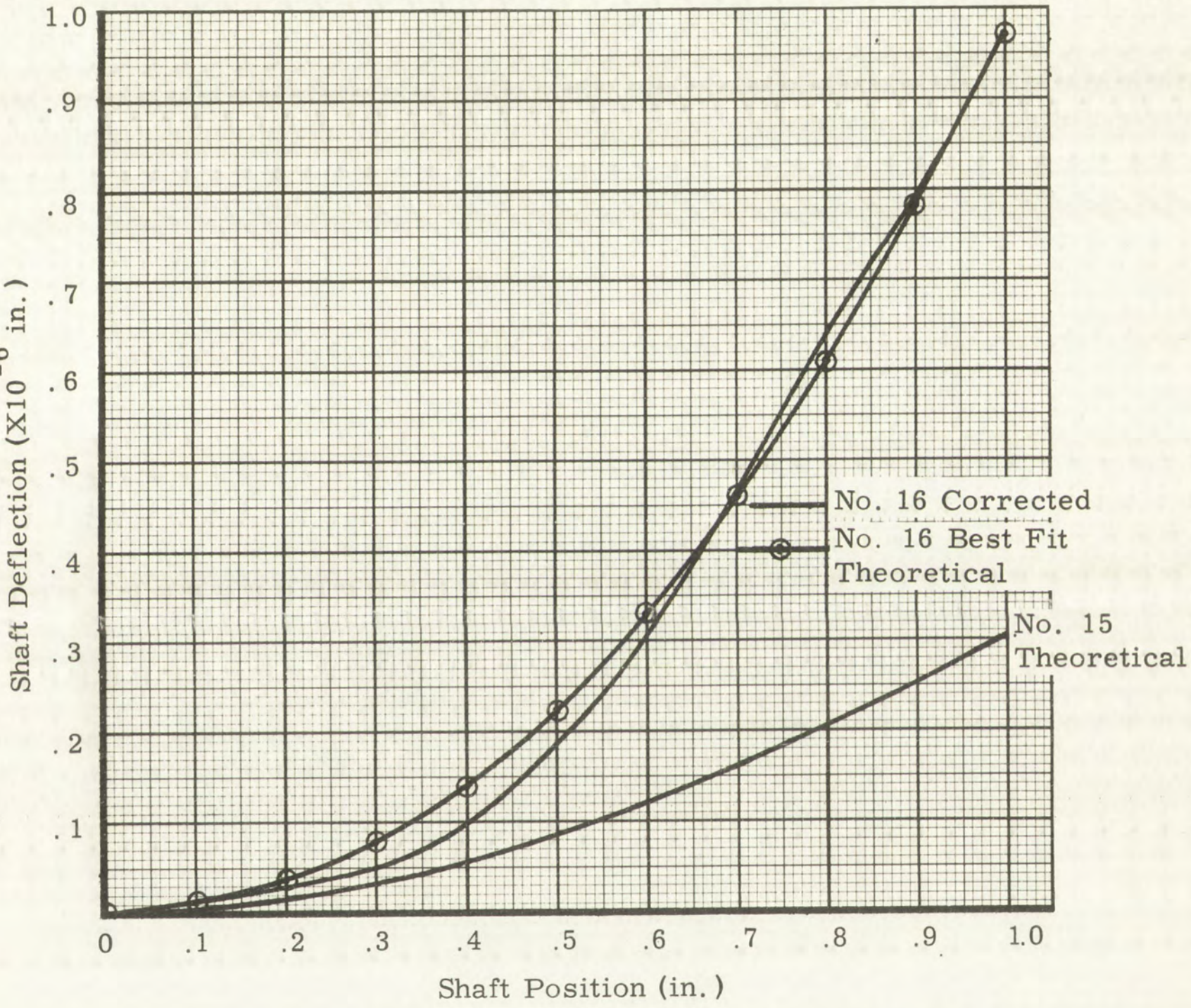

Figure 46. No. 16 Final Corrected Data Compared with Best Fit Theoretical Curve and No. 15 Theoretical Shaft Deflection Versus Shaft Position

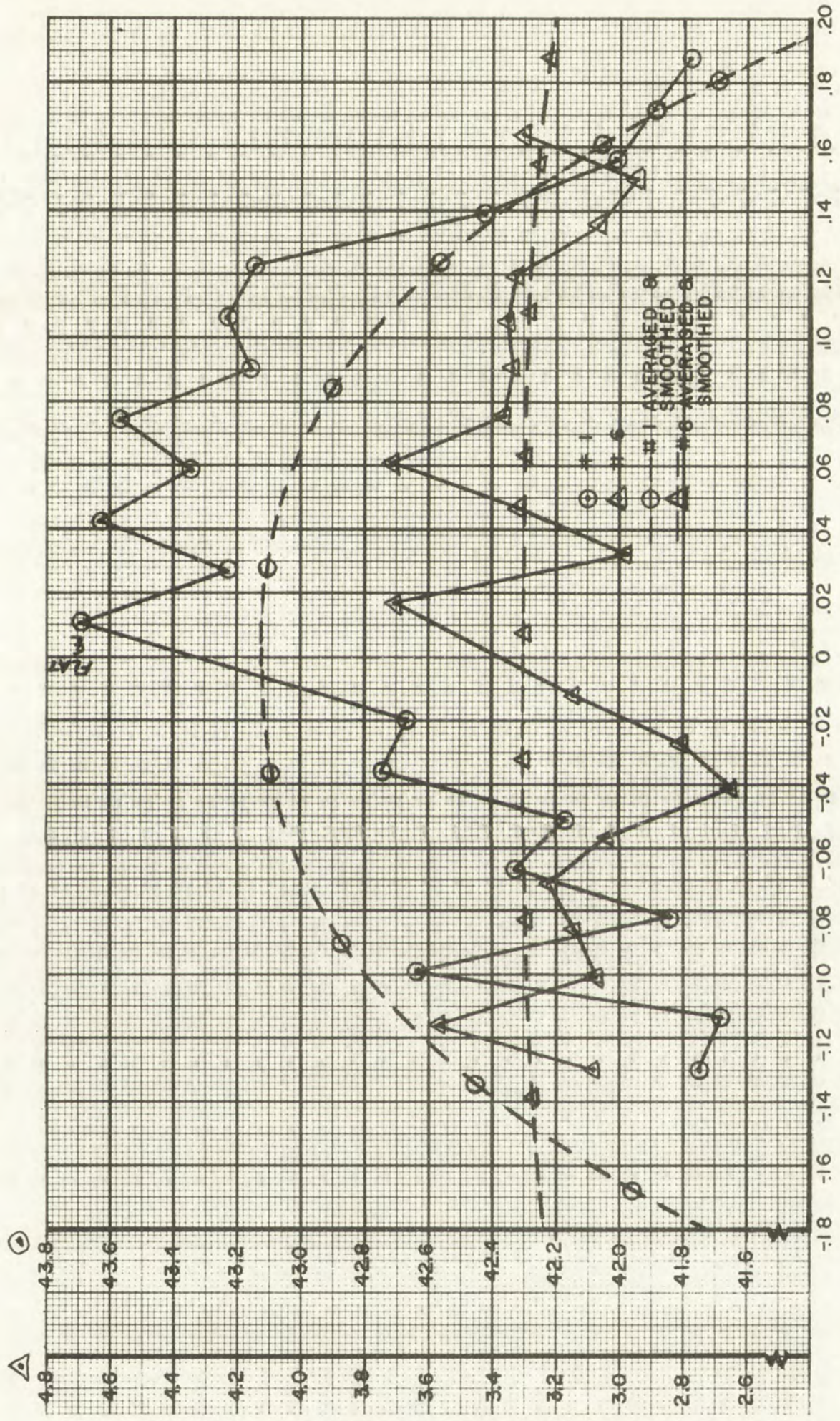

Figure 47. Statistical Measuring Error Analysis #1 and #6 Measured Data (Central Section)
Measured Shaft Deflection Versus Shaft Position

which occurs due to rotation, (2) the other errors which occur during transfer due to movement of load points, etc., and (3) indicator drift.

The first type of error may be analyzed in general, but the other two are functions of the amount of shaft curvature and time required. The moment of inertia of view (a) will be very closely approximated by the moment of inertia of a circular section; hence,

$$I_1 \approx \frac{\pi r_1^4}{4} = \frac{\pi(0.21890)^4}{4} = 1.80332 \times 10^{-3} \text{ in}^4 \qquad r = 0.21890$$

$$I_2 = 4\int_0^{y_m} xy^2\,dy = 4\int_0^{y_m} \sqrt{r^2 - y^2}\; y^2\,dy$$

$$= 4\left[-\frac{y_m}{4}\sqrt{\left(r^2 - y_m^2\right)^3} + \frac{r^2}{8}\left(y_m\sqrt{r^2 - y^2} + r^2 \arcsin\frac{y_m}{r}\right)\right]$$

$$I_2 = 1.8026988 \times 10^{-3} \text{ in}^4$$

The ratio of these two moments of inertia is

$$\frac{I_{flat}}{I_{round}} = \frac{1.802699}{1.80332} = 0.999666$$

or the error is about 0.033 percent, which is completely negligible.

The optically flat surfaces were found to have about a 2-μ inch finish rms with nearly all lapping marks running longitudinally and a few much deeper scratches. A portion of a fringe pattern with about a 3-μ inch surface finish under very high magnification, say 1000x would appear as shown on the following page (remember the light spots are really the fringes on a negative).

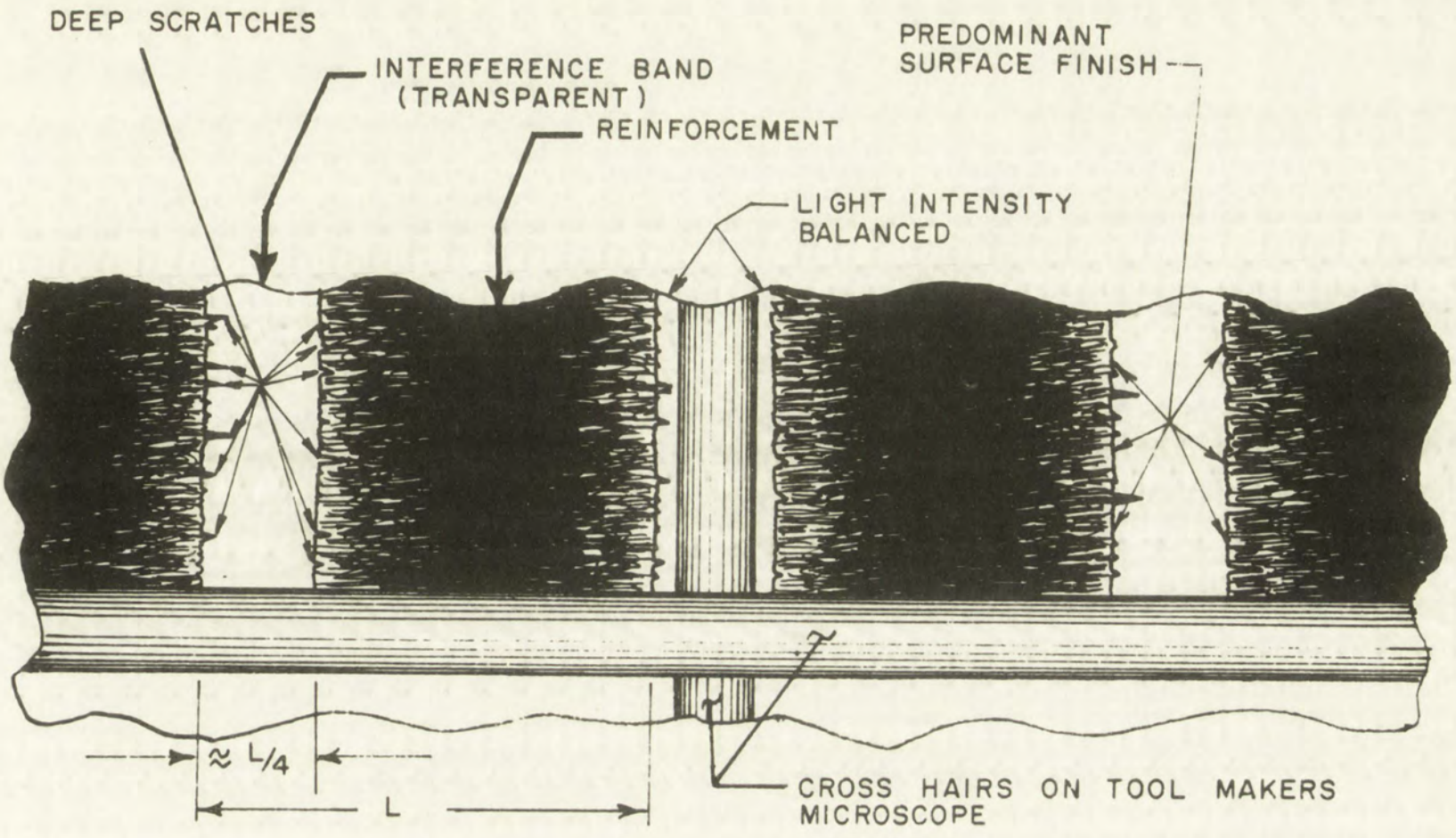

Figure 48. Measuring a Photographic Negative of Fringes (Shown Under High Magnification)

It is evident that the longitudinal lay of the finish marks affects the sharpness of the fringe edges but would not materially affect the measured center of the fringe at far less magnification because, optically, one can only balance the intensity of light showing through on each side of the cross hair in centering on the fringe, and both edges are of approximately equal roughness. This suggests that the effect of surface finish on the final measurements should be almost negligible. An estimate of the error due to surface finish would be not greater than 0.05 of the fringe spacing. The average fringe spacing on the negatives was about 0.002 inch, or an error of not over 0.00010 inch. The optical flat on the shaft was flat to within about two millionths in a 5-1/2-inch length, hence should have been flatter than one millionth in a 2-inch length. The toolmaker's microscope in repeated trials gave axial position on the negative within $\pm \times 10^{-5}$ inches. Thus, the maximum axial measuring error would be $\pm 1.1 \times 10^{-4}$ inches. The maximum deflection error for the average spacing, then, should be about

$$\frac{1.1 \times 10^{-4}}{2 \times 10^{-3}} \approx 5.5 \text{ percent}$$

of the $\lambda/2$ for the helium green light used. This corresponds to approximately

$$5.5\% \times 10.745 \times 10^{-6} \approx 0.6 \times 10^{-6} \text{ inches.}$$

Verification of Calibration

The primary method used for verification of the straining-frame calibration was a comparison of period measurements of bushing vibration on the seismometer with different straining-frame settings. At the time these measurements were taken, the electrical spin motor was introducing restoring forces which caused the bushing to vibrate with a 55-second period for small amplitude oscillations, even though no strain was introduced into the shaft by the frame. That is, only the shaft weight and bushing weight were contributing to the shaft deflection. According to the final calibration (Figure 20), the period should have been about 412 seconds. Thus, the forces introduced by the curved shaft were only

$$\left(\frac{55}{412}\right)^2 = 0.013 \text{ or } 1.3 \text{ percent}$$

of the motor forces (because restoring force varies inversely as the square of the period). With straining-frame setting of 800, which should have yielded a period of 20.4 seconds according to the strain-gage calibration, an average period of 18.9 seconds was obtained, based on 10 measurements. Lack of better correlation is attributable to three factors: (1) the timing was done with a stop watch; (2) the presence of the operator near the seismometer disturbed the bushing; and (3) the motor restoring forces. In this case, the latter effect should have been by far the greatest. A calculation of the error due to motor restoring forces follows.

$$T_{set} = 20.4 \text{ seconds}$$

$$T_{motor} = T_{\substack{\text{shaft and} \\ \text{bushing weight}}} + T_{measured}$$

$$= \sqrt{1.013} \times 55 \approx 55.3 \text{ seconds}$$

Therefore,

$$T_{actual} = T_{set}\sqrt{1 - \left(\frac{T_{set}}{T_{motor}}\right)^2} = 20.4\sqrt{0.864}$$

$$= 20.4 \times 0.931 \quad 19.0 \text{ seconds}$$

Thus, a 0.1-second error (19.0 - 18.9 = 0.1) is left for the other two sources of error mentioned. The calibration for an 800 setting as corrected for motor restoring force agrees with the experimentally obtained period within $\frac{0.2}{19.1} \times 100 \approx 1$ percent. Similar checks throughout the period range of from 20 to 30 seconds were made during the course of the seismometer development with different motor forces, but always about 1 percent correlation was obtained if the readings were corrected to account for these forces.

A second check was made with a flywheel mounted to the bushing and spun up to high speed with an air jet, then left to coast down. The flywheel was designed to have a 3-minute coast time. Here, the average of five good runs (again at a setting of 800) was 20.8 seconds. Attempts to measure periods longer than 30 seconds with this method were completely unsucessful due to the forces induced into the air bearing by gyroscopic coupling. Even at 20 seconds, about every other run went wild, so no great reliance is placed on this correlation.

These verifications were only good at the very high end of the calibration curve, so an attempt was made to check the long period settings with the optical-fringe-pattern method, employing the transfer straining frame. The results of Run No. 1, in which a setting of 250 was attempted, and Run Nos. 6 and 20, in which 160 settings were attempted, are shown in Figures 44 and 45, in comparison with the theoretical 250- and 160-setting curves. Curve No. 1 is seen to agree with the theoretical curve to within about 8.7 percent; No. 6, within about 35.3 percent; and No. 20, within about 34.6 percent. The difference in period between the measured curve and the theoretical curve would be as follows: (1) No. 1, about 2 seconds or 4.5 percent ($T_{measured} = 46.2$ seconds, $T_{theoretical} = 44.2$ seconds);

(2) No. 6, about 17.6 seconds or 24.1 percent ($T_{measured}$ = 90.6 seconds, $T_{theoretical}$ = 73 seconds; and (3) No. 20, about 17 seconds or 24.1 percent ($T_{measured}$ = 88.6 seconds, $T_{theoretical}$ = 71.6 seconds). The accuracy obtained in No. 1, while less than expected, is sufficient for most purposes and does tend to support the accuracy of the calibration. The errors in Nos. 6 and 20 are too large to be of any assurance. An analysis of the errors introduced by the transfer of settings from the principal straining frame to the transfer frame, based on repeated trials under the toolmaker's microscope, showed that the maximum deflection error in five transfers for the No. 1 setting was approximately ±15 percent compared with the -8.7 percent actually obtained. The same maximum deflection error due to transfer for the No. 6 and No. 20 settings would represent an error of approximately ±30 percent compared with the 35.3 percent actually obtained. Indicator drift errors were no doubt present. The conclusion one is forced to make is that the transfer straining frame employed was not accurate enough to reproduce small deflections. The use of dead weights, rather than a spring, would greatly improve the transfer accuracy; but, also, additional checks on indicator drift would be needed.

Fine Detail and Continuous Plots

The plotting of the continuous elastic curves and the results of the fine details of loading were both done from optical interference data. The five loading situations described in Figure 49 were plotted for this phase of the study. See Figure 43 for a comparison of the final corrected data for these five situations. These data also appear in numerical form in Figure 2. Notice that the effect of the 32-gram bushing is small (about 8 μ inch difference in deflection in the center 2 inches of the shaft) but clearly discernible between curves 6 and 20 and also between curves 15 and 16. The curvature due to shaft weight is very small and is shown in curve 15 (only 0.31 μ inch in the center 2 inches).

Figures 44, 45, and 46 show the same data presented in Figure 43 (usually with an increase in vertical scale) along with the theoretical curves

Negative No.	Straining frame used ?	Attempted setting	Bushing used ?	Period corresponding to measured curvature (sec)
1	Yes	250	No	46.2
6	Yes	160 (without bushing)	No	90.6
20	Yes	160 (with bushing)	Yes	88.6
15	No	-	No	55.4
16	No	-	Yes	41.2

Figure 49. Loading Situations Measured With Optical Interference Technique

of the attempted settings and of the best-fit theoretical curves (which pass through the end point of the final corrected curve). The formulas for the theoretical curves were derived for the three components of deflection due to (1) primary loading from the straining frame, (2) shaft weight, and (3) bushing weight. These formulas were for the deflection measured from the shaft centerline, assuming the deflection at the centerline to be zero since this form yielded data which was best suited for comparison with the measured data. See Appendix III for the derivation of these formulas and the final tabulated theoretical deflection data. Figure 44 shows the very close agreement obtained between the measured curve (shown as a solid line) for No. 1 and the closest fit theoretical curve (shown by circled dots). Here, 0.6 μin is the largest error and the rms error is 0.313 μin. Even closer agreement between the measured and closest fit theoretical curves was obtained for Nos. 6 and 20, shown in Figure 45. The vertical scale graduations are one-half the values in Figure 44 (twice the magnification) and still almost no deviation is discernible. Here, 0.04 μin is the largest error for No. 6; 0.07 μin, the largest for No. 20. The rms for No. 6 is

0.02 μin and for No. 20 is 0.04 μin. Figure 46, showing Nos. 15 and 16 to 10 times the vertical magnification of Figure 4, again shows remarkably close correlation between No. 16 as measured and the best-fit theoretical curve. Here, the largest error was only 0.053 μ in and the rms error was 0.025 μin. Thus, the average rms value for these four curves is only 0.099 μin. As discussed previously under the section on verification of calibration, the transfer operation was not very successful in establishing the intended settings; but, on the basis of the close fits obtained with best-fit theoretical curves, it at least shows that the curves obtained were correctly shaped. The close fits also show that the correction for reference-flat sag must have been highly accurate. A better appreciation of this may be gained by comparing the measured data shown in Figures 35 and 41 with the corrected data in Figure 43.

Another interesting question is "What accuracy was obtained on individual points in the continuous plots?" Figure 47 shows the uncorrected data obtained by measuring every fringe (instead of every tenth fringe) in the central part of the shaft for curves 1 and 6. The center 20 fringes in each case were measured. For each curve, the averaged and smoothed but uncorrected curves are shown as dotted lines. Notice that the points do have a random distribution on either side of the centerline but that the statistical means on the right of the centerline are above the dotted lines in both cases, and on the left of the centerline, are both below the dotted line. This is because a discontinuity of about 0.4-μin height occurred at the center cross hair of the reference optical flat. These two curves in themselves would not prove the existence of this discontinuity, but the same condition was noted in all of the 11 negatives analyzed. In all cases, the discontinuity occurred at the centerline of the flat rather than at the centerline of the shaft or straining frame. (These features could not be accurately aligned in the interferometer.) In spite of the central discontinuity, the rms measuring error between the averaged and smoothed curves and the unsmoothed data for both curves was 0.45 μin.

Results and Conclusions

A number of specific conclusions may be drawn from this thesis work.

1. The straining-frame design was satisfactory in all respects.

2. The semiconductor resistance strain gages were ideal for the straining-frame calibration.

3. An rms resolution in strain of about 3×10^{-8} in/in for a single setting of the straining frame was obtained using the semiconductor gages and a conventional SR-4 strain indicator.

4. The optical interference method of plotting elastic curves was laborious, but uncorrected data did give an rms resolution about the mean for the deflection measurements of a single point on the shaft of about 0.4 μin. Even with the most precise interferometers, adequate cross checks to obtain corrections for reference flat sag and photographic distortions would be needed to insure accurate results.

5. The comparison of the straining-frame period calibration obtained with strain gages for a setting of 800 with actual period measurements show agreement within 1 percent. Direct correlation for periods over 30 seconds was not possible because of the presence of electrical motor forces and ground instability.

6. The optical interference verification of the strain-gage calibration was poor (4.5-percent period difference at a 250 setting and 24.1-percent period difference at a 160 setting), not because of any inherent barrier, but primarily because of poor transfer straining-frame design. Another significant source of error was the lack of time to allow perfect setup and strain-indicator drift corrections.

7. Repeatable transfers of loading conditions using strain gages would be possible in a simple transfer frame if better load-point guidance were provided and dead-weight loading were used in place of leaf-spring loading.

8. The average rms deviation (in deflection of four sets of elastic curves) plotted from corrected optical interference data from the best-fit

theoretical curves was 0.099 μin. This degree of fit would not have been possible if there were significant differences between the theoretical and experimental curves.

9. Based on the close agreement between experiment and theory shown in item 8, the accuracy of the correction made to the measured optical interference data must have been better than 0.099 μin rms for each point.

10. The use of theoretical elastic curvatures for future calibrations and analyses is completely justified by the test results.

11. Controlled use of elastic deformations is a valuable technique for obtaining precision adjustments, particularly if these adjustments are of a relative nature and can be monitored by some other suitably sensitive means.

12. Controlled elastic deformation of structural elements can be used to generate certain types of precise geometric shapes, provided proper consideration is given to the elastic properties and yield stresses.

The tangible results of this thesis are to be found in the following contributions to the seismometer development program:

1. The straining frame (proven by 1 year of testing) acted as a forerunner for the final seismometer straining frame and base.

2. The accurate straining-frame calibration, made possible by semiconductor resistance strain gages, has been a great aid in setting up specific periods of vibration and in locating and measuring undesirable axial force fields in the developmental seismometer.

3. The continuous plots of typical elastic curvatures, both measured and theoretical, have allowed nonlinear axial force fields in the seismometer, due to aerodynamic forces, electrical forces, magnetic forces, internal-bearing forces, and gyroscopic effects to be plotted with great accuracy. From this knowledge and other observations, the sources have been located and steps taken to eliminate or reduce these effects.

4. Realistic design goals for the final seismometer design were calculated from the information gained.

In addition to these tangible results, this work has created increased confidence in the final long-period horizontal air-beaming seismometer design.

BIBLIOGRAPHY

1. Oliver, J., "Long Earthquake Waves," Scientific American, Vol. 200, No. 3, March 1959, pp 131-143.

2. Thomson, W. J., "Mechanical Vibrations," Prentice Hall, 1948.

3. Smith, S., "Piezoresistance Effect in Germanium and Silicon," Physical Review, Vol. 94, 1954, pp 42-49.

4. Mason, W. P., and Thurston, R. N., "Use of Piezo-Resistive Materials in the Measurement of Displacement, Force and Torque," Journal of the Acoustical Society of America, Vol. 29, October 1957, pp 1096-1101.

5. Forst, J. J., "Preparation of Piezo-Resistive Transducers from Germanium Rods," Internal Publication at Bell Telephone Laboratories, Inc., Technical Memorandum, February 24, 1958.

6. Vogt, C. O., "The Strainistor-A Semiconductor Strain Sensor," Paper presented at the Sixth National Flight Test Instrumentation Symposium, San Diego, California, May 2-5, 1960.

7. Herring, C., "Transport Properties of Many-Valley Semiconductor," Bell System Technical Journal, Vol. 34, pp 251-258.

8. Keys, R. W., "Temperature Dependence of the Elastoresistance in N-Type Germanium," Physical Review, Vol. 100, 1955, p 1104.

9. Forst, J. J., and Geyling, F. T., "Applications of Semiconductor Transducers in Strain Gages and Rigid Dynamometer," Proceedings S.E.S.A., Vol. XVII, No. 1, 1959, pp 143-148.

10. Perry, C. C., and Lissner, H. R., "Strain Gage Primer," McGraw-Hill, 1955.

11. Ausman, J. S., and Wildmann, M., "How to Design Hydrodynamic Gas Bearings," Product Engineering, November 25, 1957, pp 103-106.

12. Sternlicht, B., and Elwell, R. C., "Theoretical and Experimental Analysis of Hydrodynamic Gas Lubricated Journal Bearings," Transactions of A.S.M.E., Vol. 80, No. 4, May 1958, pp 865-875.

13. Born, M., and Wolf, E., "Principles of Optics (Electromagnetic Theory of Propogation, Interference and Diffraction of Light)," Pergamon Press, 1959, pp 259-368.

l 82.-87 omitted for security reasons

APPENDIX II

STRAINING FRAME PARTS DRAWINGS

See Figures II-1 through II-12 for drawings of the straining frame parts.

NOTES

1. STRESS RELIEVE BEFORE MACHINING.
2. CENTERLINE TO BE PERPENDICULAR TO DATUM CENTERLINE X AND BISECT THE MEASURED DISTANCE BETWEEN SURFACE "A" AND SURFACE "B".

PART NO. TABLE	REVISIONS					
	SYM	ZONE	DESCRIPTION	DATE	APPROVED CHK	ENG
	1			6/3/60		

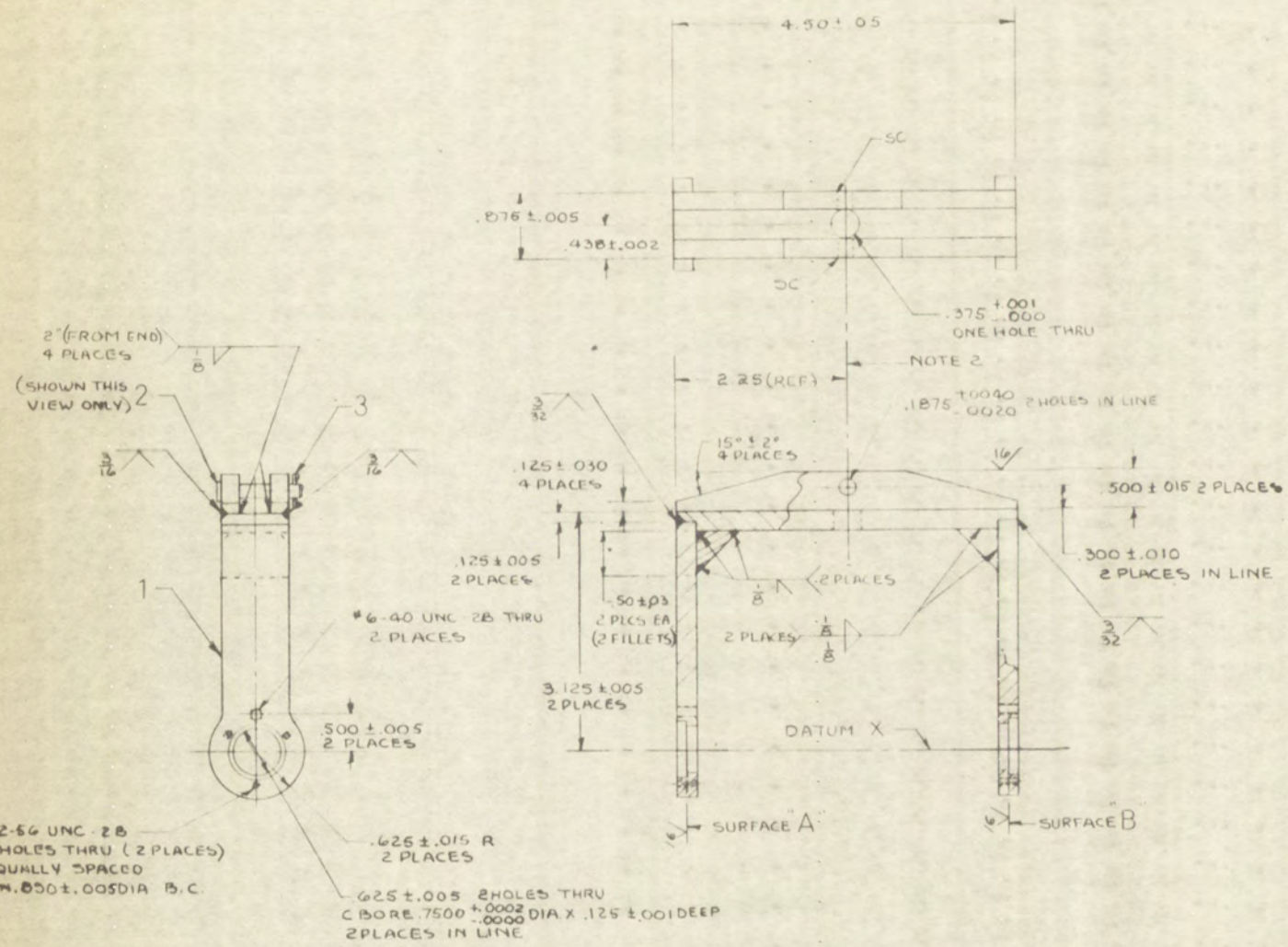

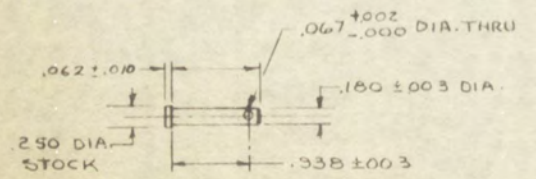

DETAIL - ITEM 2

ITEM	ZONE	NOTE	PART NO.	MFR'S. NO.	DESCRIPTION	MATERIAL	MATERIAL SPEC.
3					PIN, COTTER 1/16 DIA X 3/8 (808942)		
2					PIN	STEEL (1020) C.R	
1					FRAME	STEEL (1020) HOT ROLLED .250 THK STOCK	

LIST OF MATERIAL

PART CLASSIFICATION — DWG. CLASSIFICATION —

REQUIRED PER NOTED ASSY. (✓ DENOTES AS REQD)

N12211
N12210
NEXT ASSY
APPLICATION

MATERIAL: L/M
ADDITIVE FINISH
C* NOTATION IS FOR DESIGN AGENCY INFORMATION ONLY — NOT REVIEWED

UNLESS OTHERWISE SPECIFIED
DIMENSIONS ARE IN INCHES.
LIMITS APPLY OVER NON-PAINTED FINISHES.
SURFACE ROUGHNESS HEIGHT RATING EXPRESSED AS MICRO-INCHES.
LIMITS OF ACCEPTABLE WORKMANSHIP ARE DEFINED IN SC-7013 (5M).
FOR EXPLANATION OF TOLERANCES OF POSITION AND FORM, INCLUDING RMC, SEE SC-7016 (5M).

DRWN R J — CHKD — APPD — DWG — INITIALS
CONTRACTOR PREPARED

TITLE: FRAME, SHAFT

MFR'S. DWG. NO.

SCALE FULL — RAW STK WT LBS — UNIT WT LBS

SUPERSEDES 5Y DWG. SIZE D DWG. REV. 1

DWG. NO. N 12212

SHEET 1 OF 1

PRINTED IN U.S.A. SC-6402-D (3-69)

DWG. NO. N12212

68

NOTES

1. STRESS RELIEVE BEFORE MACHINING.

PART NO. TABLE

REVISIONS					
SYM.	ZONE	DESCRIPTION	DATE	APPROVED CHK	APPROVED ENG
1			6/3/60		

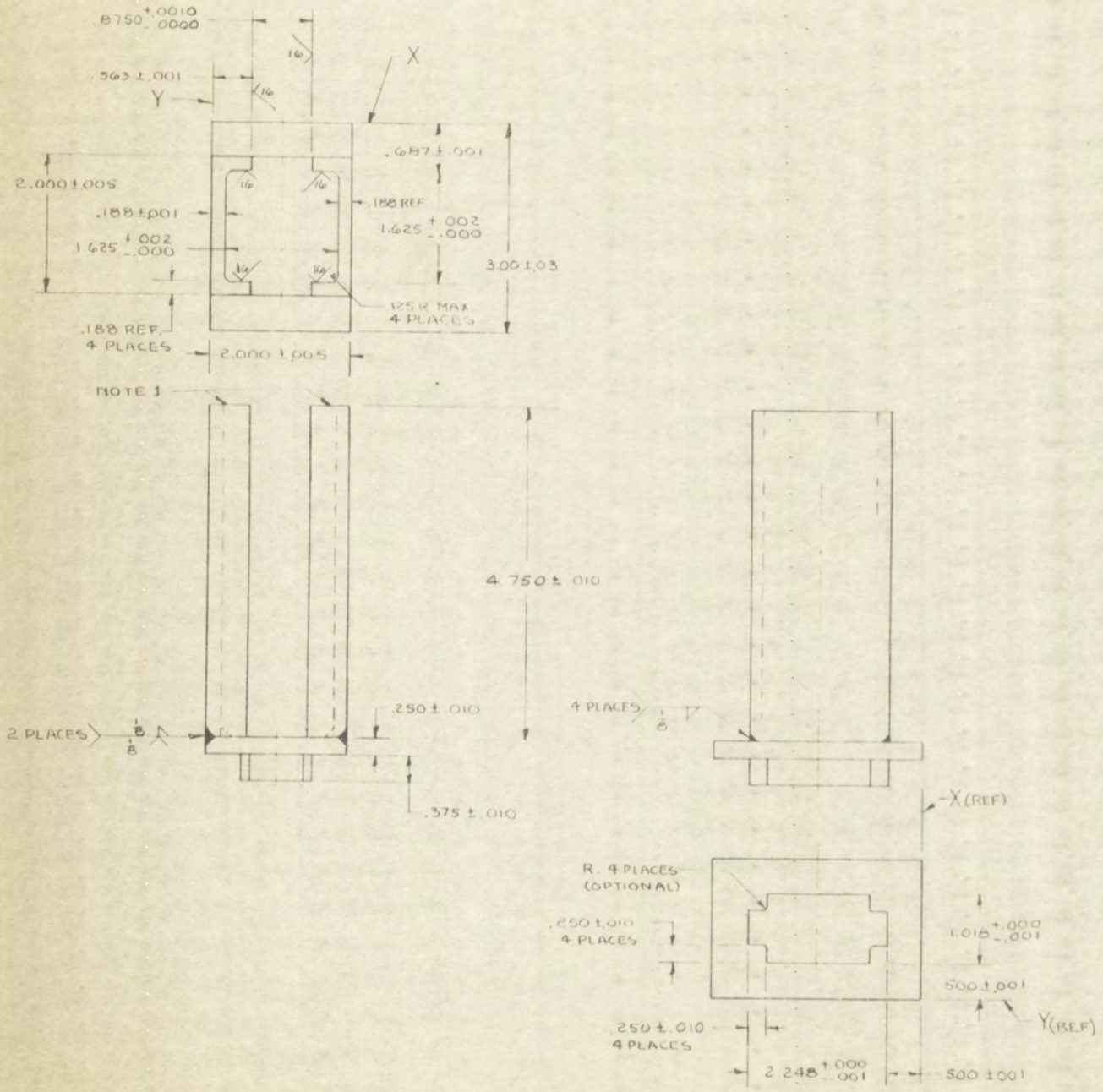

PART NO.	MFR'S. NO.	DESCRIPTION	MATERIAL	MATERIAL SPEC.		NOTE	ZONE	ITEM

LIST OF MATERIAL

PART CLASSIFICATION	DWG. CLASSIFICATION
—	—

REQUIRED PER NOTED ASSY. (✓ DENOTES AS REQD)	MATERIAL	UNLESS OTHERWISE SPECIFIED	DRWN RS	CHKD H	TITLE
	STEEL (1020) HOT ROLLED	DIMENSIONS ARE IN INCHES. LIMITS APPLY OVER NON-PAINTED FINISHES. SURFACE ROUGHNESS HEIGHT RATING EXPRESSED AS MICRO-INCHES. LIMITS OF ACCEPTABLE WORKMANSHIP ARE DEFINED IN SC-7012 (SP) FOR EXPLANATION OF TOLERANCES OF POSITION AND FORM, INCLUDING MMC, SEE SC-7016 (SP)	APPD. / DES. / INITIAL	CONTRACTOR PREPARED	FRAME, SPRING
N 2210 NEXT ASSY	ADDITIVE FINISH	C* NOTATION IS FOR DESIGN AGENCY INFORMATION ONLY — NOT REVIEWED			SUPERSEDES 5Y DWG SIZE D SHT 1
APPLICATION			DRWG	CHKD	MFR'S. DWG. NO.
			SCALE FULL	RAW STK WT LBS	UNIT WT LBS
					DWG. NO. N12213
					SHEET 1 OF 1

DRAWING SIZE

PRINTED IN U.S.A. SCRAID-D 10-961 K&E 196 PHOENIX

DWG. NO. N12213

06

OUTSIDE DIA	1.500
INSIDE DIA	1.146
FREE LENGTH	AS SHOWN
TYPE ENDS	AS SHOWN
NO. ACTIVE COILS	5 MIN.

6/3/60

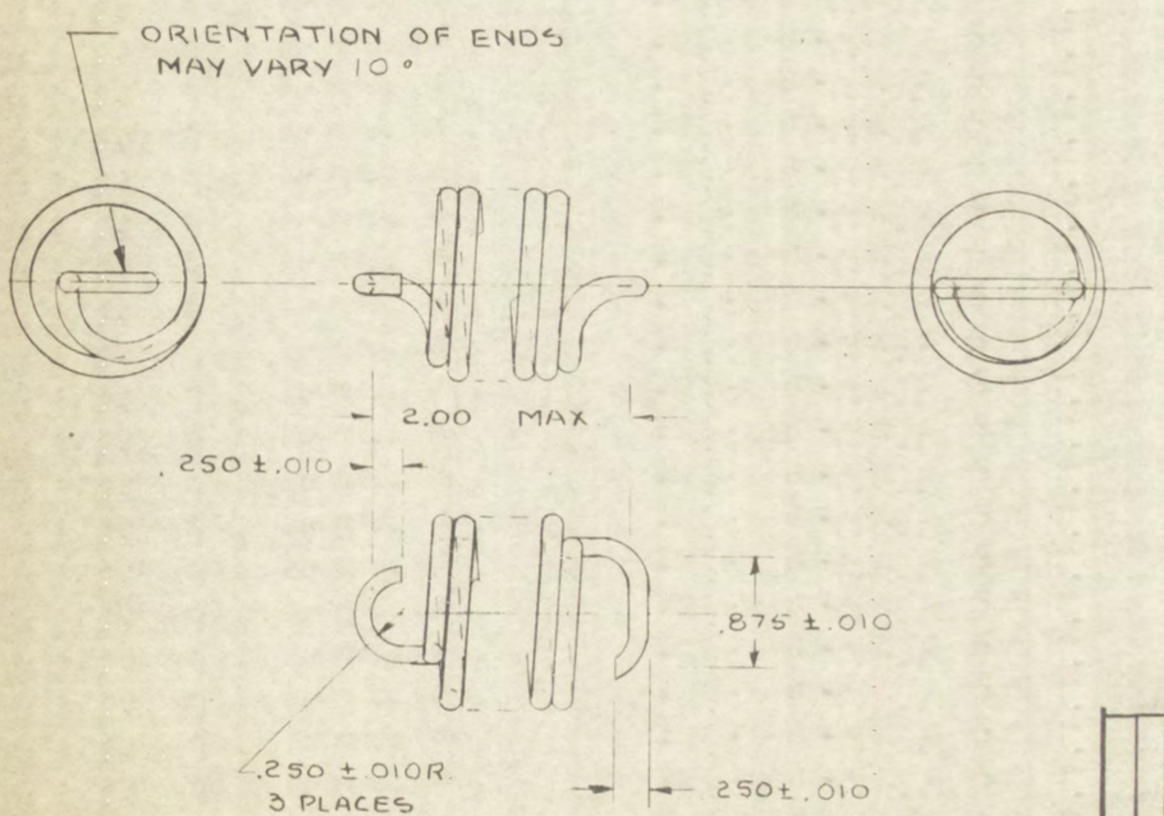

PART NO.	MFR'S. NO.	DESCRIPTION	MATERIAL	MATERIAL SPEC.	NOTE	ZONE	ITEM
LIST OF MATERIAL							

PART CLASSIFICATION — DWG. CLASSIFICATION

DRAWING SIZE

REQUIRED PER NOTED ASSY. (✓ DENOTES AS REQD)

NEXT ASSY: N12210

APPLICATION

MATERIAL: HARD DRAWN SPRING WIRE A.S.20 ASTM. A 227-47

ADDITIVE FINISH

C* NOTATION IS FOR DESIGN AGENCY INFORMATION ONLY

NOT REVIEWED

UNLESS OTHERWISE SPECIFIED
DIMENSIONS ARE IN INCHES.
LIMITS APPLY OVER NON-PAINTED FINISHES.
SURFACE ROUGHNESS HEIGHT RATING EXPRESSED AS MICRO-INCHES.
LIMITS OF ACCEPTABLE WORKMANSHIP ARE DEFINED IN SC-7012 (SP)
FOR EXPLANATION OF TOLERANCES OF POSITION AND FORM, INCLUDING MMC. SEE SC-7016 (SP)

DRWN: RJ — CHKD
APPD — ORG — INITIALS
DES
STR
MATL
MFG
DFTG

CONTRACTOR PREPARED: DRWN — CHKD — ENGR

TITLE: SPRING, TENSION

MFR'S. DWG. NO.

SCALE: FULL — RAW STK WT LBS — UNIT WT LBS

SUPERSEDES

5Y — DWG. SIZE: C — DWG. ISS.: 1

DWG. NO. N 12214

SHEET 1 OF 1

PRINTED IN U.S.A. SC 8402-C 3-59

DWG. NO. N12214

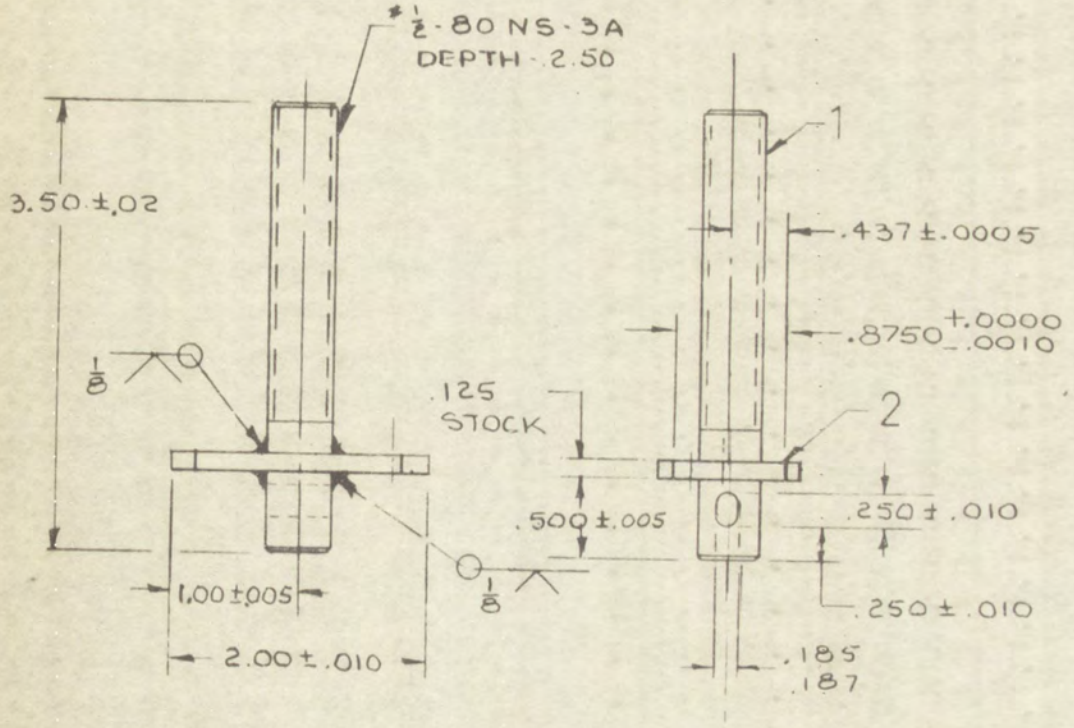

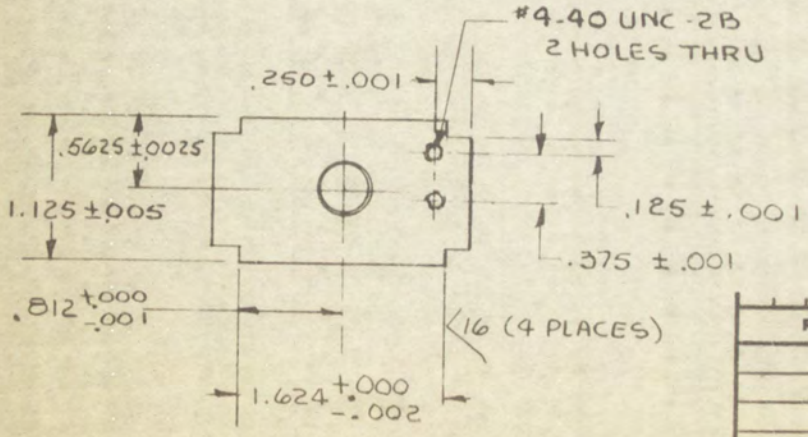

PART NO.	MFR'S. NO.	DESCRIPTION	MATERIAL	MATERIAL SPEC.	NOTE	ZONE	ITEM
		PLATE	STEEL (1020) HOT ROLLED				2
		SHAFT					1

LIST OF MATERIAL

PART CLASSIFICATION

DWG. CLASSIFICATION

DRAWING SIZE

REQUIRED PER NOTED ASSY. (✓ DENOTES AS REQD)

MATERIAL: L/M

ADDITIVE FINISH

N12210

NEXT ASSY

APPLICATION

C* NOTATION IS FOR DESIGN AGENCY INFORMATION ONLY

NOT REVIEWED

UNLESS OTHERWISE SPECIFIED

DIMENSIONS ARE IN INCHES.

LIMITS APPLY OVER NON-PAINTED FINISHES.

SURFACE ROUGHNESS HEIGHT RATING EXPRESSED AS MICRO-INCHES.

LIMITS OF ACCEPTABLE WORKMANSHIP ARE DEFINED IN SC-7012 (SP)

FOR EXPLANATION OF TOLERANCES OF POSITION AND FORM, INCLUDING MMC, SEE SC-7016 (SP)

DRWN RJ CHKD

APPD	DATE	INITIALS
DES		
STR		
MATL		
MFG		
QPTG		

CONTRACTOR PREPARED

DRWN | CHKD | ENGR

TITLE: SHAFT THREADED

MFR'S. DWG. NO.

SCALE FULL | RAW STK WT LBS | UNIT WT LBS

SUPERSEDES

5Y | DWG. SIZE C | DWG. REV. 1

DWG. NO. N 12216

SHEET 1 OF 1

PRINTED IN U.S.A. SC 8403-C 3-66

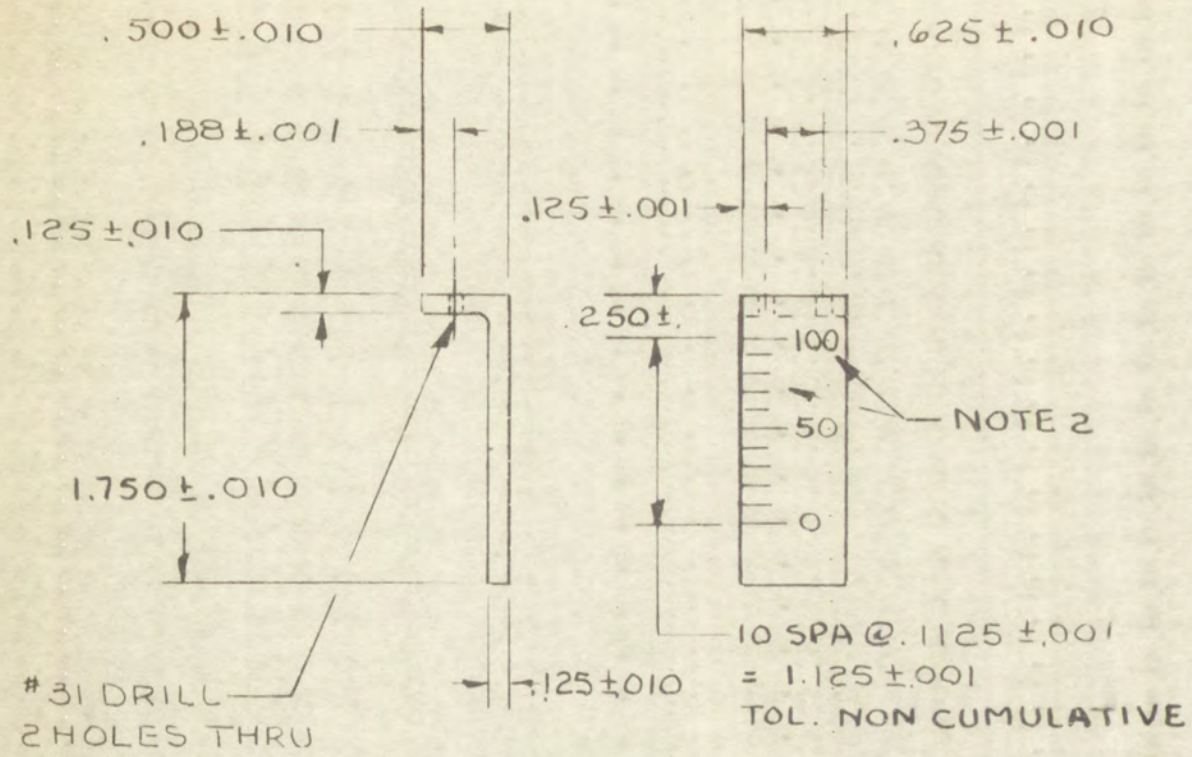

PART NO. TABLE	REVISIONS				
	SYM.	DESCRIPTION	DATE	APPROVED CHK	APPROVED ENG
	1		6/3/60		

NOTES

1. BRASS, SHEET OR STRIP (65-35) PER QQ-B-613.
2. ENGRAVE CHARACTERS, 1/8 HIGH, GOTHIC, .015 STROKE WIDTH, AND GRADUATION MARKS .006 WIDE, .250 LONG FOR MAJOR DIVISIONS AND .125 LONG FOR MINOR DIVISIONS. FILL WITH BLACK AND POLISH.

PART NO.	MFR'S. NO.	DESCRIPTION	MATERIAL	MATERIAL SPEC.		NOTE	ZONE	ITEM

LIST OF MATERIAL

DRAWING SIZE

PART CLASSIFICATION	DWG. CLASSIFICATION
—	—

REQUIRED PER NOTED ASSY. (✓ DENOTES AS REQD)

N 12210
NEXT ASSY
APPLICATION

MATERIAL: SEE NOTES

ADDITIVE FINISH

C* NOTATION IS FOR DESIGN AGENCY INFORMATION ONLY

NOT REVIEWED

UNLESS OTHERWISE SPECIFIED

- DIMENSIONS ARE IN INCHES.
- LIMITS APPLY OVER NON-PAINTED FINISHES.
- SURFACE ROUGHNESS HEIGHT RATING EXPRESSED AS MICRO-INCHES.
- LIMITS OF ACCEPTABLE WORKMANSHIP ARE DEFINED IN SC-7012 (SP)
- FOR EXPLANATION OF TOLERANCES OF POSITION AND FORM, INCLUDING MMC, SEE SC-7016 (SP)

DRWN	R J	CHKD	
APPD	ORG	INITIALS	
DES			
STR			
MATL			
MFG			
DFTG			

CONTRACTOR PREPARED

DRWN	CHKD	ENGR

TITLE: CALIBRATION, BRACKET

MFR'S. DWG. NO.

SCALE FULL | RAW STK WT LBS | UNIT WT LBS

SUPERSEDES

5Y | DWG. SIZE B | DWG. REV. 1

DWG. NO. N 12217

SHEET 1 OF 1

PRINTED IN U.S.A. SC5402-B (3-59)

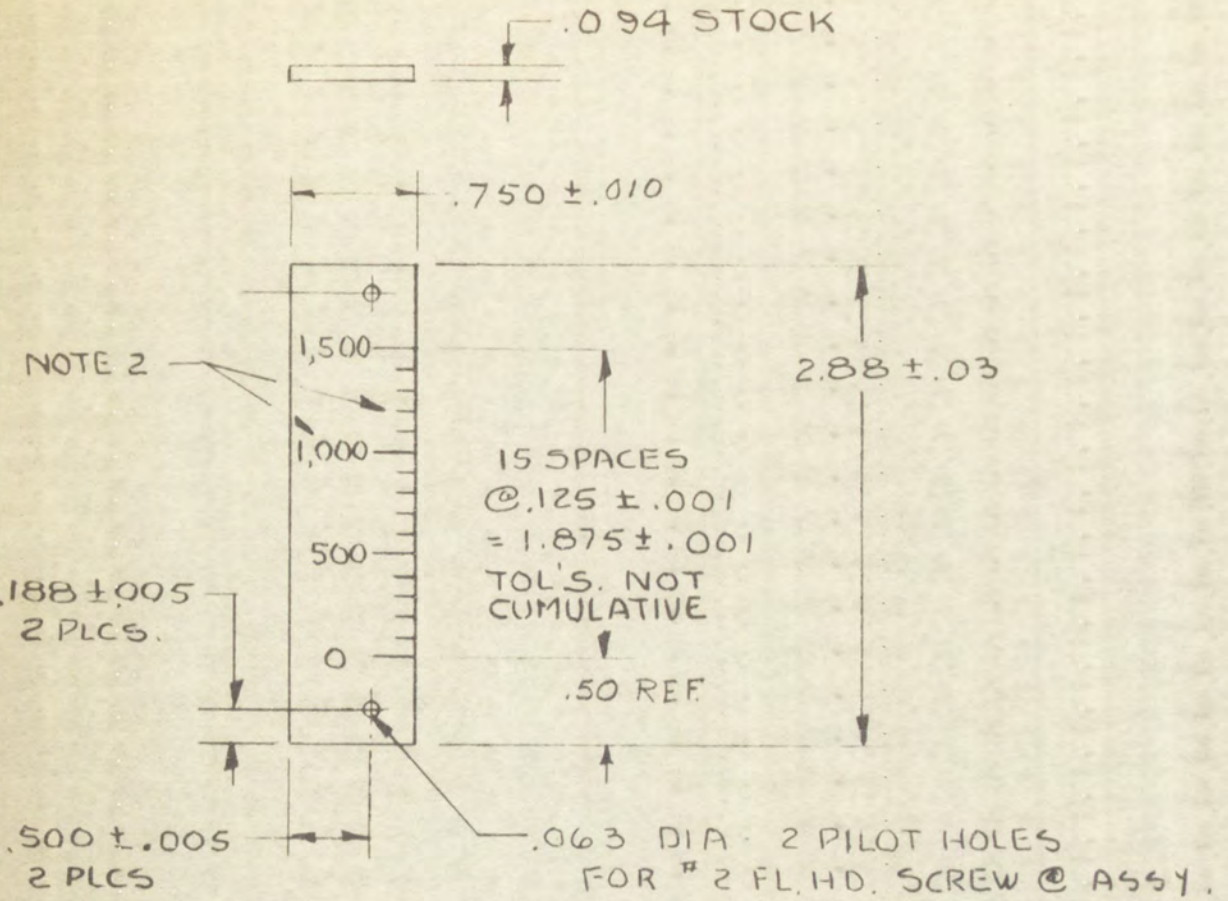

PART NO. TABLE	REVISIONS				
	SYM.	DESCRIPTION	DATE	APPROVED CHK	APPROVED ENG
	1		6/3/60		

NOTES

1. BRASS, SHEET OR STRIP (65-35) PER QQ-B-613.
2. ENGRAVE CHARACTERS, 1/8 HIGH, GOTHIC, .015 STROKE WIDTH, AND GRADUATION MARKS .006 WIDE, .250 LONG FOR MAJOR DIVISIONS AND .125 LONG FOR MINOR DIVISIONS. FILL WITH BLACK AND POLISH.

PART NO.	MFR'S. NO.	DESCRIPTION	MATERIAL	MATERIAL SPEC.		NOTE	ZONE	ITEM

LIST OF MATERIAL

PART CLASSIFICATION: ———

DWG. CLASSIFICATION: ———

DRAWING SIZE

REQUIRED PER NOTED ASSY. (✓ DENOTES AS REQD)

N 12210
NEXT ASSY
APPLICATION

MATERIAL: SEE NOTES

ADDITIVE FINISH

C* NOTATION IS FOR DESIGN AGENCY INFORMATION ONLY

NOT REVIEWED

UNLESS OTHERWISE SPECIFIED

DIMENSIONS ARE IN INCHES.

LIMITS APPLY OVER NON-PAINTED FINISHES.

SURFACE ROUGHNESS HEIGHT RATING EXPRESSED AS MICRO-INCHES.

LIMITS OF ACCEPTABLE WORKMANSHIP ARE DEFINED IN SC-7012 (SP)

FOR EXPLANATION OF TOLERANCES OF POSITION AND FORM, INCLUDING MMC, SEE SC-7016 (SP)

DRWN	RJ	CHKD	
APPD	ORG	INITIALS	
DES			
STR			
MATL			
MFG			
DFTG			

CONTRACTOR PREPARED

DRWN	CHKD	ENGR

TITLE: CALIBRATION, PLATE

MFR'S. DWG. NO.

SCALE: FULL | RAW STK WT LBS | UNIT WT LBS

SUPERSEDES

5Y | DWG. SIZE B | DWG. ISS. 1

DWG. NO. N12218

SHEET 1 OF 1

PRINTED IN U.S.A. SCS402-B (3-59)

94

GRADUATION MARKS .006 WIDE, .250 LONG FOR MAJOR DIVISIONS AND .125 LONG FOR MINOR DIVISIONS. FILL WITH BLACK AND POLISH.

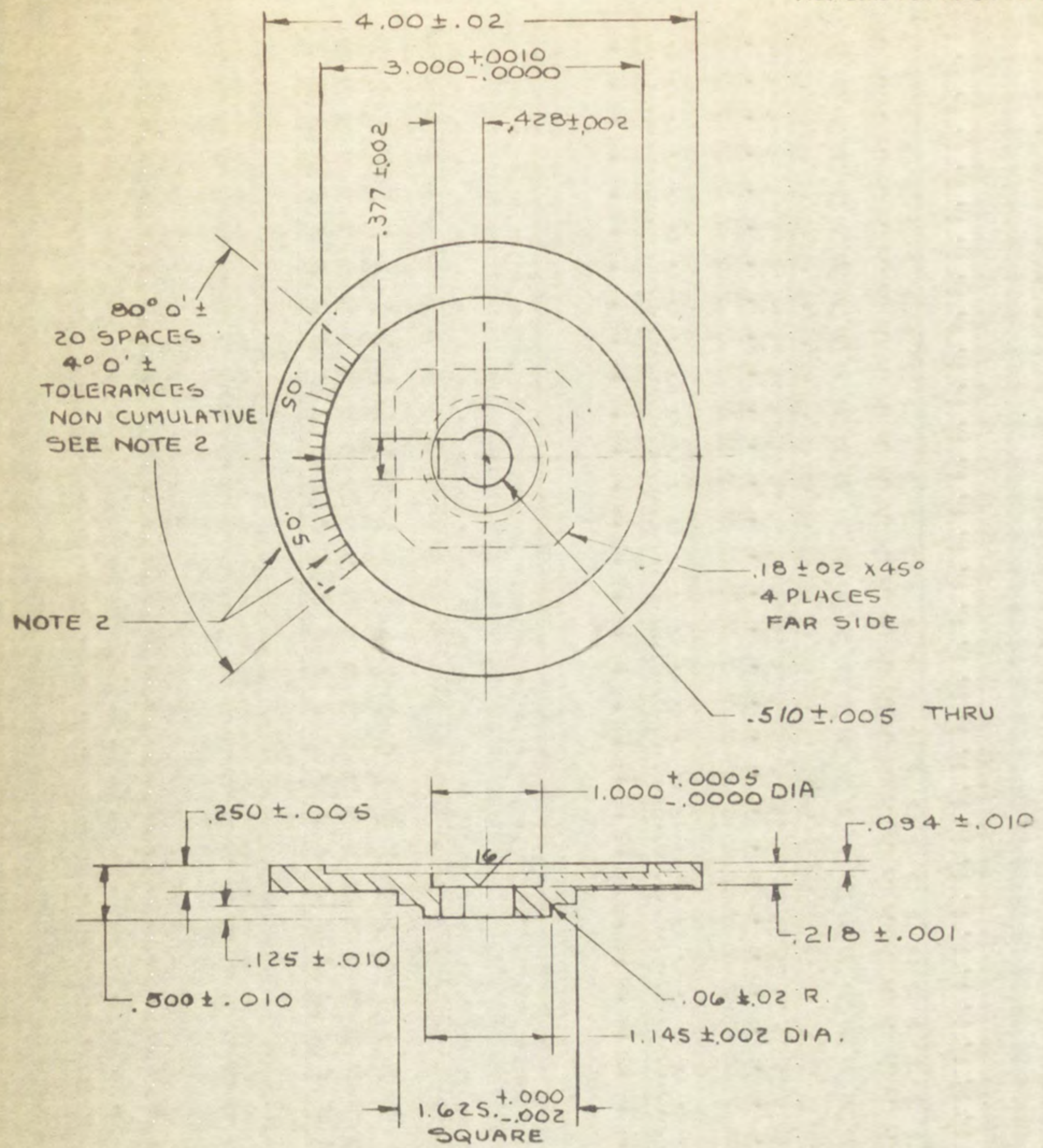

PART NO. | MFR'S. NO. | DESCRIPTION | MATERIAL | MATERIAL SPEC. | NOTE | ZONE | ITEM

LIST OF MATERIAL

PART CLASSIFICATION | DWG. CLASSIFICATION

DRAWING SIZE

REQUIRED PER NOTED ASSY. (✓ DENOTES AS REQD)

NEXT ASSY: N12211, N12210

APPLICATION

MATERIAL: STEEL (1020) COLD ROLLED

ADDITIVE FINISH

C* NOTATION IS FOR DESIGN AGENCY INFORMATION ONLY

NOT REVIEWED

UNLESS OTHERWISE SPECIFIED
DIMENSIONS ARE IN INCHES.
LIMITS APPLY OVER NON-PAINTED FINISHES.
SURFACE ROUGHNESS HEIGHT RATING EXPRESSED AS MICRO-INCHES.
LIMITS OF ACCEPTABLE WORKMANSHIP ARE DEFINED IN SC-7012 (SP)
FOR EXPLANATION OF TOLERANCES OF POSITION AND FORM, INCLUDING MISC. SEE SC-7010 (SP)

DRWN: RJ | CHKD: H

CONTRACTOR PREPARED

TITLE: COVER PLATE

MFR'S. DWG. NO.

SCALE: FULL | RAW STK WT LBS | UNIT WT LBS

SUPERSEDES

5Y | DWG. SIZE: C | DWG. NO. 1

DWG. NO. N 12219

SHEET 1 OF 1

PRINTED IN U.S.A. SC 8403-C 2-60

N12219

NOTES

1. ENGRAVE CHARACTERS, 1/8 HIGH, GOTHIC, .015 STROKE WIDTH, AND GRADUATION MARKS .006 WIDE, .250 LONG FOR MAJOR DIVISIONS AND .125 LONG FOR MINOR DIVISIONS. FILL WITH BLACK AND POLISH.

PART NO. TABLE	REVISIONS				
	SYM.	ZONE	DESCRIPTION	DATE	APPROVED CHK / ENG
	1			6/9/60	

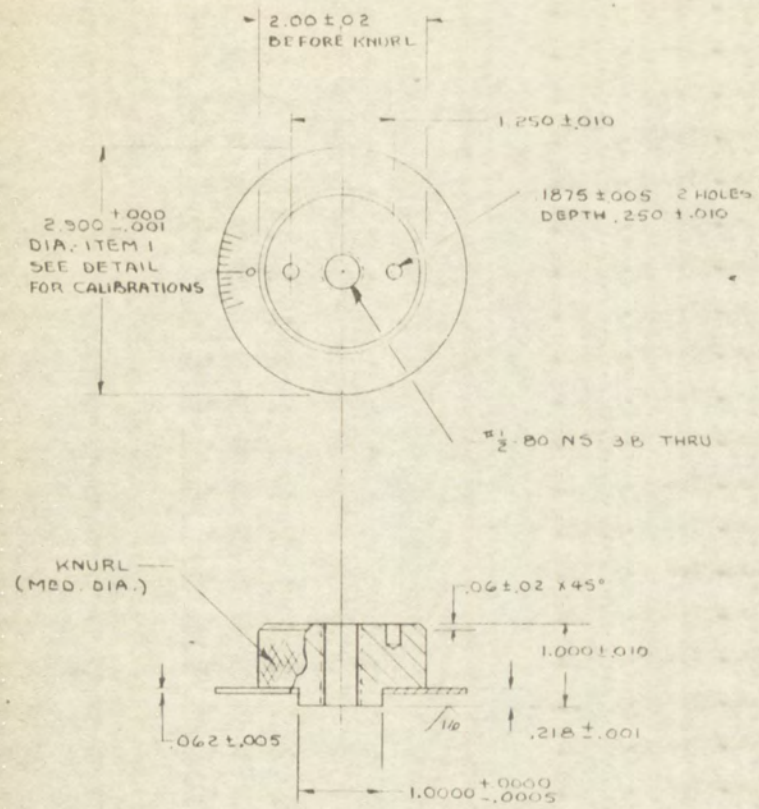

DETAIL ITEM 1

PART NO.	MFR'S. NO.	DESCRIPTION	MATERIAL	MATERIAL SPEC.		NOTE	ZONE	ITEM
		KNOB	STEEL (1020) COLD ROLLED					2
		DIAL	BRASS, SHEET OR STRIP (65-35)	PER QQ-B-613				1

LIST OF MATERIAL

PART CLASSIFICATION — DWG. CLASSIFICATION —

REQUIRED PER NOTED ASSY. (✓ DENOTES AS REQD)

N 12211
N 12210
NEXT ASSY
APPLICATION

MATERIAL L/M
ADDITIVE FINISH
C* NOTATION IS FOR DESIGN AGENCY INFORMATION ONLY
NOT REVIEWED

UNLESS OTHERWISE SPECIFIED
DIMENSIONS ARE IN INCHES.
LIMITS APPLY OVER NON-PAINTED FINISHES.
SURFACE ROUGHNESS HEIGHT RATING EXPRESSED AS MICRO-INCHES.
LIMITS OF ACCEPTABLE WORKMANSHIP ARE DEFINED IN SC-7012 (SP)
FOR EXPLANATION OF TOLERANCES OF POSITION AND FORM, INCLUDING MMC, SEE SC-7010 (SP)

DRWN | CHKD
INITIALS
CONTRACTOR PREPARED
DRWN | CHKD | ENGR

TITLE: KNOB
MFR'S. DWG. NO.
SCALE: FULL | RAW STK WT LBS | UNIT WT LBS

SUPERSEDES
5Y DWG. SIZE D DWG. REV. 1
DWG. NO. N 12220
SHEET 1 OF 1

PRINTED IN U.S.A. SC-9000-D (5-66) P.O.E. 1496 PHOENIX

96

1			6/3/60		
2	LENGTH WAS 1.00	RJ	6/15/60		M

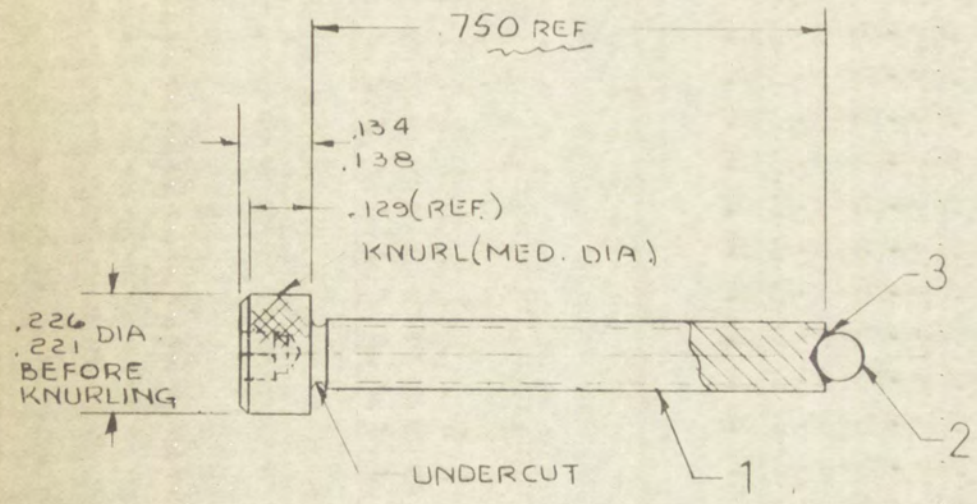

✓			ADHESIVE				2		3
1	MS134378		BALL, STEEL (.0938 DIA)						2
1	MS 35457-10		SCREW, MACH, SOC HD, CAP. (BS 3705)				1		1
PART NO.	MFR'S. NO.		DESCRIPTION	MATERIAL	MATERIAL SPEC.		NOTE	ZONE	ITEM

LIST OF MATERIAL

PART CLASSIFICATION

DWG. CLASSIFICATION

DRAWING SIZE

REQUIRED PER NOTED ASSY. (✓ DENOTES AS REQD)

MATERIAL: L/M

ADDITIVE FINISH

N12211
N12210
NEXT ASSY
APPLICATION

C* NOTATION IS FOR DESIGN AGENCY INFORMATION ONLY

NOT REVIEWED

UNLESS OTHERWISE SPECIFIED

DIMENSIONS ARE IN INCHES.

LIMITS APPLY OVER NON-PAINTED FINISHES.

SURFACE ROUGHNESS HEIGHT RATING EXPRESSED AS MICRO-INCHES.

LIMITS OF ACCEPTABLE WORKMANSHIP ARE DEFINED IN SC-7012 (SP)

FOR EXPLANATION OF TOLERANCES OF POSITION AND FORM, INCLUDING MMC, SEE SC-7016 (SP)

DRWN	RJ	CHKD		
APPD	DRG	INITIALS		
DES				
STR				
MATL				
MFG				
QMTG				

CONTRACTOR PREPARED

DRWN 4/1 CHKD ENGR

TITLE: SCREW, BALANCING

MFR'S. DWG. NO.

SCALE 4/1 RAW STK WT LBS UNIT WT LBS

SUPERSEDES

5Y DWG. SIZE C DWG. REV. 1

DWG. NO. N 12221

SHEET 1 OF 1

PRINTED IN U.S.A. SC 5402-C 3-59

N12221

97

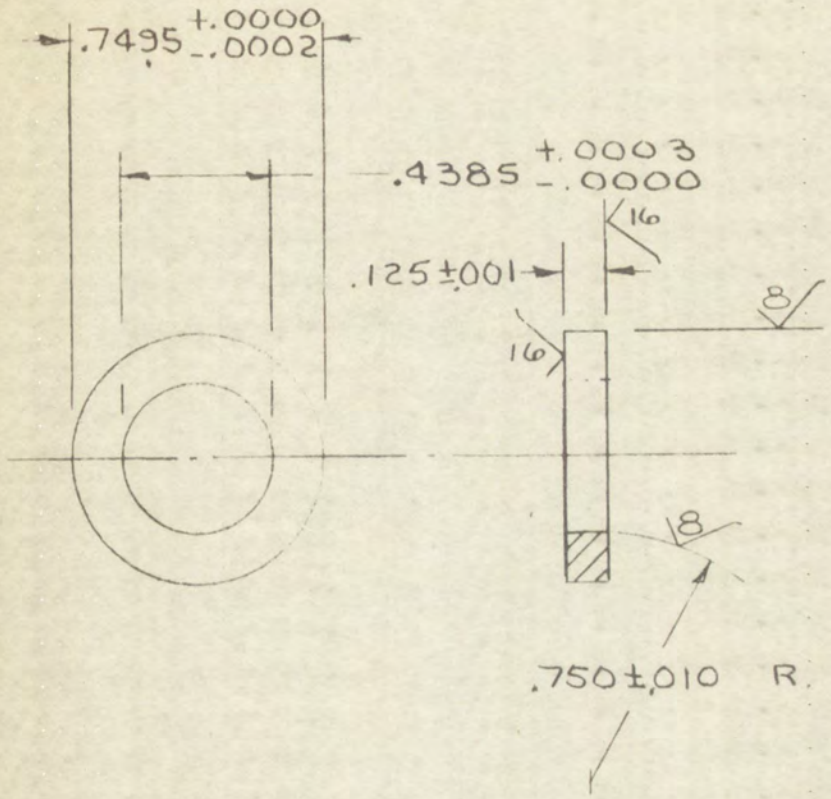

PART NO. TABLE	REVISIONS				
	SYM.	DESCRIPTION	DATE	APPROVED CHK	APPROVED ENG
	1		6/3/60		

NOTES

PART NO.	MFR'S. NO.	DESCRIPTION	MATERIAL	MATERIAL SPEC.		NOTE	ZONE	ITEM

LIST OF MATERIAL

DRAWING SIZE

PART CLASSIFICATION

DWG. CLASSIFICATION

REQUIRED PER NOTED ASSY. (✓ DENOTES AS REQD)

MATERIAL: STEEL (1020) COLD ROLLED

ADDITIVE FINISH

N12210 NEXT ASSY

APPLICATION

C* NOTATION IS FOR DESIGN AGENCY INFORMATION ONLY

NOT REVIEWED

UNLESS OTHERWISE SPECIFIED

DIMENSIONS ARE IN INCHES.

LIMITS APPLY OVER NON-PAINTED FINISHES.

SURFACE ROUGHNESS HEIGHT RATING EXPRESSED AS MICRO-INCHES.

LIMITS OF ACCEPTABLE WORKMANSHIP ARE DEFINED IN SC-7012 (SP)

FOR EXPLANATION OF TOLERANCES OF POSITION AND FORM, INCLUDING MMC, SEE SC-7016 (SP)

DRWN	RJ	CHKD	
APPD	ORG	INITIALS	
DES			
STR			
MATL			
MFG			
DFTG			

CONTRACTOR PREPARED

DRWN	CHKD	ENGR

TITLE: BEARING

MFR'S. DWG. NO.

SCALE 2/1 | RAW STK WT LBS | UNIT WT LBS

SUPERSEDES

5Y | DWG. SIZE B | DWG. REV. 1

DWG. NO. N12223

SHEET 1 OF 1

				CHK	ENG
1		6/15/60			

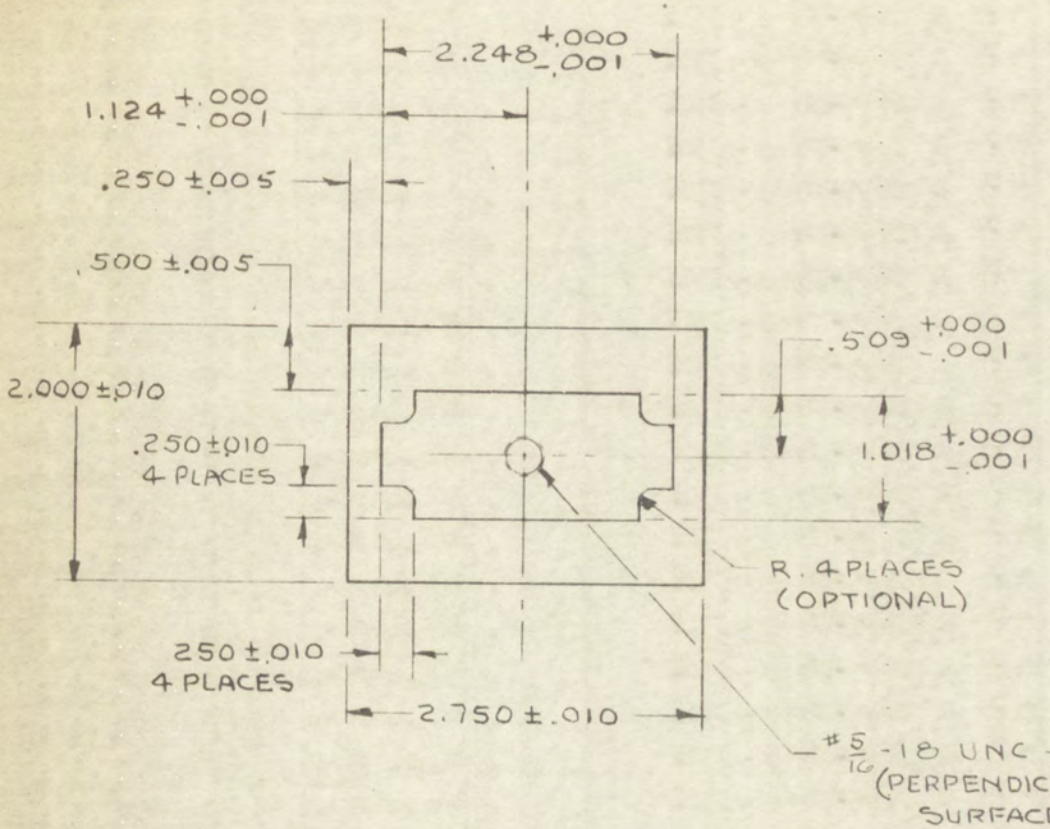

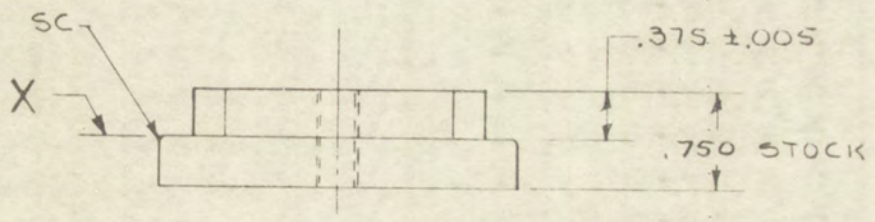

PART NO.	MFR'S. NO.	DESCRIPTION	MATERIAL	MATERIAL SPEC.		NOTE	ZONE	ITEM

LIST OF MATERIAL

PART CLASSIFICATION —

DWG. CLASSIFICATION —

DRAWING SIZE

REQUIRED PER NOTED ASSY. (✓ DENOTES AS REQD)

N12211
NEXT ASSY

APPLICATION

MATERIAL
STEEL (1020)
COLD ROLLED

ADDITIVE FINISH

C* NOTATION IS FOR DESIGN AGENCY INFORMATION ONLY

NOT REVIEWED

UNLESS OTHERWISE SPECIFIED

DIMENSIONS ARE IN INCHES.

LIMITS APPLY OVER NON-PAINTED FINISHES.

SURFACE ROUGHNESS HEIGHT RATING EXPRESSED AS MICRO-INCHES.

LIMITS OF ACCEPTABLE WORKMANSHIP ARE DEFINED IN SC-7012 (SP)

FOR EXPLANATION OF TOLERANCES OF POSITION AND FORM, INCLUDING MMC, SEE SC-7016 (SP)

DRWN RJ CHKD

APPD	ORG	INITIALS
DES		
STR		
MATL		
MFG		
DFTG		

CONTRACTOR PREPARED

DRWN | CHKD | ENGR

TITLE
BASE, SHAFT

MFR'S. DWG. NO.

SCALE FULL | RAW STK WT LBS | UNIT WT LBS

SUPERSEDES

5Y | DWG. SIZE C | DWG. REV. 1

DWG. NO.
N 12226

SHEET 1 OF 1

PRINTED IN U.S.A. SC 5402-C 3-59

DWG. NO. N12226

NOTES

1. MATERIAL: STEEL (1020) HOT ROLLED PLATE PER QQ-S-741(3) TYPE II GRADE A .250 STOCK UNLESS OTHERWISE NOTED.
2. STRESS RELIEVE BEFORE MACHINING.

PART NO. TABLE

REVISIONS				APPROVED	
SYM.	ZONE	DESCRIPTION	DATE	CHK	ENG
1			6/11/65		

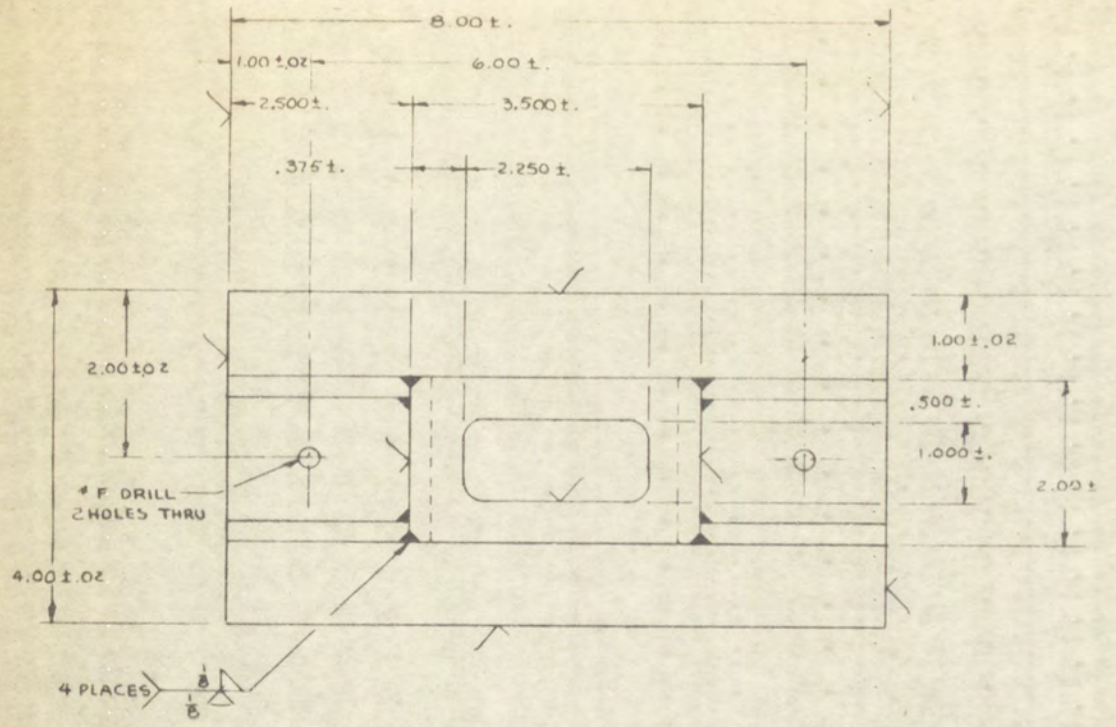

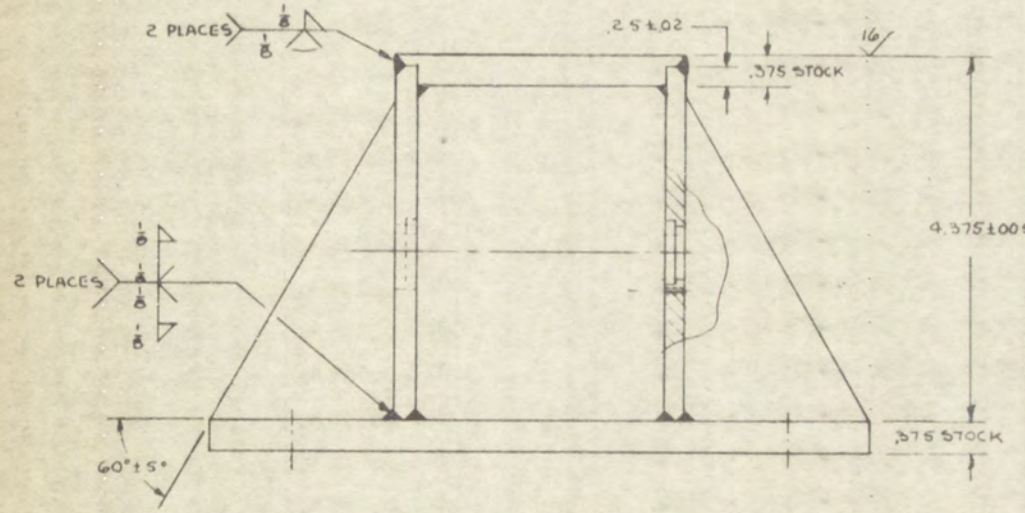

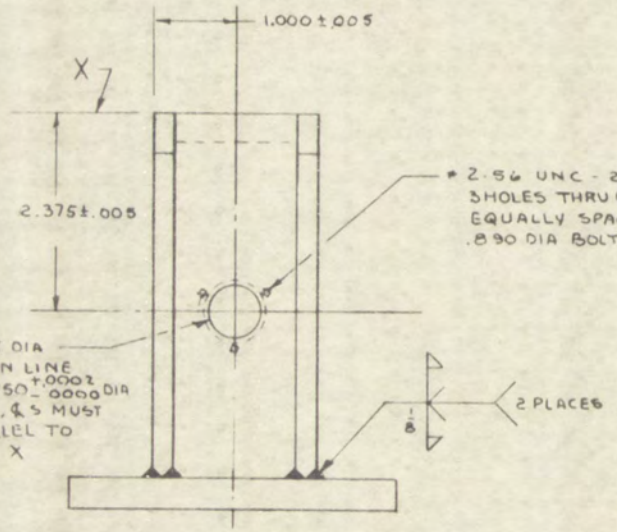

PART NO.	MFR'S. NO.	DESCRIPTION	MATERIAL	MATERIAL SPEC.		NOTE	ZONE	ITEM

LIST OF MATERIAL

PART CLASSIFICATION	DWG. CLASSIFICATION
—	—

REQUIRED PER NOTED ASSY. (✓ DENOTES AS REQD)

DRAWING SIZE

MATERIAL: SEE NOTES

ADDITIVE FINISH

NEXT ASSY

APPLICATION

C* NOTATION IS FOR DESIGN AGENCY INFORMATION ONLY

NOT REVIEWED

UNLESS OTHERWISE SPECIFIED
DIMENSIONS ARE IN INCHES.
LIMITS APPLY OVER NON-PAINTED FINISHES.
SURFACE ROUGHNESS HEIGHT RATING EXPRESSED AS MICRO-INCHES.
LIMITS OF ACCEPTABLE WORKMANSHIP ARE DEFINED IN SC-7910 (ISP)
FOR EXPLANATION OF TOLERANCES OF POSITION AND FORM, INCLUDING MMC, SEE SC-7910 (ISP)

DRWN RJ CHKD

CONTRACTOR PREPARED

TITLE: BASE

MFR'S. DWG. NO.

SCALE FULL | RAW STK WT LBS | UNIT WT LBS

SUPERSEDES 5Y DWG. SIZE D SHTS. 1

DWG. NO. N 12230

SHEET 1 OF 1

PRINTED IN U.S.A. SC8400-0 (8-65) 5.65 10M PHOENIX

8 7 6 5 4 3 2 1

100

APPENDIX III

DERIVATION OF THEORETICAL CURVES (CONSIDERING THE LONGITUDINAL SHAFT CENTER AS ZERO)

Due to the symmetry of loading, only the right half of each curve will be evaluated.

Deflection Due to Spring Force, F_S

The diagrams for loading, vertical shear force, and bending moment are shown below.

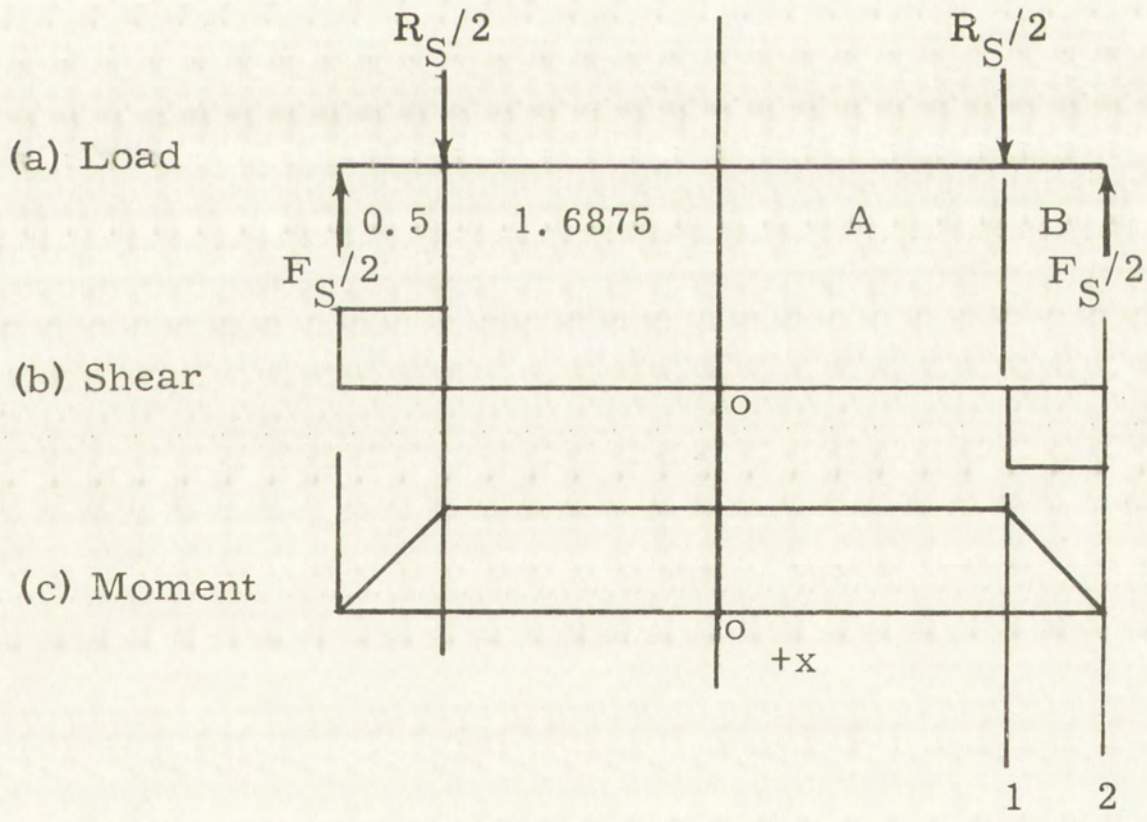

Figure III-1. Loading Due to Straining Frame

As shown in Figure III-1a, the vertical shear equations are:

$$V_{01} = 0 \tag{1a}$$

and

$$V_{12} = -0.5\ F_S\ . \tag{1b}$$

The moment equations are formed by integrating the slope equations with respect to x.

$$M_{01} = C_1 \tag{2a}$$

$$M_{12} = -0.5\ F_S x + C_2 \tag{2b}$$

Integration of moment equations, 2a and 2b, and division by EI yield the slope equations:

$$\theta_{01} = \frac{1}{EI}(C_1 x + C_3) \tag{3a}$$

$$\theta_{12} = \frac{1}{EI}(-0.25\ F_S x^2 + C_2 x + C_4) \tag{3b}$$

The deflection equations are found by integrating the slope equation.

$$\delta_{01} = \frac{1}{EI}(0.5 C_1 x^2 + C_3 x + C_5) \tag{4a}$$

$$\delta_{12} = \frac{1}{EI}(-0.0833\ F_S x^3 + 0.5 C_2 x^2 + C_4 x + C_6) \tag{4b}$$

The constants are evaluated from the known boundary conditions as follows: The central point has been selected as zero; thus, from Equation 4a,

$$EI\delta_0 = C_5 = 0\ . \tag{5}$$

The slope at the center of a symmetrical span is zero; thus, from Equation 3,

$$EI\theta_0 = C_3 = 0\ . \tag{6}$$

From Figure III-1c the moment is zero at point 2, thus from Equation 2b,

$$C_2 = 0.5\ F_S x\Big|_0^{A+B} = 0.5\ F_S(A + B)\ . \tag{7}$$

Equating Equations 2a and 2b at position 1 gives C_1.

$$C_1 = -0.5\ F_S x\Big|_0^{A} + C_2 = -0.5\ F_S A$$

$$+ 0.5\ F_S(A + B) = 0.5\ F_S B \tag{8}$$

The additional constants, C_4 and C_6, remain to be evaluated. The slopes given by Equations 3a and 3b must be equal at point 1. Thus,

$$C_1 A = -0.25\ F_S A^2 + C_2 A + C_4$$

or

$$C_4 = 0.25\ F_S A^2 - 0.5\ F_S(A + B)A + 0.5\ F_S BA$$

$$= 0.25\ F_S A^2 - 0.5\ F_S A^2 = -0.25\ F_S A^2\ . \tag{9}$$

Likewise, the deflections given by Equations 4a and 4b must be equal at point 1. Therefore,

$$0.5 C_1 A^2 = -0.0833\ F_S A^3 + 0.5 C_2 A^2 + C_4 A + C_6$$

or

$$C_6 = 0.0833\ F_S A^3 - 0.25\ F_S BA^2 - 0.25\ F_S A^3 + 0.25\ F_S BA^2$$

$$+ 0.25\ F_S A^3 = 0.0833\ F_S A^3\ . \tag{10}$$

Inserting the values obtained for the constants into the deflection equations, 4a and 4b, yields

$$\delta_{01} = \frac{0.25\ F_S B x^2}{EI} \qquad (11a)$$

and

$$\delta_{12} = \frac{F_S}{EI}[-0.0833x^3 + 0.25(A + B)x^2 - 0.25A^2x + 0.0833A^3] \ . \qquad (11b)$$

In this case, only the δ_{01} is of interest. For the 0.4375-inch-diameter steel shaft: $E = 30 \times 10^6$ lb/in^2 and $I = 1.8 \times 10^{-3}$ in^4. Thus, $EI = 5.4 \times 10^4$ lb/in^2. Inserting this value and the value B = 0.5 inch into Equation 11a yields the final deflection formula for the right half of the central section.

$$\delta_{01} = \frac{0.125\ F_S x^2}{5.4 \times 10^4} = 2.31 \times 10^{-6}\ F_S x^2 \ . \qquad (12)$$

Deflection Due to Bushing Weight (F_B)

The diagrams for bushing load, vertical shear force, and bending moment are shown below.

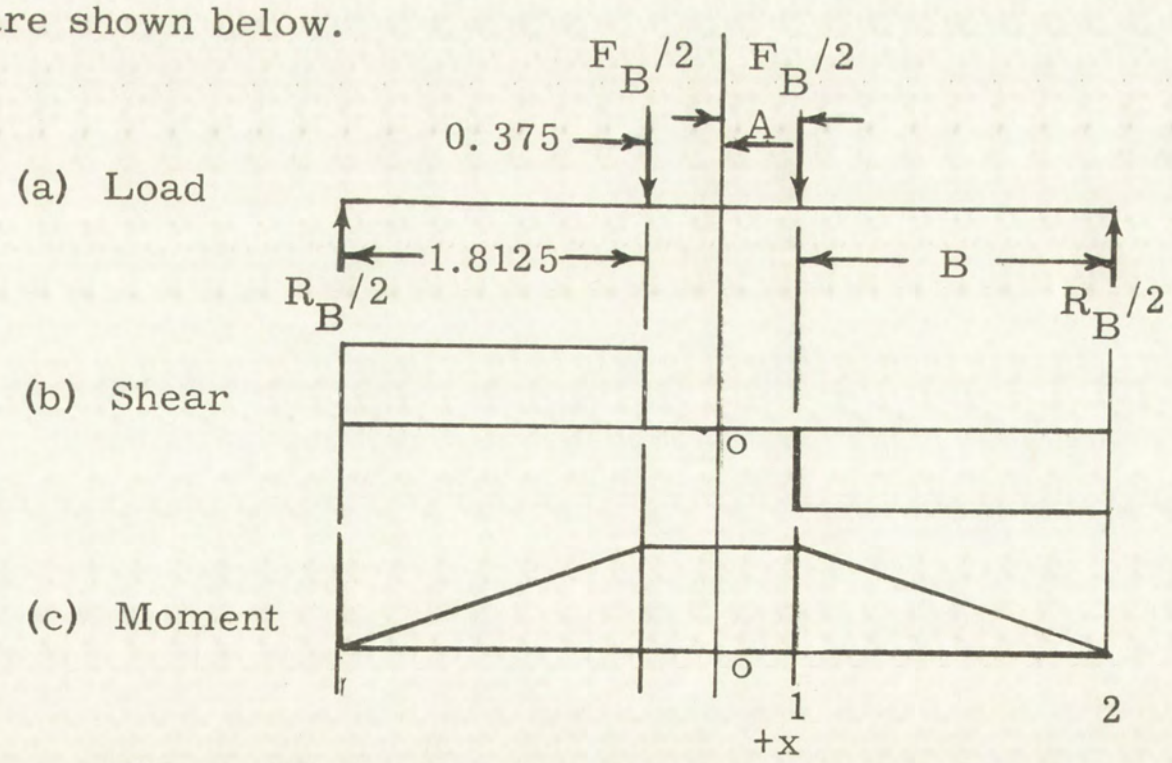

Figure III-2. Loading Due to Bushing Weight

Because of the similarity of this derivation to the preceding one, only the last step of substitution needs to be redone. Other than this, the only difference is that F_S is replaced by F_B. Substituting the values EI = 5.4 x 10^4 lb/in^2, A = 0.375 inch, B = 1.8125 inches, and F_B = 0.0706 pound, the final equations for this loading are obtained.

$$\delta_{01} = \frac{0.25 \times 0.0706 \times 1.8125x^2}{5.4 \times 10^4} = 0.5924 \times 10^{-6} x^2 \text{ in.} \qquad (13a)$$

and

$$\delta_{12} = (-0.1089x^3 + 0.7148x^2 - 0.04591x + 0.00573) \times 10^{-6}. \qquad (13b)$$

Another bushing-weight loading situation is of interest. In this case, the straining yoke is not used. Thus, A = 0.375 inch and B = 1.3125 inches, and the final equations are:

$$\delta_{01} = \frac{0.25 \times 0.0706 \times 1.3125x^2}{5.4 \times 10^4} = 0.4290 \times 10^{-6} x^2 \text{ in.} \qquad (14a)$$

and

$$\delta_{12} = (-0.1089x^3 + 0.5514233x^2 - 0.04591x + 0.00573) \times 10^{-6}. \qquad (14b)$$

Deflection Due to Shaft Weight

The diagrams for loading, vertical shear force, and bending moment are shown on the following page.

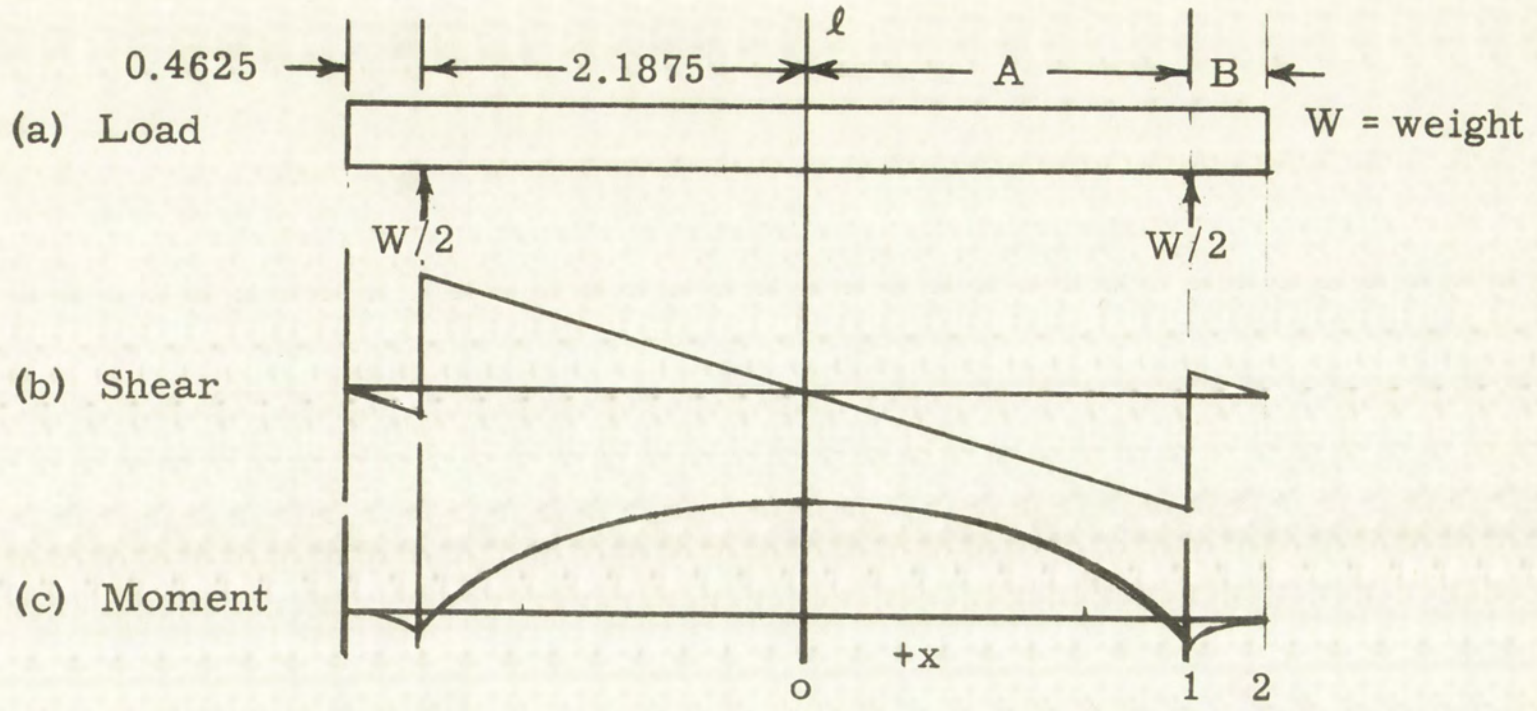

Figure III-3. Loading Due to Shaft Weight

As shown in Figure III-3a, the vertical shear equations are:

$$V_{01} = -\frac{W}{\ell}x \tag{15a}$$

and

$$V_{12} = -\frac{W}{\ell}[x - (A + B)] \ . \tag{15b}$$

Again, the moment equations are found by integration.

$$M_{01} = -\frac{W}{\ell}\left[0.5x^2 + C_1\right] \tag{16a}$$

$$M_{12} = -\frac{W}{\ell}\left[0.5x^2 - (A + B)x + C_2\right] . \tag{16b}$$

The slope equations are obtained by integration of the moment equations and division by EI.

$$\theta_{01} = -\frac{W}{EI\ell}\left[0.1667x^3 + C_1x + C_3\right] \tag{17a}$$

and

$$\theta_{12} = -\frac{W}{EI\ell}\left[0.1667x^3 - 0.5(A + B)x^2 + C_2x + C_4\right] . \tag{17b}$$

The deflection equations are obtained by integrating the slope equations.

$$\delta_{01} = -\frac{W}{EI\ell}\left[0.04167x^4 + 0.5C_1x^2 + C_3x + C_5\right] \tag{18a}$$

and

$$\delta_{12} = -\frac{W}{EI\ell}\left[0.04167x^4 - 0.1667(A + B)x^3 + 0.5C_2x^2 + C_4x + C_6\right] \tag{18b}$$

Here, only the δ_{01} is of interest, so all of the constants do not have to be evaluated.

The central point has been selected as zero; thus, from Equation 18a,

$$\frac{EI\ell}{W}\,{}_0 = -C_5 = 0\,. \tag{19}$$

The slope at the center of a symmetrical span is zero; thus, from Equation 17a,

$$\frac{EI\ell\theta}{W} = -C_3 = 0\,. \tag{20}$$

From Figure III-3c, the moment is zero at point 2; thus, from Equation 16b,

$$C_2 = \left[-0.5x^2 + (A + B)x\right]_0^{A+B} = 0.5(A + B)^2\,. \tag{21}$$

Equating Equations 16a and 16b at position 1 allows solution of C_1:

$$C_1 = -(A + B)A + C_2 = -(A + B)A + \left[0.5(A + B)^2\right]. \tag{22}$$

Inserting these values into Equation 18a yields

$$\delta_{01} = -\frac{W}{EI\ell}\left\{\left\{0.04167x^4 - 0.5\left\{(A + B)A - [0.5(A + B)^2]\right\}x^2\right\}\right\}. \quad (23)$$

Substituting the values $EI = 5.4 \times 10^4$ lb/in^2, $A = 2.1875$ inches, $B = 0.4625$ inch, $\ell = 5.5$ inches, and $W = 0.234$ pound into Equation 23 yields

$$\delta_{01} = (0.8799x^2 - 0.03282x^4) \times 10^{-6} \text{ in.} \quad (24)$$

The equation for δ_{01}, when the straining-frame yoke is not used, is derived also from Equation 23 by using $A = 1.6875$ inches, $B = 1.0625$ inches.

$$\delta_{01} = (0.33843x^2 - 0.03282x^4) \times 10^{-6} \text{ in.} \quad (25)$$

Theoretical Data

The calculated data for the theoretical curves is shown in Figure III-4.

Shaft Position (in.)	Deflection Due to Spring Force, F_S, divided by the spring force (x μin/lb) A = 1.6875 in. B = 0.50 in.	Deflection Due to Bushing Weight, F_B, (with straining yoke) (x μ in.) A = 0.375 in. B = 1.8125 in. F_B = 0.0706 lb	Deflection Due to Bushing Weight, F_B, (without straining yoke) (x μ in.) A = 0.375 in. B = 1.3125 in. F_B = 0.0706 lb	Deflection Due to Shaft Weight (with straining yoke) (x μ in.) A = 2.1875 in. B = 0.4625 in. W = 0.234 lb	Deflection Due to Shaft Weight (without straining yoke) (x μ in.) A = 1.6875 in. B = 1.0625 in. W = 0.234 lb
0	0	0	0	0	0
0.1	0.0249	0.00592	0.00429	0.00880	0.00338
0.2	0.0994	0.0237	0.01715	0.0352	0.0135
0.3	0.224	0.0533	0.0386	0.0789	0.0302
0.4	0.398	0.0944	0.0677	0.1440	0.0533
0.5	0.622	0.1487	0.1071	0.2186	0.0828
0.6	0.895	0.2130	0.1534	0.3115	0.1176
0.7	1.218	0.2893	0.2076	0.432	0.1580
0.8	1.592	0.3723	0.2663	0.549	0.2033
0.9	2.01	0.4561	0.3221	0.691	0.2527
1.0	2.49	0.5659	0.4019	0.846	0.3058

Figure III-4. Theoretical Curve Data

MISSING PAGE
EXTRA
NOT A PART OF CONTENT